APPLICATION OF REDUCED GRAPHENE OXIDE/ NATURAL RUBBER COMPOSITE FOR PETROLEUM REMOVAL IN SEA WATER

Miss Siripak Songsaeng

A Thesis Submitted in Partial Fulfillment of the Requirements
for the Degree of Master of Science in Hazardous Substance and Environmental Management
Inter-Department of Environmental Management
Graduate School
Chulalongkorn University
Academic Year 2018

การประยุกต์ของรีดิวซ์แกรฟีนออกไซด์/ยางธรรมชาติคอมพอสิตสำหรับการกำจัดปิโตรเลียมในทะเล

น.ส.สิริภัค ส่องแสง

วิทยานิพนธ์นี้เป็นส่วนหนึ่งของการศึกษาตามหลักสูตรปริญญาวิทยาศาสตรมหาบัณฑิต
สาขาวิชาการจัดการสารอันตรายและสิ่งแวดล้อม สหสาขาวิชาการจัดการสิ่งแวดล้อม
บัณฑิตวิทยาลัย จุฬาลงกรณ์มหาวิทยาลัย
ปีการศึกษา 2561

Thesis Title	APPLICATION OF REDUCED GRAPHENE OXIDE/ NATURAL RUBBER COMPOSITE FOR PETROLEUM REMOVAL IN SEA WATER
By	Miss Siripak Songsaeng
Field of Study	Hazardous Substance and Environmental Management
Thesis Advisor	Associate Professor SIRILUX POOMPRADUB, Ph.D.
Thesis Co Advisor	Associate Professor PATCHANITA THAMYONGKIT, Ph.D.

Accepted by the Graduate School, Chulalongkorn University in Partial Fulfillment of the Requirement for the Master of Science

..... Dean of the Graduate School
(Associate Professor THUMNOON NHUJAK, Ph.D.)

THESIS COMMITTEE

..... Chairman
(Associate Professor EKAWAN LUEPROMCHAI, Ph.D.)

..... Thesis Advisor
(Associate Professor SIRILUX POOMPRADUB, Ph.D.)

..... Thesis Co-Advisor
(Associate Professor PATCHANITA THAMYONGKIT, Ph.D.)

..... External Examiner
(Suwat Soonglerdsongpha, Ph.D.)

สิริภัค ส่องแสง : การประยุกต์ของรีดิวซ์แกรฟีนออกไซด์/ยางธรรมชาติคอมพอสิต สำหรับการกำจัดปิโตรเลียมในทะเล. (APPLICATION OF REDUCED GRAPHENE OXIDE/ NATURAL RUBBER COMPOSITE FOR PETROLEUM REMOVAL IN SEA WATER) อ.ที่ปรึกษาหลัก : ศิริลักษณ์ พุ่มประดับ, อ.ที่ปรึกษาร่วม : พัชณิตา ธรรมยงค์กิจ

ในงานวิจัยนี้ทำการเตรียมโฟมคอมพอสิตยางธรรมชาติเพื่อเพิ่มประสิทธิภาพในการดูดซับน้ำมัน รีดิวซ์แกรฟีนออกไซด์สังเคราะห์มากจากของเสียแกรไฟต์ด้วยกระบวนการออกซิเดชันและรีดักชัน ในกระบวนการออกซิเดชัน ทำการศึกษาการออกซิเดชันที่ภาวะแตกต่างกัน (การให้ความร้อนควบคู่กับอัลตราโซนิกส์และการปั่นกวนควบคู่กับอัลตราโซนิกส์) เพื่อให้ได้ระยะห่างระยะชั้นในโครงสร้างของแกรไฟต์สูงที่สุด หลังจากนั้นนำกรดแอลแอสคอร์บิก (L-ascorbic acid: L-AA) มาใช้เป็นตัวรีดิวซ์ นอกจากนี้ ได้ทำการศึกษาสมบัติทางสัณฐานวิทยาและสมบัติของพื้นผิวของรีดิวซ์แกรฟีนออกไซด์ที่สังเคราะห์ได้ การเตรียมคอมโฟมคอมพอสิตยางธรรมชาติทำได้โดยการผสมน้ำยางธรรมชาติและรีดิวซ์แกรฟีนออกไซด์ในสัดส่วนต่างกัน (0.25 0.5 1.0 และ 1.5 ส่วนในร้อยส่วนของยาง (phr)) ผลการศึกษาพบว่าปริมาณของรีดิวซ์แกรฟีนออกไซด์มีผลต่อลักษณะสัณฐานวิทยาและประสิทธิภาพในการดูดซับน้ำมันของโฟมคอมพอสิตยางธรรมชาติ สัดส่วนที่เหมาะสมของรีดิวซ์แกรฟีนออกไซด์ในโฟมยางธรรมชาติคอมโพสิตซึ่งให้แสดงค่าการดูดซับน้ำมันที่มากที่สุด คือ 0.5 phr ความสามารถในการดูดซับน้ำมันของ NG-0.5 สำหรับน้ำมันแก๊สโซฮอล์ น้ำมันก๊าด น้ำมันดิบ น้ำมันดีเซล และน้ำมันเตาเท่ากับ 21.50 9.31 17.04 16.53 และ 10.09 กรัมต่อกรัม ตามลำดับ นอกจากนี้ ได้ทำการศึกษาผลกระทบของอุณหภูมิและความปั่นป่วน (turbulence) ในการดูดซับน้ำมันของโฟมคอมพอสิตยางธรรมชาติ แบบจำลองจลนศาสตร์ทั้งสาม ได้แก่ pseudo-first-order pseudo-second-order และ สมการ Elovich ถูกนำมาศึกษา โดยแบบจำลอง pseudo-second-order แสดงความสอดคล้องกับข้อมูลที่ได้จากการทดลอง แบบจำลอง Langmuir ไอโซเทอร์มเป็นแบบจำลองที่เหมาะสมในการทำนายพฤติกรรมการดูดซับน้ำมันของโฟมคอมพอสิตยางธรรมชาติ นอกจากนี้ ศึกษาถึงลักษณะการนำกลับมาใช้ใหม่โดยวัฏจักรการดูดซับและการคายการดูดซับจำนวน 15 ครั้ง ผลการศึกษาพบว่าโฟมคอมพอสิตยางธรรมชาติสามารถนำกลับมาใช้ได้หลายครั้ง

สาขาวิชา	การจัดการสารอันตรายและสิ่งแวดล้อม	ลายมือชื่อนิสิต .....
ปีการศึกษา	2561	ลายมือชื่อ อ.ที่ปรึกษาหลัก .....
		ลายมือชื่อ อ.ที่ปรึกษาร่วม .....

5987544720 : MAJOR HAZARDOUS SUBSTANCE AND ENVIRONMENTAL MANAGEMENT
KEYWORD: natural rubber composite foam, reduced graphene oxide, oil adsorption

Siripak Songsaeng : APPLICATION OF REDUCED GRAPHENE OXIDE/ NATURAL RUBBER COMPOSITE FOR PETROLEUM REMOVAL IN SEA WATER. Advisor: Assoc. Prof. SIRILUX POOMPRADUB, Ph.D. Co-advisor: Assoc. Prof. PATCHANITA THAMYONGKIT, Ph.D.

In this study, the natural rubber (NR) composite foam was prepared to enhance oil adsorption performance of NR foam. The reduced graphene oxide (rGO) was synthesized from graphite waste by oxidation and reduction processes. In the oxidation step, different oxidation conditions (thermal-sonication and stirring-sonication) were studied in order to achieve the highest interlayer spacing in graphite structure. Then, the reduction was carried out using L-ascorbic acid (L-AA) as a reducing agent. Furthermore, morphology and surface properties of the synthesized rGO were investigated. To prepare the NR composite foams, NR latex was mixed with various contents of rGO (0.25, 0.5, 1.0 and 1.5 parts by weight per hundred part of rubber: phr). The results showed that the amount of rGO affected the morphology and the oil adsorption capacity of NR composite foams. The optimum amount of rGO in the NR composites foam which exhibited the highest oil adsorption performance was 0.5 phr. The oil adsorption capacity of NG-0.5 for gasohol, kerosene, crude oil, diesel and fuel was 21.50, 19.31, 17.04, 16.53 and 10.09 g g^{-1}, respectively. In addition, the effect of temperature and turbulence on the oil adsorption capacity of the NR composite foams was determined. Three kinetic models, i.e. pseudo-first-order, pseudo-second-order and Elovich equation, were examined. The pseudo-second-order presented the better fit with the experimental data. The Langmuir isotherm was an appropriated model to predict the oil adsorption behavior of the NR composite foams. Finally, reusability feature of the NR composite foams was also studied through fifteen oil adsorption-desorption cycles. The result showed that the NR composite foams could be reused in many times.

Field of Study:	Hazardous Substance and Environmental Management	Student's Signature .....
Academic Year:	2018	Advisor's Signature .....
		Co-advisor's Signature .....

ACKNOWLEDGEMENTS

I am pleased to express my thankfulness to my advisor Assoc. Prof. Dr. Sirilux Poompradub for her enthusiastic encouragement and useful knowledge at all times of my thesis. I also thank my co-advisor Assoc. Prof. Dr. Patchanita Thamyongkit for her patient guidance and support. In addition, I would like to extend my sincere gratitude to my committee member, Assoc. Prof. Dr. Ekawan Luepromchai the chairman of the committee and all the committee members, Dr. Vacharaporn Soonsin and Dr. Suwat Soonglerdsongpha for their comments and suggestions which led to significant improvement of the thesis.

I would like to acknowledge financial was supported from the International Program in Hazardous Substance and Environmental Management (HSM), Graduate School Chulalongkorn University and also thanks to Department of Chemical technology for laboratory equipment and research supports.

Finally and most importantly, I extremely gratitude to my lovely family and friends for providing me with unfailing support and continuous encouragement throughout my years of study.

Siripak Songsaeng

TABLE OF CONTENTS

Page

LISTS OF TABLES

LISTS OF FIGURES

CHAPTER I INTRODUCTION

1.1 State of problem

Marine pollution is one of the most environmental concerns, especially oil spillage. The extensive of oil and petroleum products leads to increase the possibility of oil spill through extraction, industrial refinery, transportation and also storage leakage. Several advance technologies are used to control the risk of oil leakage; nevertheless, the oil spill still occurs in many areas around the world. In case of Thailand, the latest oil spill accident happened in 2013 that approximately 50,000 liters of oil discharged into the ocean, and the beaches near Ao Phraro, Samet Island (Kampa, Casarotto, Maria, Woodard-Wallace, & Whyte, 2014). When the large volume of oil released into the ocean, oil can be widely spread by the action of wind and wave and causes the adverse impacts on human health, aquatic lives, ecosystem and environmental qualities. The conventional technique for oil spill remediation can be divided into three main groups. There are mechanical, chemical and biological methods. Among of these methods, an adsorption material is commonly used in the preliminary step due to the potential of oil removal and environmental friendliness (Adebajo, Frost, Kloprogge, Carmody, & Kokot, 2003; Behnood, Anvaripour, Jaafarzade Haghighi Fard, & Farasati, 2013).

Many researchers have been studied on sorbent materials owing to the possibility of collection and high sorption capacity by transforming liquid oil phase to semi-solid phase. Sorption mechanism can be divided into absorption and adsorption. The absorption occurs when oil is penetrated into pore spaces of absorbing material, whereas, the adsorption is the attraction of the spilled oil on sorbent surfaces but does not allow to infiltrate into the material matrix. Moreover, sorbent materials are convenient transported from the contaminated site and adsorbed oil can be recovered from these materials. The important properties of an ideal sorbent are low

hydrophilicity, high oleophilicity, excellent oil/water selectivity and, great reusability. The sorbent materials can be categorized into three groups; inorganic minerals, synthetic materials, and natural organic products (Behnood et al., 2013). The synthetic materials such as polypropylene, polyester, and polyurethane, are known as commercial sorbents that show high oil sorption capacity. The drawbacks of the synthetic materials are high management cost, non- renewability and non-biodegradability. While natural materials are availability, cost-effective and biodegradability (Adebajo et al., 2003). Therefore, the natural materials are more attention in terms of an oil sorbent material.

Currently, the natural materials e.g. cotton, straws, corn cobs, coconut shells, kenaf, sawdust and kapok fiber are developed and determined their oil sorption capacity (Idris, Eyu, Mansor, Ahmad, & Chukwuekezie, 2014). These materials are oleophilicity but their efficiency is dependent on their density, wettability, retention rate and recyclability. Some natural organic material achieved high oil sorption capacity, however, the reusability and recovery of absorbed oil required mechanical equipment (H. M. Choi, Cloud, & technology, 1992). The oil sorbent material could be prepared in form of fiber, resin, gel or foam. Fiber and resin sorbent have the disadvantages such as slow oil sorption rate, unrecoverable absorbed oil and poor reusability. To overcome their limitations, the macroporous gel or sorbent foam has been studied. Nevertheless, the macroporous gels could not reuse for many times due to the destruction of their network (Ratcha et al., 2015). Foam sorbent provides a huge space for oil storage regarding to its large pore volume that is useful for oil recovery and reusability. Either synthetic or natural polymers can be prepared as a sorbent foam. Hence, natural rubber (NR), becomes more interesting material due to its special properties and environmental aspect. NR or *cis*- 1,4 polyisoprene is one of the most important renewable polymeric materials in nature. NR is commonly obtained from *Hevea Brasiliensis* which is grown in the warm climate of Southeast Asia, especially

Thailand. NR is applied in many applications due to its high resilience, tensile strength, and tear resistance (Chapman, 2007). The demand of NR has continuously increased, especially NR foam because it was used as adsorbing material for noise and vibration control (Najib, Ariff, Bakar, Sipaut, & Design, 2011). The special characteristics of NR foam are high porosity, low density, and hydrophobic property that are very useful to adsorb the spilled oil or organic pollutant also (Ratcha et al., 2015). However, its limitations are low oil uptake and poor weather resistance. Many treatments have been proposed to solve these disadvantages, especially the low oil sorption capacity such as functional group modification, and preparation in form of polymer composite, are developed (Venkatanarasimhan & Raghavachari, 2013). Generally, carbon materials (carbon black, graphite and carbon-nanotube) are used as a filler to improve the properties of NR products. Reduced graphene oxide (rGO) is one kind of carbon-materials and becomes more interesting material. The two-dimensional honeycomb lattice structure of rGO shows excellent properties (Fan et al., 2008). Recently, rGO is widely applied in several field of technologies including water purification and sorption technology owing to the hydrophobicity and high surface area (M. T. H. Aunkor, I. M. Mahbubul, R. Saidur, & H. S. C. Metselaar, 2016). Furthermore, rGO can be made in form of the polymer composite into the NR matrix in order to improve physical, mechanical, thermal and electrical properties of the composite materials.

In this study, we aimed to enhance the oil sorption efficiency of the NR by preparing NR composite materials. The rGO was synthesized via an oxidation-reduction process and mixed into NR latex to produce NR composite materials. The NR composite materials were investigated their physical and oil sorption properties. Additionally, the kinetics and adsorption isotherm of the NR composite materials were determined. The NR composite material is expected to be able to serve as the efficient sorbent materials for remediating the oil contaminated area.

1.2 Hypothesis

- The composite material can provide higher hydrophobic and oleophilic properties.
- The rGO can increase the surface area and the oil sorption capacity of the resulting composite material.

1.3 Objectives

The goal of this research is to produce the NR composite material that is practically useful for the oil spill remediation. To achieve this goal, the following objectives are established.

- To synthesize and characterize rGO sheet using oxidation-reduction process
- To produce an NR composite material and to determine the performance of material for petroleum oil removal from seawater

1.4 Scope of the study

This work is divided into two parts as the first part is to synthesis rGO and the second part is to produce NR composite materials and characterize its properties. The experimental framework is summarized in Figure 1.1.

1.4.1 Part I: Synthesis of rGO and characterization

1.4.1.1 Synthesis of rGO by oxidation-reduction processes

- Two methods used in oxidation were the stirring-sonication and thermal-sonication methods
- The concentration of L-AA in reduction process was varied as follows: 0.25M, 0.5M and 1.0M

1.4.1.2 Characterization of graphite, GO and rGO

- Structural study by X-ray diffraction characterization (XRD)
- Morphological study by transmission electron microscopy (TEM)

- Elemental composition analysis by CHNS analyzer
- Functional groups by fourier transforms infrared spectroscopy (FTIR)
- Elemental binding energy by X-ray photoelectron spectroscopy characterization (XPS)
- Surface area measurement using Brunauer-Emmett-Teller (BET) method

1.4.2 Part II: Preparation of NR composite foams and characterization

1.4.2.1 Preparation of composite foams by using a cake mixer

1.4.2.2 Morphological study of composite materials by scanning electron microscope (SEM)

1.4.2.3 Oil adsorption study

- Effect of oil types: gasoline, kerosene, crude oil, diesel and fuel oil
- Effect of environmental conditions: temperature, turbulence
- Adsorption kinetic
- Adsorption isotherm
- Reusability test

1.4.2.3 Weathering test

1.5 Beneficial outcome

The NR foam and composite can be used as oil sorbent materials and replaced the synthetic sorbent.

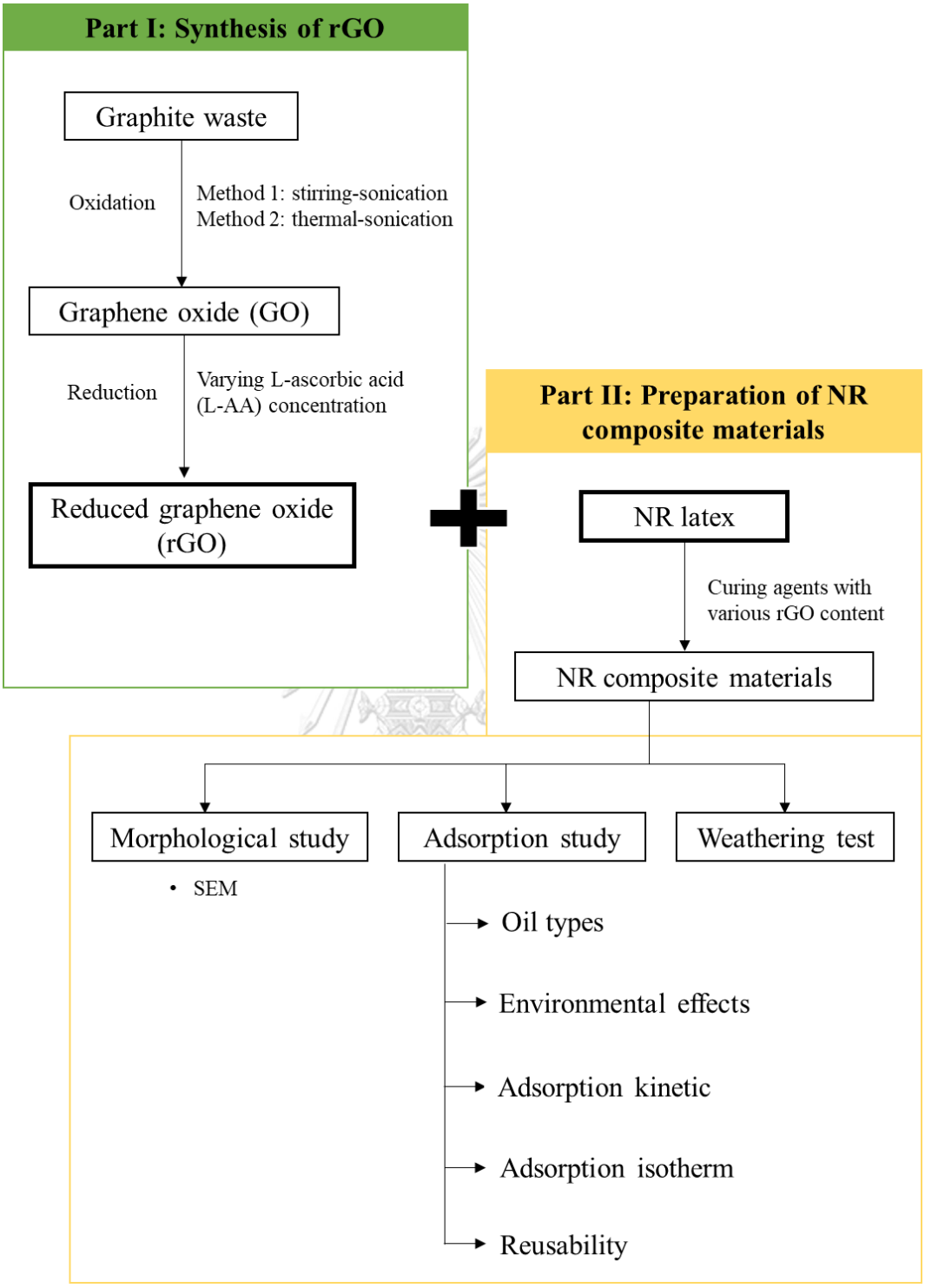

Figure 1.1 Experimental framework.

CHAPTER II
THEORETICAL BACKGROUND AND LITERATURE REVIEWS

2.1 Petroleum oil

Petroleum oils are an underlying element that mostly used as a fundamental component in many products. They describe a substance contained hydrocarbon and other components such as sulfur, nitrogen and oxygen. The variable amounts of other components relatively display different physical and chemical properties of the oil (Board, Board, & Council, 2003). Basically, the petroleum oil can be divided into two main types. There are natural hydrocarbon substance or crude oil and refined petroleum products. The petroleum oils are a crucial factor in driving the economy of countries corresponding to the increasing consumption of petroleum products. Therefore, petroleum-oil contamination is greatly concerned due to the high probability of being released into the environment through seepage, extraction, transportation and storage. The toxic chemicals containing in the oil substance cause both long-term and short-term effects in all ecosystems. When the oil is introduced into the environment, it can distribute among the four major environmental compartments: air, water, soil and biota (Speight, 2016). The movement of oil is governed by the physicochemical properties and the environmental processes. Understanding the characteristics and behavior of oil in the environment are useful for conceiving the potential effects and the appropriate response techniques (White, 2000)

The important properties of oil are specific gravity, distillation characteristic, pour point, flash point, vapor pressure, solubility and viscosity. All of the physical characteristics also relate to the chemical composition of the oil substance such as the proportion of volatile components and the content of asphaltenes, resins and waxes. To realize the physiochemical of oil provides a suitable approach for oil spill

removal (Emergency, Response, & Division, 1993; Ltd., 2012; National Academies of Sciences & Medicine, 2016; Parker, 1997).

2.1.1 Oil properties

2.1.1.1 Specific gravity

Specific gravity is a dimensionless unit defined as the ratio of the substance density to the water density (1 g/cm^3). The specific gravity uses to classify light or heavy petroleum oils and indicates that the oil is floating or sinking into water. The density of the oils ranges from 0.7 to 0.99 g/cm^3, thus the oils float on water surface (Board et al., 2003; Merv Fingas, 2014). When the oil released into seawater which typically has a density 1.03 g/cm^3, light oils and most heavy oils usually float on seawater (National Academies of Sciences & Medicine, 2016). Additionally, the proportion of evaporative components significantly affects the oil density, instance, the loss of evaporative components leads to the oil density increasing. The American Petroleum Institute gravity scale, °API, is commonly used to describe the specific gravity of crude oil and petroleum products as follows (Merv Fingas, 2012):

$$°API = \frac{141.5}{density\ at\ 15\ ℃} - 131.5$$

The specific gravity information can predict other properties of oil, for example, a low API oil tends to contain low proportion volatile components and to be high viscosity.

2.1.1.2 Distillation characteristics

This characteristic describes the volatility of oil and indicates the maximum evaporation. It provides a useful information for environmentalists about the chemical composition of oil. The distillation property correlates strongly to the composition of the oil such as bituminous, asphaltenic or waxy residues which do not readily distill, even at high temperatures. Thus, these chemical compositions are likely

to persist in the marine environment for extending a period of time (Mervin Fingas, 2016; X. Zhu, Venosa, Suidan, & Lee, 2001).

2.1.1.3 Flash point

The flash point is directly relate to the risk of ignition. A liquid is considered to be flammable when its flash point is below 60 °C (Merv Fingas, 2012). Most of the oil types are concerned as flammable substances, especially when fresh. Gasoline is generally known as a flammable substance under all ambient conditions and poses a serious hazard when spilled and volatized. This characteristic relates to the volatility of oil. Many oils with high volatile components (low density) are possible ignition at low temperature. On the other hand, heavy oils normally are not flammable under environmental conditions due to their low volatile components (Jokuty et al., 1999).

2.1.1.4 Vapor pressure

The vapor pressure provides the partitions of the oil between the liquid and gas phases that usually quoted as Reid Vapor Pressure measured at 100 °F. A vapor pressure greater than 3 kPa (23 mmHg) is the criteria for evaporation under environmental conditions. The substance has a vapor pressure above 100 kPa (760 mmHg), it changes into a gas form. Gasoline has a vapor pressure of 40-80 kPa (300-600 mmHg) that it is very volatile with a high proportion of components boiling at low temperature. Furthermore, the vapor pressure relates to the density and viscosity of the spilled oil (Jokuty et al., 1999; Speight, 2014).

2.1.1.5 Solubility

Solubility refers the amount of an oil dissolves in the water. In the environmental condition, the amount of dissolved oil is always small which is less than 100 part per million (ppm), this is not a significant mechanism as evaporation. Although solubility represents a minor process, the soluble fraction of oil can cause toxic effect to aquatic life (Board et al., 2003; Merv Fingas, 2012).

2.1.1.6 Viscosity

The viscosity of oil is the resistance to flow and affects the information in terms of spreading. This property is largely determined by the proportion of lighter and heavier fractions contained in oil compounds. The greater percentage of light components or lower the amount of asphaltene causes the low viscosity of the oil. Highly viscous oils cause the spilled oil does not spread into a thin film. The temperature or ambient condition also impacts viscosity, with lower temperature resulting in a high viscosity (National Academies of Sciences & Medicine, 2016). The increase of oil viscosity caused the transformation of a liquid petroleum into a heavy or semi-solid substance. All oil types become more viscous as the temperature falls and as the volatile component evaporates overtimes (Board et al., 2003; Emergency et al., 1993).

2.1.2 Types of oil

Types of oil is one of the most important factors in any spills due to its probable persistence in the environment. The oils can be divided into four major groups (Doerffer, 2013; Speight, 2014).

Class A: Light oils, volatile oils or non-persistent oils

Light oils mostly refer to light refined products (e.g. jet fuel, gasoline, kerosene, light virgin naphtha, heavy virgin naphtha, petroleum ether, petroleum spirit, and petroleum naphtha) and some light crude oil. These oils are highly volatile with low density and low viscosity which are spared rapidly on the sea surface. They are non-persistent due to their high evaporation, but they are low flash point and tend to be flammable at low temperature. When light oils spilled on the seashore, they penetrate and persistent into the porous surface of the matrix such as sand, adsorbent. However, they can be easily removed from the matrix because the oils do not tend to adhere to the surface of adsorbent. This type is highly danger to humans, organisms and the environment (Emergency et al., 1993).

Class B: Medium oils or non-sticky oils

Fuel oil, diesel fuel oil and domestic fuels are representatives of this class that are moderately volatile. The physical property of non-sticky oils is a waxy or oily feel. This type is less toxic and more adhere to the matrix surface than previous oil types. However the non-sticky oils are less toxic, they can be persisted and caused long-term effects in the environment.

Class C: Heavy oils or sticky oils

Heavy oil is a brown or black liquid petroleum with high viscosity. This class tends to long-term persistence in the environment due to their greater proportion of non-volatile components. The density of these oils is near the water density. When the heavy oils leaked, the cleanup methods are very difficult and expensive. This type is relatively low toxic to human, conversely, it causes the long-term effect to the environment and wildlife.

Class D: Very heavy oils or non-fluid oils

Non-fluid oils are relatively nontoxic and black color including heavy crude oils and bunker oils. Their characteristics are low or no evaporation, dissolution, and high density. Mostly, the heavy oils sink down into depths of the ocean due to their heavy weight. Moreover, these oils possibly cause the long-term contamination in soil or sediments. When they released into the environment, it severs impacts to waterfowl and fur-bearing mammals and also difficult to clean up under all conditions. The comparison important properties of different oil types are summarized in Table 2.1 (Mervin Fingas, 2016).

2.1.3 The effect of oil spill

An oil released into the environment causes both acute and chronic effects (Michel & Fingas, 2016). Acute effects are short duration, limited impact or they described as long-term community level impacts. Chronic effects is defined as the

long-term and consecutive exposure covering the incorporation of spilled oil into sediments (Board et al., 2003). The effects of an oil spill not only damaged the ecosystem but also affected the economic part. Therefore, the public attention towards oil spills has grown in the last three decades, and their effects are more obvious today.

2.1.3.1 Environmental effects

The major oil spill effect is the animal lives such as changing their reproductive, feeding behavior, losing of their habitats and reducing the biodiversity. Aquatic environment is the most concern areas due to the complex interrelations between plant and aquatic animals. Plankton is important species because they tend to eliminate low oil concentration within a few days. Moreover, they are the bottom of an aquatic food chain that leads to damage for other species further up the chain (Michel & Fingas, 2016). Oil exposure can change both physiological and pathological of fish, moreover, the disruption of growth of surviving. Fish species live close to the water surface, shore and seabed are the most vulnerable to oil spills. The adversely visible impacts of the oil spill on seabirds have been well documented, estimating between 100,000 and 500,000 seabirds are killed in the North and Baltic Seas (Clark, Frid, & Attrill, 1989). The exposure pathways of birds are fouling of the feathers and ingestion. When oil trapped plumage of birds, the protective layer of feathers and insulating down is disrupted and allowing seawater direct contact with the skin. Hence, the birds are loss of body heat and ultimately succumb to hypothermia. The ingestion effects of birds are the reduction in reproduction, the destruction of red blood cells and the increase susceptibility to disease (Michel & Fingas, 2016). Marine mammals, such as whales, dolphins, porpoises and seals, are highly visible and cause much public concern when oil spill. All of these mammals are sensitive to oil exposure, however, the reports of oil pollution damage to theses mammals are very rare (Parker, 1997).

2.1.3.2 Commercial effects

Contamination of the coastal area causes adverse economic consequences in a wide variety of direct and indirect ways. In commercial part, the spilled oil affects creation of a port and navigation hazards, interferes with commercial or recreational fisheries, contamination of fish farming facilities and products. In part of tourism, the tourism industry suffers financial loss, as a result of contamination of popular beaches both as soon as the leakage occurred and in the longer. The oil spill also affects the banning of seafood products from the contaminated area, resulting in the loss of consumer confidence. Moreover longer term and damaging economic impacts can occur when public perception of prolonged and wide-scale pollution remains long after the oil has disappeared. In these situations, it takes longer than usual for business activities to return to normal (Parker, 1997).

2.2 Oil spill response techniques

Remediation of oil spill from the marine environment is a critical to minimize danger and potential damage to aquatic lives, human and environmental qualities. The spill location magnitude can determine the strategy and technology applied for cleanup. The oil spill on seawater and coastal required different response techniques than an oil spill on land. Currently, the traditional techniques manage the marine oil spill can be categorized into four groups: biological decomposition, chemical dispersion, burning and mechanical recovery (EO, FA, & DA, 2014). However, there is no simple procedure that can remove all spills due to the difference of oil types and environmental conditions. In most cases, two or more methods are combined to achieve an effective removal (Al-Majed, Adebayo, & Hossain, 2012). The detail of various strategies is explained in this section.

2.2.1 Biological decomposition

The biological degradation of oil is a very simple and cheap remediation technique, involved in weathering and the eventual removal of pollutants from the environment. Biodegradation can mitigate toxic impacts of spilled oil without causing ecological harm and environmental conditions as shown in Figure 2.1. This mechanism has the potential to assist recovery in depth-ocean or sensitive area such as bottom sediment, shorelines, marshes and wetlands, but the rates of biodegradation are often too slow. Bioremediation techniques include two main approaches: biostimulation and bioaugmentation. Biostimulaion is the addition of nutrients or other co-substrates for stimulation native organisms to degrade petroleum pollutants. While bioaugmentation enhances oil degradation by the addition of oil-degrading organisms to supplement the existing microbial populations (Al-Majed et al., 2012; Mohajeri, Aziz, Zahed, & Isa, 2008; Tewari & Sirvaiya, 2015). Bioremediation was shown to be effective in highly porous shorelines where nutrients and oxygenated seawater could reach the surface and sub-surface oil residue (Al-Majed et al., 2012; Ivshina et al., 2015). The rate of biodegradation is controlled by biodiversity, bioavailability of nutrients, oil toxicity, oxygen supply, environmental conditions and time consuming. All petroleum hydrocarbons cannot be completely degraded, then the asphaltenes and resin compounds still remain (Asadpour et al., 2013; Schratzberger et al., 2003). Therefore, the decision to use this technique should be based on a net environmental benefit analysis. If residual oil poses no ecological risk, it should be left to undergo natural biodegradation.

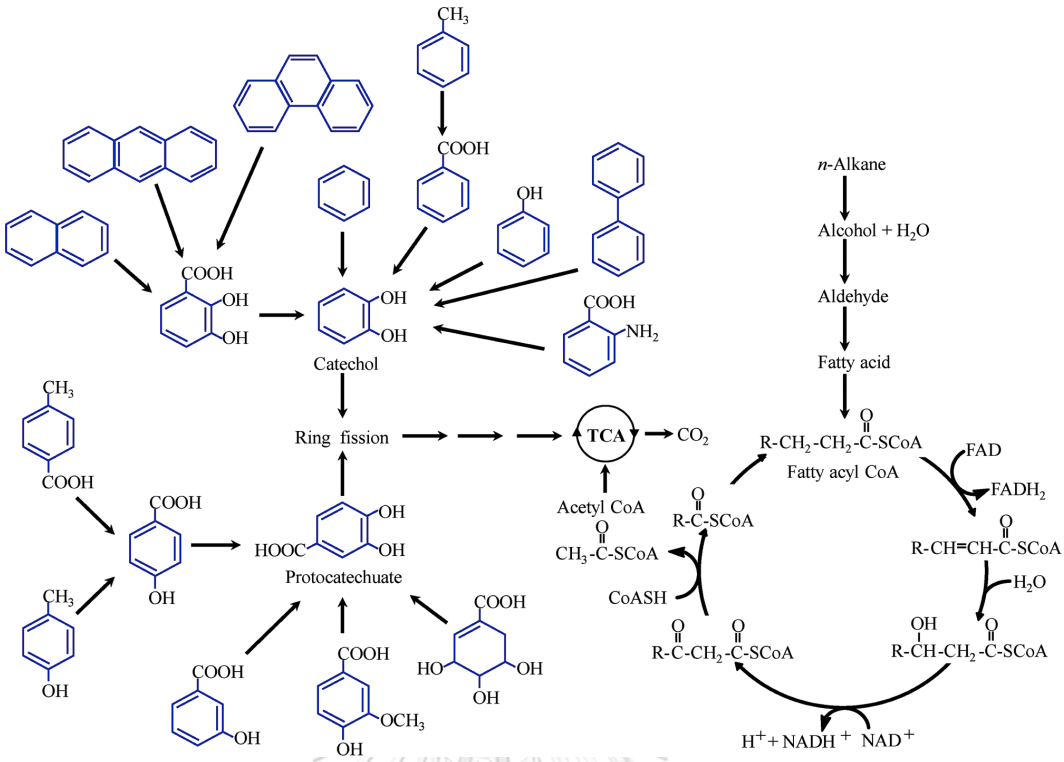

Figure 2.1 Pathways of biodegradation for hydrocarbon compounds (Ivshina et al., 2015).

2.2.2 Chemical dispersant

Chemical dispersant is designed to enhance the natural dispersion which is useful for oil disappearance from water surface. The formulation of chemical dispersant consists of two or more different surfactants that are partially soluble in both oil and water (Al-Majed et al., 2012). Several chemical dispersants have the capabilities to change the physical and chemical properties of oil. The dispersant is often applied to disperse oil at sea or shorelines, rather than the sensitive resources. This technique makes small oil droplets by reducing the surface tension between oil and water (Figure 2.2), resulting in to increase the rate of biodegradation. Nevertheless, spray equipment is required to mix the chemical and oil for maximum effectiveness. The chemical dispersants are not efficiency on all oil types and all circumstances. They are less effective with highly viscous oil. Conversely, they are effective with viscous

oils on shorelines because the contact time is prolong, allowing better penetration of the dispersant into the oil (Ivshina et al., 2015; Parker, 1997). The calm condition is one of the limitations of using dispersant because it is no sufficient mixing energy needed to mix dispersants with oil and to also aid the immediate dispersion of the oil (Al-Majed et al., 2012). The inflammable nature of most dispersants can cause human health hazards during applications and potential damage to marine life (Dave & Ghaly, 2011). Currently, chemical dispersants have been developed to be less toxic, but fewer long-term environmental effects have been conducted after its application. The decisions to use chemical dispersant involve sea condition, cost effectiveness, ecological considerations and regulations. This technique has not been used extensively in the United States due to its effectiveness and concerns about the toxicity of the dispersant mixtures.

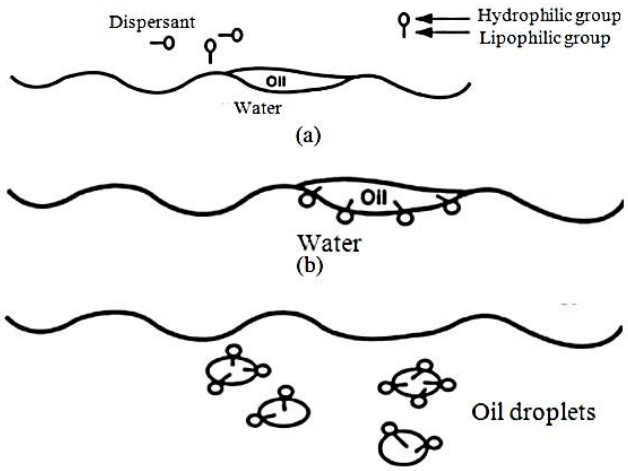

Figure 2.2 The use of chemical dispersant to break down spilled oil into small droplets (Dave & Ghaly, 2011).

2.2.3 Thermal remediation

This technique involves the ignition and controlled combustion of oil on water surface with minimal specialized equipment that is high rates of oil removal

efficiency. This method is effective to ignite the oil, when the thickness of spilled oil is at least 0.1 inches (2 to 3 millimeters). The more weathered, the emulsified oil and the greater oil thickness are harder for ignition and sustained combustion (Al-Majed et al., 2012; Asadpour et al., 2013). The residual compounds after oil burning, which are higher molecular weight, low volatilization and low solubility, has no detectable acute toxicity (Ivshina et al., 2015). This technique has been used in many large spills and it normally used under the approval of governmental agencies. The limitations of this method are the thickness of oil on water surface and environmental conditions. This method is effective in calm wind conditions and spills of fresh oils or light-oils which quickly burn without causing any danger to marine life. The meaningful disadvantage of burning is the generation of large quantities of toxic smoke including carbon monoxide, sulfur dioxide, and polycyclic aromatic hydrocarbons (PAHs) (Al-Majed et al., 2012). Therefore, the balance between oil elimination and toxic gases occurring are concerned for thermal application.

2.2.4 Mechanical method

The most efficient and environmentally friendly techniques for oil spill removal is mechanical techniques. Generally, mechanical cleanup is the primary step of defense against oil spill because they are normally used as a barrier to control the spreading of spilled oil without changing the physical and chemical characteristic of oil. These methods required to use booms, skimmer or sorbent materials which consist of two steps for oil spill controlling: containment and recovery (Tewari & Sirvaiya, 2015). The performance of these techniques can be severely limited by ocean conditions and weather including wind, wave and current.

2.2.4.1 Booms containment

Booms are temporary floating barriers used to limit oil spreading into larger areas and to reduce the possibility of polluting shorelines. This

equipment is useful to divert oil spills to areas where cleanup can be performed, to contain spilled oil and to protect environmentally sensitive areas threatened (Clark et al., 1989). The important features of booms include the freeboard flotation that extends over the surface and prevents the oil from flowing through the top of the boom. The skirt extends beneath the surface to prevent the oil to fall out underneath the boom. The tension improves the strength of booms to withstand the force of waves and winds. Booms can be categorized into three groups: frence, curtain and fire-resistant booms. The frence booms are designed like semi-rigid materials providing a vertical screen against contaminating oil. This boom is light weight, minimal oil sorption and easy to handle, but its low stability in strong winds and currents. Curtain booms are non-adsorbent floating structure that are reliable in clam condition (Dave & Ghaly, 2011). Fire containment booms, which are created by the fire proof metal, mostly used in conjunction with *in-situ* burning technique (Ventikos, Vergetis, Psaraftis, & Triantafyllou, 2004). Additionally, this boom type prefers in calm water conditions to ensure that a thick layer of oil is maintained for burning. Environmental conditions affect booms operation that they mostly operate satisfactorily under the prevailing wind and wave conditions. The limitations of using booms are the applicable safety under adverse conditions and the maintenance that are be a big deal if weather condition is high current speed exceed 0.7 knots and the cost is considerable.

2.2.4.2 Skimmers

A skimmer is a device for oil recovery from the surface water that is either self-propelled devices or can be operated from vessels. The skimmer can use with the operation of booms to recover spilled oil without changing its properties. This equipment must be brought immediately to deal with the oil before it has spread out into a thin layer. The skimmers can be divided into three types; weir, oleophilic and suction skimmers, depend on their basic operating principles (Dave & Ghaly, 2011; Ivshina et al., 2015; Michel & Fingas, 2016). Weir skimmers which float on water surface

use with enclosure the oil/water interface position. They are high stability in wave condition and have the potential for oil recovery by oil trapping inside. Oleophilic skimmers have an affinity for oil in preference to water; therefore, this type usually achieves the highest ratio of recovered oil in relation to free or entrained water. This type can recover more than 90% of spilled oil from water, however, it can be applied with the oil mixed with dispersants. Suction skimmers operate like a vacuum cleaner which are generally very efficient, but they work the best on smooth water. They have the ability in handling a wide range of oil viscosity. Moreover, their efficiency depends on weather conditions. In wavy water, skimmers tend to recover water more than oil that is the important limitation of this equipment. Furthermore, this method is expensive for large spills (Al-Majed et al., 2012; Saleem, Riaz, & Gordon, 2018).

2.2.4.3 Sorbent materials

Sorbent materials are hydrophobic and oleophilic materials having a high capacity to adsorb oil. Oil sorbents are able to transform liquid oil to the semi-solid phase which can then be removed from the spilled area in a convenient manner (Asadpour et al., 2013). Sorption mechanism can be divided in two mechanisms; absorption and adsorption. Oil can be penetrated into pore spaces in the material, it can call absorption, whereas adsorbents attract the spilled oil to their surfaces but do not allow to penetrate into the material. The important properties of an ideal sorbent material for oil removal are low hydrophilicity, high oleophilicity, excellent oil/water selectivity and, great reusability. These properties determine the time consuming and oil adsorption (Bernard & Jakobson, 1972). Generally, sorbent materials can be categorized into three groups; inorganic mineral, synthetic material, and natural organic products (Behnood et al., 2013). This approach is insensitivity to sea conditions; therefore, it can be used in all environmental conditions. However, the sorbents should be employed with caution to minimize inappropriate and excessive use that can present major logistical difficulties associated with secondary

contamination, retrieval, storage and disposal. Sorbents have been recorded to be one of the most effective and cheapest methods of cleaning oil spills both on sea water and shoreline (Al-Majed et al., 2012; EO et al., 2014). In general application, this technique is applied on the spill before the oil viscosity increases due to the decrease of the sorbent efficiency. The following characteristics must be considered when choosing sorbents for cleaning up spills including adsorption rate, retention capacity and applications. The advantages and disadvantages of adsorbents are summarized in Table 2.1.

Table 2.1 Adsorbant types and their properties (Al-Jammal & Juzsakova, 2017; Dave & Ghaly, 2011).

Adsorbents	Advantages	Disadvantages
Inorganic minerals	- High adsorption capacity - Inexpensive - Environmental availability	- Ability of water adsorption - Sensitivity to fouling - Need to dispose with regulation - Weather sensitive
Synthetic materials	- No maintenance require - Excellent hydrophobic and oleophilic properties - Reusability	- Expensive - Need to landfill disposal - Non-biodegradation
Natural organic materials	- Inexpensive - Environmental availability - Biodegradation	- High water adsorption - Hydrophilic property - Low buoyancy

2.3 Sorbent materials

As mentioned above, oil sorbent materials can be classified into three categories and the detail of each category is described as follows.

2.3.1 Inorganic mineral sorbents

Mineral adsorbents represent a very large group material, including zeolite, silica, graphite, vermiculite, sorbent clay and volcanic ash, can be used as oil sorbent materials due to their specific surface area that is suitable for the oil adsorption (Behnood et al., 2013). They are available in the environment, however, they show abundant drawbacks. Inagaki (2001) indicated that exfoliated graphite presented higher the oil adsorption capacity compared polypropylene mats and natural sorbents (e.g. cotton, milkweed and kenaf). Their sorption capacity is much higher than synthetic mats because their structure is a network of worm-like which had least two kinds of pore. Sakthive et al. (2013) reported that the conjunction of fly ash and zeolite could produce high surface area material. The result showed functionalization of the zeolite with two different hydrophobic sites led to increasing in the oil sorption capacity of up to 500%. In addition, the material could be used in the power plant as a fuel energy to retrieve oil from sorbent. Okiel et al. (2011) investigated the removal of oil by adsorption on bentonite, powered activated carbon (PAC) and deposited carbon (DC). The bentonite and DC were more efficient in removing oil compared with PAC. The ability of three adsorbents had been influenced by various factors, for example contact time, the weight of adsorbents and oil concentration. This study recommended that the bentonite could be used due to its low cost, natural and abundant source for oil removal. The disadvantages of inorganic sorbents are low oil sorption efficiency, insufficient buoyancy, low reusability and non-degradation compared to polymer or organic sorbents Furthermore, they cause contamination on seabed and harmful

effects to aquatic habitats. Therefore, they are not preferred for oil removal from surface water (Al-Majed et al., 2012; White, 2000).

2.3.2 Synthetic organic products

Synthetic sorbents are made from high molecular weight polymers, for example polypropylene (PP), polyurethane (Monks et al.), polystyrene (Ventikos et al.) and polyvinyl chloride (PVC), are extensively used for oil spill cleanup. Their significant characteristics are oleophilic-hydrophobic properties, high oil/water selectivity, low density, and availability in large-scale (H. Zhu, Qiu, Jiang, Wu, & Zhang, 2011). Hence, they are generally known as commercial sorbents. Liu et al. (2015) improved the oil sorption capacity and retention performance of PP fibers to 15.53% and 70%, respectively, with reusability of 10 times through surface graft polymerization. Lin et al. (2008) studied using waste tire powder for recovery the spilled oil that showed oleophilic property. Due to its elastic property, the waste tire powder could be used for more than 100 times without decreasing its oil sorption efficiency. Wu (2014) reported the preparation of PU sponges with silica sol and gasoline. The result showed that 0.1 g of the prepared sorbent could adsorb more than 100 g of motor oil with less water adsorption. This material showed the high oil adsorption performance, oil/water selectivity and reusability. However, synthetic sorbents have the drawbacks such as they cause a great waste after their application and they are non-biodegradation material (Adebajo et al., 2003).

2.3.3 Natural organic materials

Several natural organic products have an affinity for oil sorption because they contain natural oils or wax in their structure. Natural products are low density, abundant, inexpensive and environmentally friendliness. Currently, various natural materials have been developed to replace synthetic sorbents such as straw, corn cob,

wood fiber, cotton fiber, cellulosic, kapok fiber, kenaf, milkweed floss and peat moss (Adebajo et al., 2003). Some natural materials show higher oil sorption capacity than those synthetic or inorganic materials. The only disadvantage of natural sorbents is they are improper to use in aqueous medium because they tend to absorb water as well. Paulauskienė et al. (2014) evaluated the oil sorption capacity of natural sorbents (sawdust, peat, wool, straw and moss) compared with synthetic materials. The result implied that various sorbent materials showed the different oil sorption capacity depended on their characteristic. To enhance the sorption efficiency and buoyancy of natural sorbents, different materials could be used in complex mixtures. Ali et al. (2012) determined the characteristics and the oil sorption effectiveness of kapok fiber, sugarcane bagasse and rice husks compared with synthetic sorbent. Kapok fiber displayed a microstructure with hollow tubular structure, therefore, it exhibited excellent oil sorption capacity comparable to synthetic sorbent. Sugarcane bagasse showed rough surface morphology causing it was able to adsorb different oil types. In contrast, rice husks showed the lowest oil sorption capacity due to their interconnected dome-shaped regions structure. Additionally, rice husks tended to adsorb water more than 50% and sink to the bottom. In this study, they suggested that the oil sorption efficiency of all sorbents might depend on sorbent structure, and some biomass sorbents might be properly used in matrix form for oil removal. Ratcha et al. (2015) studied the structural modification of the NR with various types of poly (alkyl acrylate), such as poly (methyl methacrylate) (PMMA), poly (butyl methacrylate) (PBMA) or poly (butyl acrylate) (PBA), to increase hydrophobicity and oleophilicity. The result indicated that the addition of poly (alkyl acrylate) could decrease hydrophilicity resulting in the increase on oil sorption performance of NR. Additionally, NR material could be reuse for oil sorption in many times. The application and limitations of different sorbent materials for oil spill cleanup were summarized in Table 2.2.

Table 2.2 The comparison of oil sorption capacity and the applications of different sorbent materials.

Types	Oil type	Sorption capacity ($g\ g^{-1}$)	Eco-friendly
PU sponge (D. Wu et al., 2014)	Motor oil	103	No
	Peanut oil	108	
	Diesel	95	
Polyvinyl chloride/Polystyrene fibe (H. Zhu, Qiu, Jiang, Wu, Zhang, et al., 2011)	Motor oil	149	No
	Peanut oil	119	
	Diesel	81	
Butyl rubber (Ceylan et al., 2009)	Crude oil	23	No
	Diesel	20	
Wool (Paulauskiene & Research, 2018)	Crude oil	9	Yes
	Diesel	6	
Silkworm cocoon waste (Moriwaki et al., 2009)	Motor oil	52	Yes
	Vegetable oil	60	
Kapok fiber (Ali, El-Harbawi, Jabal, & Yin, 2012)	Diesel oil	19	Yes
Raw cotton (Singh, Kendall, Hake, Ramkumar, & Research, 2013)	Crude oil	30.5	Yes
Waste tyres (B. Wu & Zhou, 2009)	Crude oil	24.0	Yes

2.3.4 Selection criteria

Many factors which also influence the efficiency of oil sorbent should be taken in account. The important criteria are wettability, capacity and reusability.

2.3.4.1 Wettability

Oil-removing materials are special wettable surface materials that are attributed to their unique hydrophobic and oleophilic properties. These characteristics provides high oil/water separation efficiency in the oil spill cleanup process. The wettability of sorbent materials is controlled by their chemical composition and topographical structure and also surface energy (Xue, Cao, Liu, Feng, & Jiang, 2014). Hydrophobic property enhances corrosion resistance, water proof capability and stability against organic and inorganic pollutants. This property is defined by two factors. There are the degree of wettability which is commonly known in terms of contact angle, and the surface free energy. The apparent water contact angle described by Yong's equation relating to the solid-vapor, solid-liquid and liquid-vapor surface tension (Darmanin & Guittard, 2015). If the liquid droplet spreads with a large area on the solid surface, the solid sorbents are considered as a hydrophilic material. Whereas, the contact angle of liquid droplet is greater than 90 degree, the materials mention to hydrophobic material. The materials have the contact angle over than 150 degree, they are characterized as superhydrophobic materials (Doshi, Sillanpää, & Kalliola, 2018). The degree of contact angle (θ) increases with the decrease of the solid-vapor interface free energy. In addition, the roughness factor affects the wettability of a smooth solid surface. The increase of surface roughness reduces the degree of contact angle because the solid surface is filled with air rather than liquid. Therefore, a good oil sorbent material composes of low surface energy and suitable roughness (Ge et al., 2016). However, the number of natural sorbents exhibit low contact angle due to their associated hydroxyl functionalities. These groups are extremely available in natural materials, responsible for their hydrophilicity (Joseph O Nwadiogbu, Okoye, Ajiwe, &

Nnaji, 2014). The improved hydrophobic and oleophilic properties of oil sorbent materials remarkably enhance oil sorption ability, with a strong decrease of water sorption. The hydrophobic-oleophilic characteristics influence the amount of the surface wax, corresponding to the buoyancy of the material. Natural sorbents including inorganic and organic materials have poor buoyancy and tend to sink in the bottom that may risk to depth-aquatic life and persist in the sediment. Therefore, buoyancy can exhibit the oil adsorption performance of a sorbent. A good buoyant sorbent may present long and branched hydrocarbon chains (Abdullah, Rahmah, & Man, 2010; Wahi, Chuah, Choong, Ngaini, & Nourouzi, 2013).

2.3.4.2 Sorption capacity

The capacity and rate of oil sorption powerfully hinge on the accessible active surface. The surface morphology, surface area and pore size are main the factors affect the oil sorption capacity of sorbent materials. Some natural sorbents displayed excellent oil sorption and retention capacity due to their hallow structure. Kapok fiber is a representative material with hollow structure, and it was reported to make up 80-90% adsorption efficiency of the fiber volume (Dong, Xu, & Wang, 2015). This kind structure causes the high performance for oil capturing within their empty lumens. The surface modification generally changes the available surface area of sorbents, resulting in affects oil sorption capacity (Wahi et al., 2013). The sorbent structure with high surface roughness provides more active sites for oil adsorption rather than smooth surfaces. Not only active surface sites affect oil sorption efficiency, but also pore size of sorbents. The big pore size of sorbents decreases oil sorption efficiency, but small pore size enhances oil sorption efficiency because oil droplets are completely captured in the pore. The small pore size synergistically stimulates the capturing of oil droplets depending on the viscosity of oils. When the spilled oil is more viscous, small pore size becomes obstructed the oil distribution and reduced oil sorption capacity (Nishi, Iwashita, Sawada, & Inagaki, 2002). Therefore, the surface

morphology affects the area of oil capturing in the oil separation process (Bansal, von Arnim, Stegmaier, & Planck, 2011; Gupta & Tai, 2016).

2.3.4.3 Reusability

Nowadays, the recyclability of a sorbent becomes an important criteria for sorption process. The reusability refers to the ability for a sorbet to be reused that minimizes the total amount of waste generation for disposal and decrease the cost of oil spill cleanup. After oil picked up, all used sorbents are ultimately disposed in landfill or incinerator. The unrecoverable sorbents dramatically need a large area for disposal, resulting in undesirable environmental qualities. The reusability of sorbents can recover the spilled oil from the materials. The possibility to recover the spilled oil and recyclability of sorbents are definitely the sustainable of environmental and economic points. Moreover, the biodegradability of sorbents is one of the interesting factors. If the sorbent materials are difficult to recover, the environmentally safe and biodegradable are concerned (Doshi et al., 2018; Ge et al., 2016).

2.4 Natural rubber (NR)

NR is an important natural resource and tends to use a wide verity application. The large amount of rubber needed in the military, industrial, transportation, medical and consumer sectors has led to NR being repeatedly defined as a strategic raw material over the last decade. The manufacture of rubber tires is a significant sector consumed a lot of NR (Puskas, Chiang, & Barkakaty, 2014; Warren-Thomas, Dolman, & Edwards, 2015). More than 2,500 plant species can produce the rubber latex, for example *Heavea brasiliensis*, *Parthenium argentatum*, *Taraxcum kok-saghy*, *Lactuca sativa*, *Ficus elatica* and *Helianhus annuus* (Cornish, 2014). The rubber tree is mostly grown in the tropical regions of Asia such as Malaysia, Indonesia, Thailand, Philippines and Myanmar (K. P. Nair, 2010). However, NR latex can get from *H. brasiliensis* by

trapping. In only one important commercial source. The trapping is usually done once every 2-3 days for 9 months each year (Sakdapipanich & Rojruthai, 2012) A cut, about 22° to horizontal, is made into the bark of the tree cutting the latex vessels nearby. The latex exuding from the cut follows a vertical channel at the lower end of the cut into a small ceramic or glass cup in the cutting process a small portion of the bark is excised. The latex flows for 4 h and then coagulation and drying can generate a high molecular weight polymer (Mn > 1 million g/mol) (Ciesielski, 1999). The chemical structure of NR shows the isoprene repeat units with double bond connection in *cis*-1,4 configuration (Figure. 2.3). The molecular weight (Mn) of NR is 10^5-10^6 g/mol with very broad molecular weight distribution (Mw/Mn =2-15) (Cornish, 2014). Not only isoprene monomer composes of NR, but also includes non-rubber components, especially, proteins. The proteins containing in NR latex can severe allergic response in a small percentage of the population and among medical professional following extension exposure (Arayapranee, 2012).

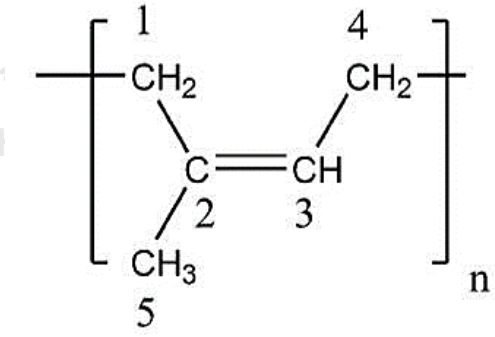

Figure 2.3 The chemical structure of cis-1,4-polyisoprene (Barlow, 1988).

2.4.1 Biochemistry of latex

NR latex contains both rubber and non-rubber particles in an aqueous serum. The non-rubber components are carbohydrates, proteins, lipids, inorganic salt and other minor substances. The main component in latex is rubber particles, which

is 30-40% of volume (Ciesielski, 1999). Table 2.4 shows the typical components of NR latex (Sentheshanmuganathan, Yapa, Nadarajah, & Kasinathan, 1975). The latex particle size is ranging from 0.05 to 3 μm with a spherical shape. The collected latex is treated with formic acid and transfers into a consolidated rubber particle. Then, the solid rubber is pressed into thin crepe sheets and it is called air-dried sheet (ADS) or ribbed smoked sheet (RSS) (Sakdapipanich & Rojruthai, 2012). As a result of proteins and lipids containing in latex, the surface of rubber particles has a negative charge and causes the latex stability. Although, proteins are a significant component corresponding to the characteristic of NR and an allergic response (Arayapranee, 2012). Besides the mechanical properties of NR relate to the chain connection and the crystallization of NR. The rubber chain composes of long-chain fatty acids (e.g. stearic, oleic and linoleic acids) and phospholipids covalently links to the end-chain. The long-chain fatty acids refer to both saturated and unsaturated fatty acids. The saturated fatty acids make the crystallization of rubber chain, whereas, the unsaturated acids stimulate synergistically of the crystallization process. The structure of chain-end groups relate to control the major properties of NR. The specific weight of fresh NR latex is 0.96 – 0.98 g cm^{-3} and its pH is varying within 6.5 – 7.0 (Brydson, 1978). The NR latex can transform into high quality latex concentrate of 60% dry rubber content (DRC) by several processes (e.g. evaporation, electro-decantation, creaming and centrifugation) (K. P. Nair, 2010). This process separates the latex into two fractions: the concentrated more than 60% dry rubber and the other containing 4-6% dry rubber. Centrifuged latex is today available commercially in two different varieties with high ammonia (max. 0.7% of ammonia) and low ammonia (max. 0.3% of ammonia). For long-term preservation, the ammonia content is added up to 0.6-0.7% to maintain the latex concentration.

Table 2.3 The typical composition of NR latex.

Composition	Content (% by weight)
Water	58.7
Rubber compound	35.0
Neutral lipids	2.4
Proteins	2.2
Glycolipids and phospholipids	1.0
Carbohydrate	0.4
Ash	0.2
Other compounds	0.1

2.4.2 Properties of NR

Vulcanized NR is an important material in the rubber industry due to its excellent physical properties. Additionally, NR is considered a renewable resource and an environmental friendly. The general properties of NR were summarized in Table 2.5. Vulcanized products made from NR have high mechanical strength and can be compounded to have high elasticity. NR has very good abrasion resistance and dynamic mechanical properties, thus it is an important material for the manufacture of rubber tires. The mechanical properties of NR depend on chain structure and temperatures. The high molecular weight of rubber causes the NR tends to crystallize spontaneously at low temperatures or when it is stretched. The crystallization of NR can reverse by warming. The crystallization process affects resilience, tear, tensile strength, abrasion and also low heat build-up. Although, NR has some undesirable properties such as low flame resistance, poor aging properties, low heat degradation and also low oil resistance. These defects result from the high unsaturation of the molecular chain and the non-polar character of NR. Moreover, weather conditions, such as UV light and ozone, also affect elastomer of NR. Therefore, several processes

have been reported to overcome its limitation including the adjustment of the NR compounding formulation, chemical modification and blending with other materials (Phinyocheep, 2014).

Table 2.4 The general properties of NR

Properties	Value
Specific gravity	0.93
Refractive index (20°C)	1.52
Coefficient of cubical expansion	0.00062/ °C
Cohesive energy density	63.7 cal/cc.
Heat of combustion	10,700 cal/g
Thermal conductivity	0.00032 cal/sec/cm^3/ °C
Dielectirc constant	2.37
Volume resistivity	10^{15}-10^{19} ohms/cc.
Dielectric strength	1000 V/mm.

2.4.3 Improvement of NR

Studied on the physical and chemical development of NR have resulted in many modified forms suitable for specific processes and applications. Therefore, the two major approaches including chemical modification and other material blending have been reported to improve the physical and chemical of NR.

2.4.3.1 Chemical modification

Chemical modification of polymer is an interesting method for improving the physical and chemical characteristics of both synthetic and natural polymers. The extensive applications of NR can be achieved through chemical modification. For example viscosity-stabilizer rubber, thermoplastic NR, oil-extended

NR, epoxidized NR, graft polymer, chlorinated rubber and liquid NR (K. P. Nair, 2010). This process has generally followed two purposes correlating with improving undesirable properties and transforming into new polymeric materials. Although, the chemical process of NR can occur under various conditions, environmentally friendly conditions for NR modification become interesting. The modified reaction of NR can be categorized into three main parts. There are the transformation of rubber structure, the modification of carbon-carbon double bond and the grafting with different polymer chain. The NR structure is transformed through the addition of acidic reagents, thermal treatment and degradation (Riyajan & Sakdapipanich, 2006; Van Veersen & Technology, 1951) The double bond modification refers to halogenation, hydrogenation and epoxidation reactions (Roberts, 1988) Another modification of NR is grafted with various polymer types such as maleic anhydride (maleinization) and vinyl monomers (graft copolymerization) (Bacon, Farmer, & Technology, 1939). Each technique causes different properties of NR, for instance, the hydrogenation reaction enhanced thermal stability of NR. Chlorinated rubber is developed for chemical resistance, anti-corrosive and heat resistance. The epoxidation method improved resistance to hydrocarbon, which enhanced the polarity of NR, and low air permeability. Additionally, NR could transform into a thermoplastic character by the graft copolymerization (Phinyocheep, 2014).

2.4.3.2 Rubber composites

The properties of a single rubber can develop by rubber composite method which combine two or more materials together. The rubber composite does not provide a homogenous material due to the different properties of the components. However, the new material exhibits unique properties with the overall properties being better than the individual material. Composite materials are usually classified by the type of material used for the matrix (Zweben, 2014). The characteristics of rubber composite are dependent on the content, structure and

particle size of filler (Arayapranee, 2012). The fillers always use in polymer composites can be divided into reinforcing and non-reinforcing fillers. The filler obtained by grinding or minerals is mentioned as non-reinforcing fillers due to their big particle. For filler reinforcement, the interaction between the filler particles and polymer is strong corresponding to the covalent bond between functional groups on the filler surface and polymer. To prepare composite materials, well mixing is required to reduce non-uniformity of the compound. To control the specified and acceptable properties of the rubber composite, some additives are blended to achieve a good combination of filler and rubber compound (Poompradub, 2014). Carbon black and fiber are two common fillers used to reinforce rubbers. The interaction of carbon black and rubber is considered as chemical bonding. There describe a van der Waals force between carbon and rubber, chemical crosslink on the carbon surface or mechanical interlocking of rubber chain (Donnet & Custodero, 2005; Hariwongsanupab, 2017). The schematic of carbon black reinforced in rubber shows in Figure 2.4 Fiber reinforcement presents the improvement of physical rather than chemical properties, in contrast, adhesion of the composite materials reduces (A. Nair & Joseph, 2014).

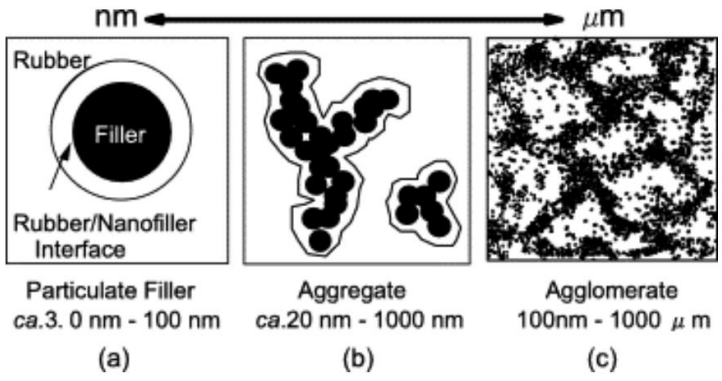

Figure 2.4 Schematic representation of carbon black reinforced rubber (Hariwongsanupab, 2017).

Recently, nanocomposites have been studied to open a new and interesting area of material science. The considered aspects directly relate to the

degree of filler dispersion and filler loading in the polymer matrix. Nano graphite and its derivatives (expanded graphite or exfoliated graphite) have been improved physicochemical properties to produce conducting nanocomposites. Several studied reported expanded and exfoliated graphite composites based on a range of polymer such as epoxy (Jing Li, Sham, Kim, Marom, & Technology, 2007). polypropylene (Kalaitzidou, Fukushima, Drzal, & Manufacturing, 2007).polystyrene (Xiao, Sun, Liu, Li, & Gong, 2002)., etc. The advantages of these nanocomposites are the enhancement in the mechanical characteristics and electrical conductivity. Many factors affect the interaction of polymer/nanocomposites such as, the polarity, molecular weight, hydrophobicity, reactive groups, etc. (Ayalew, Gonte, & Balasubramanian, 2012; Kuilla et al., 2010) produced polymer composite beads from sugarcane molasses and cellulose for dry sorption capacity. The resulting polymer composite beads exhibited 84.83% and 81.71% adsorption efficiency for blue and yellow dyes, respectively, after an exposure time of 150 min at 25 °C. NR composites are new kind materials that have been studied to enhance the physical properties and the sorption ability by adding reinforced fillers, such as silica, zeolite, graphene, etc. The filler materials greatly affect the physicochemical and chemical properties of the NR composite. Perera et al. (2015) prepared the NR composite with zeolite to enhance ammonia and carbon dioxide adsorption. The result showed that zeolite incorporated NR latex foam had higher capacity to adsorb inorganic gas, compared with the conventional NR latex foam (Perera, Kumanayaka, & Walpalage, 2015). Jobish and Johns & Rao (2011) used NR/ chitosan blends as an adsorbent material to remove methylene blue from aqueous solution. In addition, this study showed that maleic anhydride significantly improved the tensile strength, elongation at break, Young's modulus and thermal stability of NR/CS vulcanization (Johns & Rao, 2011). The biggest advantage of composite materials is a new material, stronger material and flexibility material.

2.5 Graphene

Carbon-based materials have long been an interesting topic in many branches of technologies including environmental remediation. The hydrophobic surface and non-toxicity of carbon materials are an important properties for environmental applications (Gupta & Tai, 2016; Sweetman et al., 2017). Activated carbon (National Academies of Sciences & Medicine) is normally used for water purification and toxin removal. In recent times, carbon-based nanoparticles (e.g. nanondiamond, fullerenes, carbon nanotubes (CNTs), graphite nanofiber and graphene) have been developed for high-performance water purification (Wang, Liu, Lu, & Qu, 2014). These materials showed an effective adsorption strategy for removing contaminants. Since graphene was discovered, it opens a new direction in the field of materials science due to its structure feature. Graphene is considered as one of the greatest smart materials in terms of environmental protection. Additionally, the discovery of nanocomposites, which mostly used inorganic nanopraticles as fillers, played a key role in material science and technology. The interesting aspects of nanocomposites are their unique properties and numerous potential applications. Gaphene and graphene-based composites show the largely potential applications owing to their distinctive two-dimensional assembly and related band structure (Gandhi, Vasudevan, Shibayama, & Yamada, 2016; Kemp et al., 2013). Graphene can be used as a filler in composite materials and its composite shows superior mechanical, thermal, gas barrier, electrical and flame retardant properties. Therefore, graphene and its composites are widely applied in sensor, transistors, electronics, photonics, bioengineering, energy production and storage.

2.5.1 Graphene structure

Graphene refers to a single atomic layer of sp^2 two-dimensional (2D) hybridized carbon atoms arranged in a honeycomb structure, which is identified as the simplest form of carbon (Figure 2.5). The honeycomb networks are a fundamental

structure of other carbon allotropes including fullerenes, carbon nanotube and graphite. The rolling up of the honeycomb network can form into a sphere which is a zero-dimensional, calls fullerene. When it is formed with a one-dimensional cylindrical structure that knows as carbon nanotubes. Moreover, the single layers can be formed in 3-dimensional and bound by a weak van der Waals force which refer to graphite as shown in Figure 2.6 (Allen, 1988; Jianchang Li, Zeng, Ren, & Van Der Heide, 2014). Graphene has gained attention due to its theoretical properties including specific surface area (2630 m^2g^{-1}), high conductivity at room temperature (106 s cm^{-1}), fracture strength (125 GPa), breaking strength (42 N m^{-1}), high intrinsic mobility (200,000 cm^2 $v^{-1}s^{-1}$), high Young's modulus (1.0 TPa), high carried density (10^{12} cm^{-2}), thermal conductivity (5,000 $Wm^{-1}K^{-1}$), high optical transmittance (97.7%), specific mechanism and chemical stability (Chabot et al., 2014; Gandhi et al., 2016). These unique characteristics of graphene are beneficial to several fields of technology, such as catalyst engineering, chemical sensor, biosensor, thin film transistor, composite materials, water purification and absorption of non-aqueous liquid (M. Aunkor, I. Mahbubul, R. Saidur, & H. J. R. A. Metselaar, 2016) In recent years, several techniques to synthesize graphene sheets have been developed that can be divided into two approaches, e.g. top-down and bottom-up methods. (Bhuyan, Uddin, Islam, Bipasha, & Hossain, 2016; Tour, 2013). An overview of the graphene synthesis techniques is shown in the flow chart in Figure 2.7.

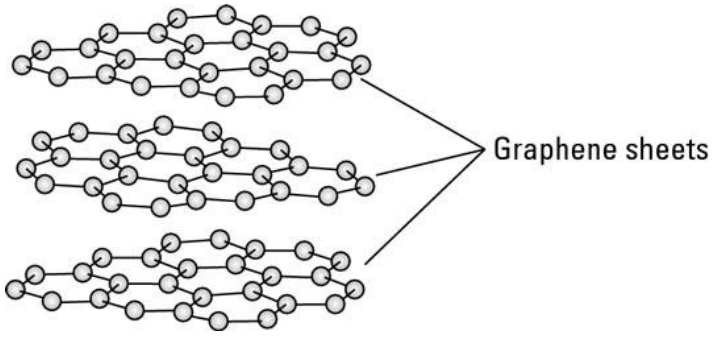

Figure 2.5 The single carbon layer of graphene (Boysen & Nancy, 2009).

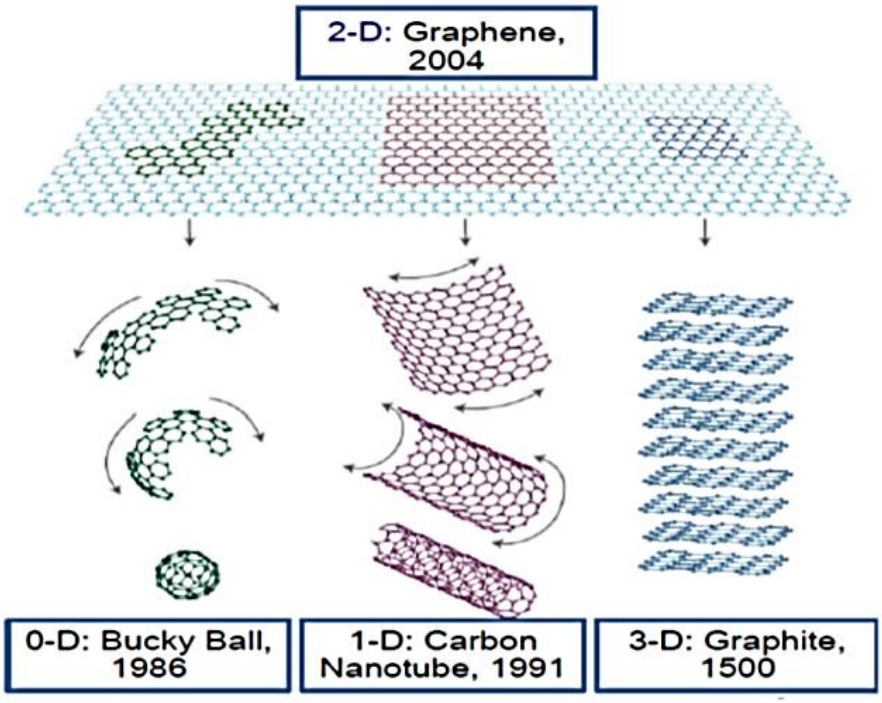

Figure 2.6 The various forms of graphene structure (Bhuyan et al., 2016).

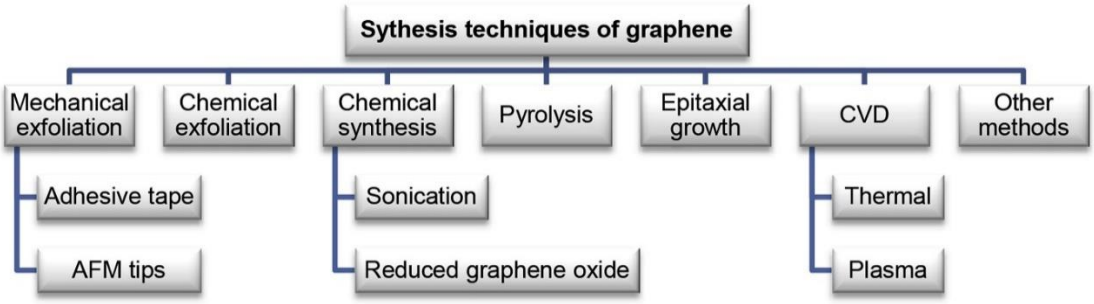

Figure 2.7 Graphene synthesis techniques (Mohan, Lau, Hui, & Bhattacharyya, 2018).

2.5.2 Synthesis of graphene

Synthesis of graphene refers to any process for fabricating or extracting graphene, depending on the desires size, purity and efflorescence of the specific product. In 2004, graphene was isolated from graphite through mechanical exfoliation using scotch tape (Allen, 1988; Yi & Shen, 2015). Although this technique gives the highest quality graphene, this method is not suitable to prepare graphene sheet in

large scale. Recently, the number of approaches has been designed for synthesis graphene sheet that commonly categorize into two primary methods as shown in Figure 2.8. The fabrications of graphene can be achieved by the separation of graphite structure into individual graphene sheets. This technique is referred to the top-down processes (Ltd.) (Shams, Zhang, & Zhu, 2015; Tour, 2013). The TD processes are widely used to synthesize graphene, including mechanical exfoliation, super acid dissolution of graphite, electrochemical exfoliation, chemical exfoliation etc., due to their simple techniques, mass produced and inexpensive. Some limitations of top-down processes are surface defects, re-agglomerating after separation and low yields. (Behabtu et al., 2010). Another technique refers to bottom-up methods (BU) that implement carbon molecules as building blocks. The BU approaches, which are grown from metal-carbon melts, epitaxial growth on silicon carbide (SiC) and chemical vapor deposition (CVD), are not suitable for the production of graphene sheets with large surface area. Moreover, the most significant deficiency in BU fabrications is the limitation in placement of the device structure (Shams et al., 2015; Tour, 2013). Therefore, this research summarized the general method of graphene synthesis, including chemical vapor deposition, mechanical exfoliation and chemical exfoliation.

Figure 2.8 Schematic showing top-down and bottom-up graphene synthesis approaches (Chaitoglou, 2016).

2.5.2.1 Chemical vapor deposition (CVD)

Chemical vapor deposition describes a chemical process that molecules are heated and changed to a gaseous state and is known as precursors. The gaseous state of molecules deposits on transition-metal substrates makes high-quality graphene. This technique has been reported to produce thin graphene films (≤ 75 cm) that are appropriable for use in applications (e.g. touch screens, smart windows, solar cells, etc.). This process requires three main components including a metal catalyst, a carbon precursor and high temperature around 1000 ^{o}C within a controlled atmosphere (Chabot et al., 2014). The first synthesis graphene by CVD was achieved on nickel (Ni) substrate. This procedure showed multiple folds and estimated approximately 35 layers of graphene sheets (W. Choi, Lahiri, Seelaboyina, Kang, & Sciences, 2010). Deposition of the single graphene layer was produced on platinum (Sakthivel, Reid, Goldstein, Hench, & Seal). This approach not only synthesized thin graphene films, but also improved these properties. With this treatment, graphene with little or no defects can be obtained having the low degree of crystallinity (I_D/I_G) as 0.22 (Shams et al., 2015). CVD has confirmed the reproducibility of high quality graphene for various applications, especially energy technologies. Using the CVD technique, the synthesized graphene materials often have a thickness distribution between 1-10 layers, which depends on the synthesis quality. Furthermore, the CVD process can be divided into various types: thermal, plasma enhanced (PECVD), cold wall, hot wall, and reactive. These types are dependent on the material quality, precursors, and the width and the structure. CVD method is favorable for future complementary metal-oxide semiconductor (CMOS) technology by replacing Si. However, the important disadvantage of this method is the need of expensive substrate materials for graphene growth, considerably limiting its applications for large-scale production (Bhuyan et al., 2016; Zheng & Kim, 2015).

2.5.2.2 Mechanical exfoliation

Graphite and its derivatives (graphite oxide (GO) and graphite fluoride (GF)) essentially uses to produce graphene. The construction of graphite is built from mono-atomic graphene layers that are stacked together by weak van der Waals forces. In graphite structure, stacking of sheets is the result of overlap of partially filled p_z or $\boldsymbol{\pi}$ orbital perpendicular to the plane of the sheet involving van der Waals forces (Gong, 2011). Thus, graphene is possible to produce, if these bonds can be broken. Within the TD concept, mechanical exfoliation is an ideal case that graphene can be peeled from graphite layer into single-layer or few-layer. The interlayer distance and interlayer bond energy is 3.34 Å and 2 eV/ nm^2, respectively. In general, there are two kinds of mechanical routes to exfoliate graphite into graphene sheet, e.g. normal force and lateral force as shown in Figure 2.9 (Novoselov et al., 2004). One can exert normal force to overcome the van der Waals attraction when peeling two graphite layers apart, such as micromechanical cleavage by Scotch tape. For mechanical cleaving, 300 nN/lm^2 external force is required to separate each mono-atomic layer of graphite (Zheng & Kim, 2015). However the exfoliation can prepare graphene without some defect, this method is not suitable to obtain larger amounts of graphene. Moreover, this method is extremely labor-intensive and time consuming. It is limited to laboratory research and seems impossible to scale up for industrial production (M. Aunkor et al., 2016; Bhuyan et al., 2016; Yi & Shen, 2015).

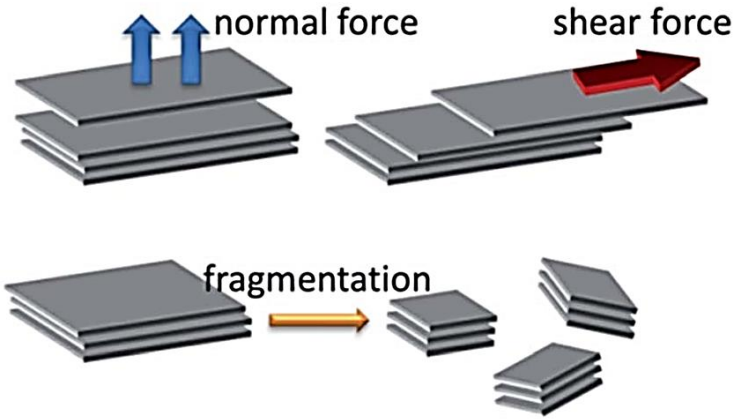

Figure 2.9 Two kinds of mechanical exfoliation routes from graphite into graphene flakes (Yi & Shen, 2015).

2.5.2.3 Chemical synthesis

Chemical method is one of the best appropriate methods for graphene synthesis that is a two-step process (Figure. 2.10). The first process is the reduction of van der Waals forces which expands the interlayer space and the exfoliation which separates into few layers by rapid heating or sonication. To expand the interlayer of graphene, the oxidation of graphite with strong oxidizing agents has been reported by Hummer (Hummers Jr & Offeman, 1958) using potassium permanganate ($KMnO_4$) and sodium nitrate ($NaNO_3$) in acidic condition (sulfuric acid or phosphoric acid). Thus, each layer of graphite can be exfoliated by rapid heating or sonication to few layers. The exfoliation by ultrasonication is followed by a dimethylformamide (DMF)/water (9:1) or water. The oxidation reaction can increase the interlayer spacing from 3.7 to 9.5 °A. Nevertheless, the oxidation process produces oxygen functional group into graphene sheet. As a result, the reduction process is required to remove oxygen-functional groups and obtain graphene-like properties (Bhuyan et al., 2016).

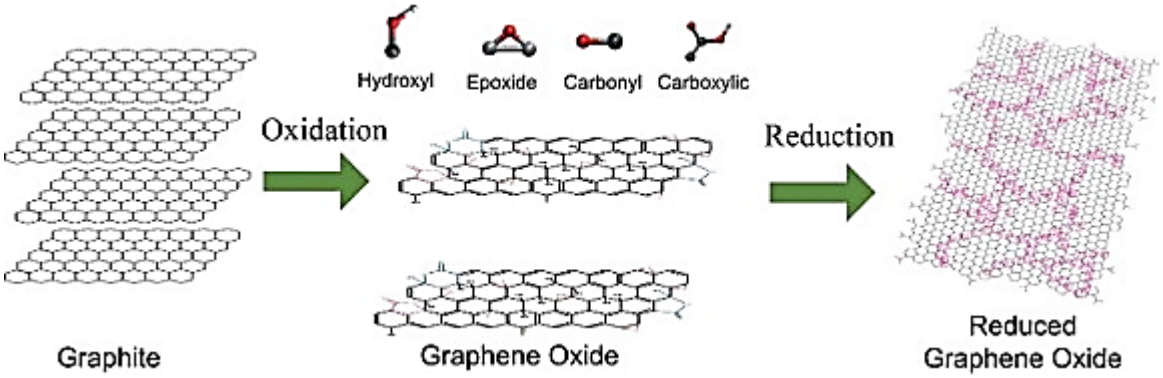

Figure 2.10 Chemical synthesis pathway of grapene (Phiri, Gane, Maloney, & B, 2017).

After oxidation process, the chemical structure of graphite composed many oxygen functional groups. The transformation of graphene oxide to graphene is often indicated by a color change of the reaction mixture from yellow-brown to black, and an increase of hydrophobicity of the material as a result of the removal of oxygen containing groups (Hou et al., 2018). Graphene was synthesized by chemical method still has some defect, hence, it can be called as partially reduced exfoliation graphite oxide sheets or reduced graphene oxide. Reduction of graphene oxide can be prepared through chemical, thermal or electrochemical reduction pathway (Rao, Maitra, Matte, GmbH, & Co. KGaA: Weinheim, 2012). The chemical reduction is considered as the easiest techniques to synthesis graphene with large scale. This process is dictated by the energy required to exfoliate graphite into single-layer graphene. Moreover, the solven-graphene interaction involves complete graphite exfoliation. The liquid based exfoliation of graphite in organic solvent is successful produced in large-scale production (W. Choi et al., 2010). While chemical methods can make graphene at low temperature and cost, obtained graphene contains lots of surface defects. This limitation led to poor electrical properties of graphene (M. Aunkor et al., 2016). The synthesized graphene can be applied in conductive inks and paints, polymer fillers, battery electrodes, supercapacitors, sensor, etc. (Shams et al., 2015). Hydrazine monohydrate is firstly used as reducing agent, however, it is a highly toxic

and potentially explosive chemical. Therefore, the production in large scale should be avoided this chemical (Fernández-Merino et al., 2010). In recent year, green reducing agents have been widely used for synthesis graphene sheet due to it is eco-friendly, easy, and scalable preparation of graphene. The alternative chemicals have been introduced as green reducing agents include organic acids, plant extracts, microorganisms, sugars, antioxidants, amino acids and proteins, etc. (De Silva, Huang, Joshi, & Yoshimura, 2017).

a) Protein

Proteins are large biomolecules consisting of one or more long chain of amino acid residues. The different form of proteins can be used as reductant for reducing GO. Ma et al. (2013) prepared composite material foam of rGO and carboxymethyl starch (CMS) which used L-lysine as a reductant. The results indicated that the reaction temperature, pH and GO/L-lysine ratio affected the reduction of GO. Moreover, glycine was used to synthesis rGO under mild conditions that was done by Bose et al. (2012). The results showed high carbon/oxygen atomic ratio of 11.24. The amine group of glycine could effectively undergo covalent interaction with GO and under refluxing conditions it could reduce GO successfully to produce graphene. Glycine can participate not only as a chemical functionalizer but also used as a reducing agent. Wang et al. (2017) described the reduction of GO using alanine (ALA) with the temperature at 85 °C for 24 has shown in Figure 2.11. ALA is an aliphatic amino acid, a simple molecule which consists of the backbone of the amino acid structure with a methyl group attached as a side chain. These results showed the successful reduction of GO to rGO without using any stabilizer or alkaline medium. Another green reductant of amino group was done by Tran et al. (2014). They reported the synthesis rGO method using non-aromatic and thiol-free amino acids as the reductant. The control of reduction time was possible to achieve rGO with different

densities of oxygen groups. The mechanism of the GO reduction process was proposed to involve the polymerization of amino acid.

Figure 2.11 The reduction of GO using alanine for 24 h (Wang et al., 2014).

b) Sugar

Sugar and polysaccharide have been studied for GO reduction. These chemicals have the ability to act as a reducing agent as well as a stabilizing agent, thereby resulting in more stable rGO dispersions (De Silva et al., 2017) reported that glucose, fructose and sucrose could be used as reducing agent of GO. The reduction of GO using glucose provided a green and facile method to produce high-quality rGO in comparison with other saccharides, such as D-fructose and sucrose, under the same condition. The aldonic acid, glucose oxidizing form, can further be converted into lactone. Thus, the oxidized products can form H-bonds with the residual functionalities on the rGO surfaces as shown in Figure 2.12. Abdolmaleki et al. (2017) studied the modification of rGO by glucose through covalent functionalization on nanocomposite. The rGO was functionalized with glucose to achieve good dispersion in the polymer matrix. As a result of increasing rGO content, the tensile strength, Young's modulus and thermal stability of composite polymer increased. Furthermore, a comparative of green chemical reductants, L-ascorbic acid (L-AA), D-

glucose and tea polyphenol (TP) was reported by Xu et al. (2015). The results showed that all these reductants were effective to synthesis rGO and to restore the electrical conductivity of rGO. Accordingly, L- AA plays the highest electrical conductivity compared to other reductants.

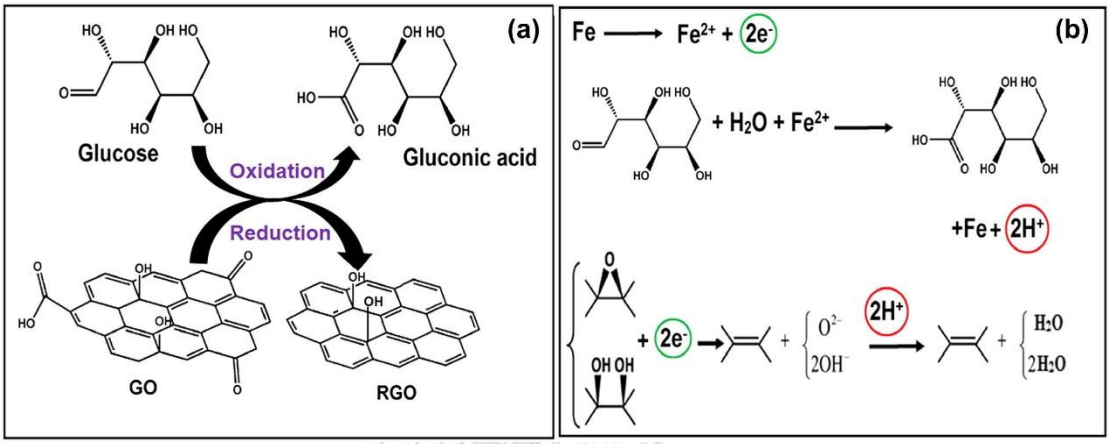

Figure 2.12 Proposed reduction mechanism using (a) glucose and (b) glucose in the presence of Fe foil (Thakur, S., & Karak, N. (2015).

c) Organic acids

Various organic acids are widely used to synthesize rGO. Bo et al. (2014) studied using caffeic acid for rGO preparation. Caffeic acid is one of the most predominant hydroxycinnamic acids that its chemical structure described as two adjacent hydroxyl groups on an aromatic ring attached to the highly conjugated propenoic side chain. The rGO proved to have high a C/O ratio (7.15) and a low oxygen content that this material showed appropriate properties for gas sensor. Gallic acid is another reducing agent which has been used to synthesize rGO (Li et al., 2013). There are three adjacent hydroxy groups on its only benzene ring and thus it might show considerable reducibility. Song et al. (2012) reported the synthesis of rGO using oxalic acid as reducing agent was successfully prepared from GO at 75 °C for 18 h. Furthermore, a Pt-graphene composite was fabricated on a glassy carbon electrode

and excellent electro catalytic activity towards methanol oxidation was observed. With advantages of low toxicity, simple purification process and high quality of the product, several organic acids provide a feasible to prepare rGO. All these green reductants as described previously, L-ascorbic acid (L-AA) shows great interesting due to its high potential of oxygen removal.

L-AA is a ubiquitous organic material with the chemical formula of (2R)-2-[(1S)-1,2-dihydroxyethyl]-3,4-dihydroxy-2H-furan-5-one, and with a molecular weight of 176.12 g/mol (De Silva et al., 2017). L-AA is not only applied as a food additive, but also undergo many chemical reactions including methylation, acid catalyzed esterification and oxidation (Davies, Partridge, & Austin, 2007). Recently, this chemical has been reported as a powerful reducing agent in aqueous solutions including rGO synthesis. L-AA can be replaced hydrazine due to its eco-friendly, low cost, and more stable rGO dispersions in water as shown in Figure 2.13. (Pei & Cheng, 2012). This stability could be achieved by guluronic acid or oxalic acid, which is an oxide form of AA. The interaction of H-bonds and the residual oxygen functionalities might disrupt the **π**-**π** stacking between rGO sheets, thereby preventing the agglomeration of residual oxygen functionalities (De Silva et al., 2017). The rGO stable suspension can be prepared in common organic solvents such as; *N,N*-dimethylformamind (DMF) or *N*-methyl-pyrrolidone (NMP) (Fernández-Merino et al., 2010). There are few factors relative the reduction rate of GO such as pH of the medium, GO and L-AA concentration, reduction temperature and the power of stirring or sonication. Accordingly, high ultrasound power, high temperature, high pH value and large amount of L-AA increase the rate of reduction.

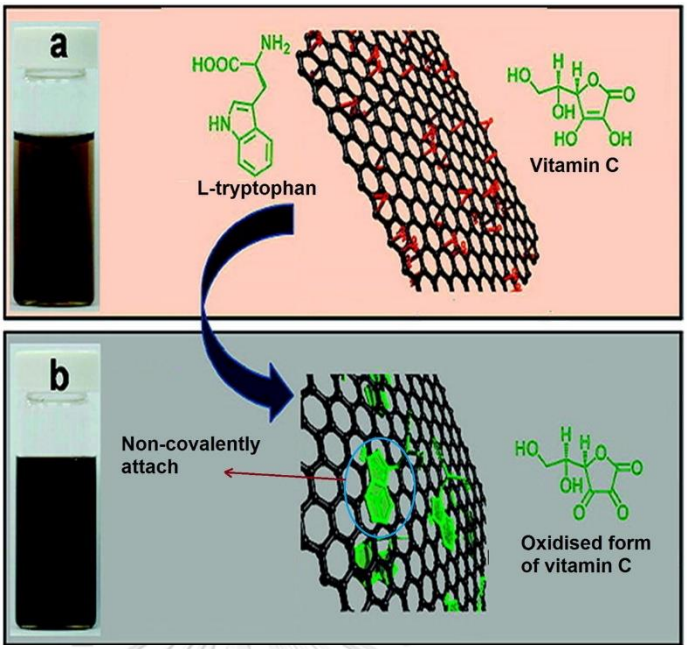

Figure 2.13 Schematic illustration of the reduction process, including photographs of (a) the graphite oxide aqueous solution and (b) the stably dispersed rGO aqueous dispersion (Thakur & Karak, 2015).

The mechanism for the chemical reduction of graphene oxide can be speculated as two-step S_N2 nucleophilic reactions followed by one step of thermal elimination. The electron withdrawing five-membered ring of L-AA makes the hydroxyls more acidic, so L-AA is ready to dissociate two protons, functioning as a nucleophile. The graphene oxide contains mainly two types of reactive species including epoxide and hydroxyl. In the case of epoxide, it could be opened by the oxygen anion of L-AA ($HOAO^-$) with a S_N2 nucleophilic attack. The reduction is followed by a back-side S_N2 nucleophilic attack with release of H_2O, resulting in the formation of an intermediate. Finally, the intermediate undergoes a thermal elimination, leading to formation of the rGO. The L-AA is oxidized into dehydroascorbic acid. The reduction of hydroxyls is similar to the case of epoxide. The hydroxyls can be displaced by the oxygen anions of L-AA ($^-OAO^-$) with a back-side S_N2 nucleophilic attack twice, which are

subsequently reduced further by thermal elimination as shown in Figure 2.14 (Gao et al., 2010).

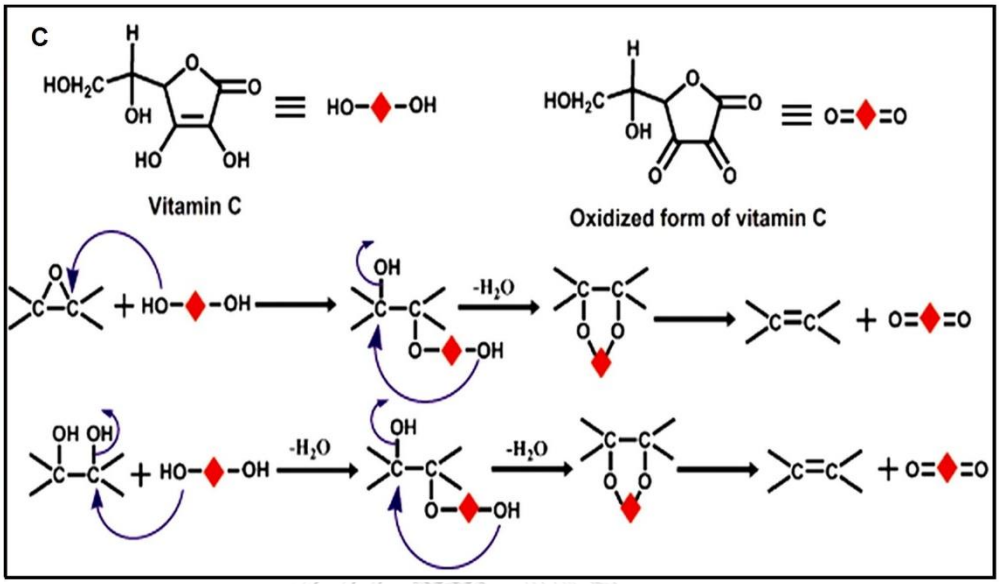

Figure 2.14 The reaction pathway for the chemical reduction of graphite oxide with L-AA (Thakur & Karak, 2015).

2.5.3 Polymer/graphene composites

Carbon-based polymer nanocomposites has been interesting over the past 20 years due to their special properties. Different carbon types can be used as filler in polymer composites, especially graphite and its derivatives. Graphene shows exceptionally good mechanical, thermal and electrical properties has been extensively used as filler in composites. Many researchers studied the effect of graphene filler based on a range of polymers for physical-chemical property development (Kuilla et al., 2010). The fillers can be formed as an agglomerate, intercalated or exfoliated structure in polymer matrix as shown in Figure 2.15. If the fillers cannot be miscible in polymer, it acts like a micro-material structure. When the polymer chains can penetrate between the filler structure, it refers to an intercalated structure. The exfoliated structure of fillers means the filler particles thoroughly detaches from each

other (Akbari, Talebanfard, Hassan, & Engineering, 2010). The properties of polymer/graphene composites depend on filler dispersion, filler and matrix bonding, filler loading, graphene quality and polymer matrix. The interaction between polymer and fillers is a fundamental factor of composites properties that depends on the polarity, hydrophobicity, molecular weight, reactive groups, etc. The different behaviors of composite materials result from the interfacial action that refer to the compatibility and adhesion of the filler in polymer matrix. The atomic and molecular bonding of graphene causes weak intermolecular forces between filler and polymer, resulting in low interfacial bond strength of polymer composites. Besides the wetting behavior of filler also affects the interaction of composite. The covalent bond of polymer molecules and the weak intermolecular forces of filler reduce the surface energy of two components thereby creating low hydrophobicity composites. The polymer chains and the different interfacial forces of graphene inhibit homogenous dispersion of filler in the polymer matrix, initiating poor electrical and thermal characteristic. The dispersion of fillers also mentions to surface energy of the fillers. The theoretical surface energy of graphene is very high surface energy, which makes the graphene sheets to be susceptible to restacking, preventing the homogenous distribution in polymer matrix (Idowu, Boesl, & Agarwal, 2018). Polymer/graphene composites can be prepared by three main techniques including in-situ polymerization, melt intercalation and solution mixing (Phiri et al., 2017).

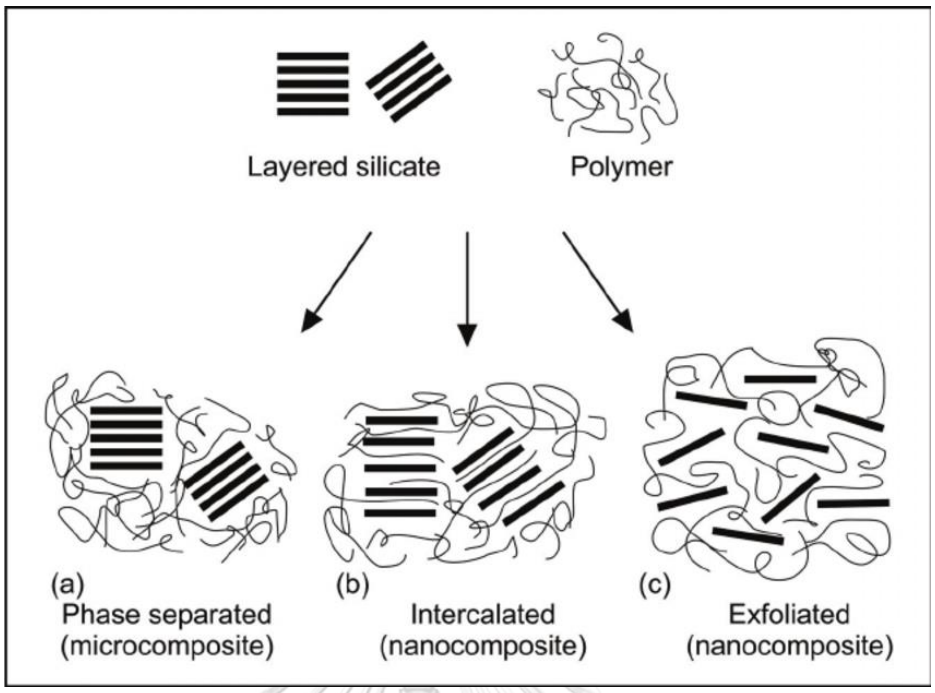

Figure 2.15 Different types of composites arising from the interaction of layered silicate and polymer (Akbari et al., 2010).

2.5.3.1 In-situ polymerization

This technique initiates with the dispersion of graphene filler in a liquid monomer at high temperature. This method causes a strong interaction between the filler and the polymer resulting in the faster stress transfer and a good filler dispersion that is appropriable for high filler loading. The polymerization increases viscous mixture, therefore, solvents are required. This technique is a promising method for a more homogeneous distribution, on the other hands, the high cost of monomer and high temperature are the main limitations (Funck, Kaminsky, & Technology, 2007).

2.5.3.2 Melt intercalation method

The melt intercalation method is a solvent-free process that a polymer melt is mixed with graphene filler. Basically, homogeneous mixing of graphene and polymers is achieved under high mechanical shear condition, through a screw extruder or a blending mixer. This method has found extensive application for

preparation of thermoplastic composites. The high temperature enhances the dispersion of melting polymer and filler. The advantages of this intercalation are applicable to both polar and non-polar polymer and large scale production. The prepared composites by this method is ineffective for filler dispersion and inadequate for adsorption field (Phiri et al., 2017).

2.5.3.3 Solution mixing

Solution mixing is the most commonly used technique for polymer composite fabrication due to its simplicity and potential for large scale application. The mechanism consists of three step including the dispersion of filler in a solvent, the incorporation of the polymer and the removal of solvents. To provide easy dispersion of fillers, several solvents are commonly used such as water, acetone, chloroform, tetrahydrofuran, dimethyl formamide or toluene. However, this method allows the composite preparation based on polymer with low or even polarity, the solvent evaporation during the mixing is one of the most concerns (Silva, Alves, & Paiva, 2018).

2.6 Adsorption

Adsorption is a surface phenomenon, which a substance (adsorbate) adheres to the surface of another substance (adsorbent). This process creates an accumulation films of adsorbate on the surface or pores of a solid adsorbent. Generally, adsorption occurs when the attractive energy between adsorbent and a substance (e.g. the adhesive work) is greater than the cohesive energy of the substance itself. Adsorption processes are classified into two types as; physical adsorption is the attraction between atoms of adsorbates and adsorbents with weak van der Waals forces or electrostatic attraction, and chemisorption is the attraction of an atom with strength bond like covalent bonding (Chiou, 2003).

2.6.1 Adsorption mechanism

The mechanism of adsorption process is divided into three steps as shown in Figure. 2.16. The first step is filming diffusion process involving with adsorbates movement from the boundary layer to the external surface of adsorbents. The intermolecular forces between adsorbate and adsorbent cause the diffusion of adsorbate on the adsorbent surface. The second step is migration intro pores of adsorbent that adsorbates transports into the interior of adsorbent particle. The last step is the energetic interaction between adsorbates and the site of adsorbents. The adsorbates are filled up into monolayer molecule covering the pores and surface area of adsorbent. Adsorption process is the fastest step; therefore, the rate limiting step might be the first or second step.

2.6.2 Physisorption and chemisorption

The adsorption forces are a key in defining whether the adsorption is physical or chemical. Physical adsorption describes the interaction force between adsorbate and adsorbent is van der Waals forces, which are the intermolecular forces and interatomic interactions with the energy of 10-20 kJ/mol). Various parameters of adsorbent affect physisorption such as pore structure, pore size, pore volume and surface area. While, chemical adsorption occurs by the chemical interaction between molecules and atom of adsorbate and adsorbent. The efficiency of chemisorption relates to specific surface area, types of active sites and stability of active sites. The basic information of physisorption and chemisorption are summarized in Table 2.5. (Musin, 2013; Repo, 2011).

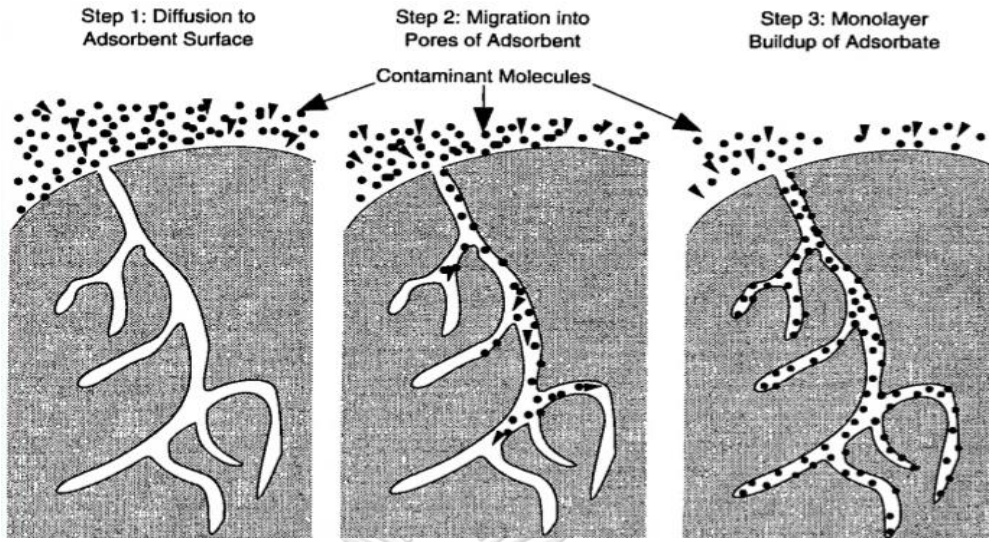

Figure 2.16 The mechanism steps of adsorption (Musin, 2013).

Table 2.5 Different characteristics between physisorption and chemisorption.

	Physisorption	**Chemisorption**
Type of interaction	van der Waals, hydrogen bonding, hydrophobic interaction	Covalent bond
Heat of adsorption (kcal/mol)	10-20	10-100
Effect of temperature	Occur at low temperature	Occur at wide temperature range
Effect of parameters	Pore size, pore structure, pore volume and surface area	Specific surface area, types of active sites, number of active sites, stability of active sites
Reversibility	Irreversibility	Irreversibility or reversibility
Layer forming	Mono or multilayers	Monolayers

2.6.3 Adsorption kinetic modeling

Adsorption is one of the most important applied techniques for pollutant removal from contaminated media. Understanding thermodynamic and kinetic aspects can be predicted the performance and mechanism of adsorption process. Adsorption kinetics describe the adsorption rate on a solid surface. Adsorption diffusion models are constructed on the basis of three consecutive steps including external diffusion (film diffusion), internal diffusion (intra-particle diffusion) and surface reaction (Qiu et al., 2009). The diffusion in porous structure (micro, meso and macropores) of adsorbents significantly affects the rate of adsorption. The total rate of kinetic process is determined by the rate of the slowest process that is generally known as the rate determining step (Dąbrowski & science, 2001). Kinetic models based on the rate determining steps are divided into two groups. There are diffusion models (external mass transfer and internal diffusional models) and adsorption models (Largitte, Pasquier, & Design, 2016).

2.6.3.1 Pseudo-first-order model

This model is the simplest empirical kinetic model presented by Legergern. The basic aspect of the model associates with the kinetic of one-site adsorption controlled by the rate of the surface reaction. General analytical derivation was achieved by assuming the high initial concentration of the adsorbate, which essentially remained constant during the kinetic experiment (Azizian & Science, 2004). The rate constant (k_1) determined as a function of initial adsobate concentration and the energy of the adsorption. The model can be determined from the equation as shown in Eq. (2.1).

$$\ln(Q_e - Q_t) = \ln Q_e - k_1 t \qquad (2.1)$$

where Q_t and Q_e are the amount of adsorbate (g g^{-1}) at time (t) and at equilibrium, respectively. The pseudo-first order rate constant shows in k_1 (min^{-1}). The value of k_1

and Q_e can be calculated from the slope and intercept of the graph between $In(Q_e-Q_t)$ and t.

However, the derivation of this model was achieved from the assumption of surface reaction, mathematically equivalent equations have been obtained for film or pore diffusion (Repo, 2011). Recently this model has been popularly used to describe the adsorption of pollutants from wastewater in different fields (Qiu et al., 2009).

2.6.3.2 Pseudo-second-order model

This kinetic model is derived by assuming a low initial concentration of the adsorbate, which has a two-site-occupancy adsorption. The assumption that the rate limiting step may be chemical sorption involving valency forces through sharing or exchange electrons between adsorbate and adsorbent mentions to pseudo-second-order model (Ho & McKay, 1999). It can be presented as the following Eq. (2.2).

$$\frac{t}{Q_t} = \frac{1}{k_2 Q_e^2} + \frac{1}{Q_e} t \qquad (2.2)$$

where k_2 is the adsorption rate constant stands (g g^{-1} min^{-1}) for pseudo-second-order adsorption. The linear plot between t/Q_t and t gave $1/Q_e$ as the slope and $1/k^2Q_e^2$ as the intercept.

2.6.3.3 Elovich model

The Elovich model is one of the most useful model to describe the kinetic of chemisorption. The assumption of this model based on the adsorption site increase exponentially with adsorption. The theory implies a multi-layer adsorption. This model widely used to explain the adsorption of gas on solid sorbent. The Elovich model can be expressed in the following form (I. Tan, A. Ahmad, & B. J. J. o. H. M. Hameed, 2009).

$$Q_t = (\frac{1}{b})\ln(ab) + \frac{1}{b}\ln t \quad (2.3)$$

Where *a* is the initial adsorption rate (g g^{-1} min^{-1}) and *b* correspond to the extent of surface coverage and activation energy of chemisorption. A plot between Q_t and ln *t* previded the (*1/b*) as the slop and (*1/b*)ln(*ab*) as the intercept. Moreover, the (*1/b*) and (*1/b*)ln(*ab*) value can be indicated the number of site available for adsorption and the adsorption quantity, respectively.

2.6.3.4 Intraparticle diffusion model

A typical intraparticle diffusion is known as a homogenous solid diffusion model which describes the mass transfer in an amorphous and homogenous sphere. This model can be expressed as Eq. (2.4) when the intraparticle diffusion is the rate-determining step.

$$Q_t = k_d t^{1/2} + I \quad (2.4)$$

where k_d is the intraparticle diffusion rate constant (g g^{-1} $s^{1/2}$). The k_d constant was obtained from the slope of the linear plot of Q_t and as a function of $t^{1/2}$. *I* is the interception of the plot indicating the presence of a boundary layer effect.

2.6.3.5 Liquid film diffusion model

The rate of a substance that accumulates in the solid phase is equal to the traformation of a substance across the liquid film. It is characterized by a mass transfer coefficient. The equation representing liquid film diffusion kinetic can be express as Eq. (2.3) (Qiu et al., 2009). Based on the fact of adsorption, it is implausible to believe that surface diffusion is the slowest step. Moreover, the mechanical mixing during the adsorption process significantly impacts film diffusion. Film diffusion usually only rates, controlling for the first few minutes (Ho & McKay, 1999).

$$\ln(1-F) = -k_{fd}t \quad (2.5)$$

$$F = \frac{Q_t}{Q_e} \tag{2.6}$$

where F refers to the fractional attainment of equilibrium and k_{fd} is the rate constant (g^{-1} $s^{1/2}$). The k_{fd} constant was obtained from the slope of the plot between Q_t versus $t^{1/2}$.

2.6.4 Adsorption isotherm models

An adsorption isotherm determines the amount of adsorbate on the adsorbent surface at equilibrium and constant temperature. The thermodynamic assumptions and parameters of the equations provide useful information about the sorption mechanism, the surface properties and affinities of the sorbent (Keshavarz et al., 2016). Adsorption isotherms are typically nonlinear because of the energetic heterogeneity and the limited active sites or surfaces of the solid. All isotherm models are based on Henry's law The, Langmuir, and Freundlich models are commonly used to investigate the equilibrium of single-component adsorption (Iakovleva, 2018).

2.6.4.1 Langmuir adsorption model

Langmuir isotherm determines the surface coverage by balancing the adsorption and desorption rates (dynamic equilibrium). The basic assumptions of this model based on the assumptions of a (i) homogeneous surface with constant adsorption energy over the all sites, (ii) localized adsorption on the surface and monolayer and (iii) each of adsorption sites contain only one adsorbate. Then, the following reaction is considered as (Limousin et al., 2007). The nonlinear and linear forms are represented as Eqs. 2.5-2.6(Langmuir, 1918):

$$Q_e = \frac{Q_m k_L C_e}{1 + k_L C_e} \tag{2.7}$$

$$\frac{C_e}{Q_e} = \frac{1}{Q_m k_L} + \frac{C_e}{Q_m} \tag{2.8}$$

where Q_m (g g^{-1}) is the monolayer capacity of the adsorbent, k_L (L g^{-1}) is a constant related to the free energy of the adsorption and C_e and q_e are equilibrium concentration and the equilibrium oil concentration on the adsorbent, respectively. For the linear method, the isotherm constants Q_m and k_L can be determined from the slope and intercept of the plot between C_e/Q_e and C_e (J. O. Nwadiogbu, Ajiwe, & Okoye, 2018).

2.6.4.2 Freundlich adsorption model

Freundlich isotherm is an empirical equation that can be used for the systems on the assumption of heterogeneous sorption energy and interaction between the adsorbate molecules. Freundlich isotherm model is not restricted to the monolayer adsorption and describes the non-ideal and reversible adsorption. This model e presence of unequal adsorption sites, leading to different affinities with the adsorbates (Radhika & Palanivelu, 2006). The nonlinear and linear form of this model can be written as Eq. 2.8 and Eq. 2.9:

$$Q_e = k_F C_e^{1/n} \tag{2.8}$$

$$\log Q_e = \log k_F + \frac{1}{n}\log C_e \tag{2.9}$$

where k_F (g g^{-1})(L·g^{-1}) and n are Freundlich constants related to the adsorption capacity and adsorption intensity, respectively. The n parameter, known as the heterogeneity factor, can be used to indicate whether the adsorption is linear (n = 1), whether it is a chemical process (n < 1) or whether it is a physical process (n > 1) and it also indicates the relative distribution of the energy and the heterogeneity of the adsorbate sites. To determine the constants K_F and n, the linear form of the equation shown below may be used to plot the log(Q_e) against log(C_e).

2.7 Literature reviews

Santos et al. (2017) described the influence of the concentration of lignin when used as a filler in polyurethane foam for crude oil sorption. The kinetic study showed that the equilibrium time of adsorption was 48 h. The 10% concentration of lignin (PUF-10) showed the best performance of oil removal with an improvement about 35.5% in sorption capacity compared to the blank one. The concentration of lignin showed that the oil removal efficiency increased while the oil removal percentage decreased with the increased oil concentration for the removal of crude oil from water. However, the large-scale production of this material properly used for environmental remediation could not be compromised by a high final cost of production and a huge waste generation.

Liu et al. (2013) prepared reduced graphene oxide coated polyurethane (rGOPU) sponges to absorb different kinds of organic liquids. The results presented that the rGPU sponge was highly porous and oleophilic resulting in a high absorbance for liquids and good oil/water separation capacity. The absorption rates of the rGPU sponge for all the oils were rapid (≤ 100 s) and were related to the viscosity of the oils. The coating of rGO not only made the rGPU sponges hydrophobic but also increased their compressive strength. Therefore, a combination of high hydrophobicity, elasticity, and strength made the rGPU sponge be a high efficient and reusable absorbent for spilling oil. Moreover, this material was also cost effective compared with graphene and carbon nanotube sponges which also had high absorption capacities.

Tjandra et al. (2015) reported that reduced graphene oxide was covalently bound onto the surface of polyurethane (PU) sponge using two different coupling agents: (3-aminopropyl) triethoxysilan (APTES) and itanium (triethanolaminato) isopropoxide (TTEAI). The modified PU sponges exhibited both hydrophobic and oleophilic properties, making it highly selective toward the absorbance of oil and other organics from water. The TTEAI-rGO sponges exhibited the highest average pump oil absorbance

compared to all of the other modified sponges. The resulting improved rGO-coated PU sponge was a highly efficient and reusable sorbent material and was a promising alternative to oil-water separation applications.

Li et al. (2015) modified graphene (GN) with c-methacryloxypropyl trimethoxy silane (KH-570), to coat the PU sponge (KH–GN sponge). The modified sponge exhibited the characteristics of superhydrophobic properties (contact angle = 161°) and a unique absorption capacity. The maximum absorption of the prepared KH–GN sponge for oil was up to 39 times. Furthermore, the coated sponge was reused more than 120 times without losing its maximum absorption capacities.

Subrati et al. (2017) reported the development of hydrothermal reduced graphene oxide foam functioned with Fe_3O_4 magnetic nanoparticles (MNP) for oil sorption. MNP was used to produce rGO-MNP hybrid foams which could be separated by a magnetic field. Motor oil was selected to use as adsorbate in this study. The experimental results showed that The MNPs had a negligible effect on the sorption capacity. Slight decrease of oil sorption capacity for the rGO-MNP foam due to the increase hydrophilicity of the composite foam. Another reason could be that the MNP loading onto the rGO foam slightly reduced the surface area and the pore volume. However, rGO foam is an excellent candidate to be used as a sorbent for oil spill cleanup due to its high specific surface area and hydrophobicity.

CHAPTER III

MATERIALS AND METHODOLOGY

3.1 Materials

All chemical reagents and equipment were summarized in Table 3.1 and 3.2, respectively.

Table 3.1 The chemical reagents in this research.

Chemical reagents	Company	Country
98% (w/v) Sulfuric acid	Quality Reagent Chemical	New Zealand
36% (w/w) Hydrochloric acid	Ajax Finechem	Australia
30% (w/w) Hydrogen peroxide	Quality Reagent Chemical	New Zealand
Potassium permanganate	Ajax Finechem	Australia
L-ascorbic acid	Ajax Finechem	Australia
Sodium hydroxide	Ajax Finechem	Australia
Graphite powder	Siam chemical	Thailand
Natural rubber latex	Rubber Research Institute	Thailand
10% Potassium oleate dispersion	Rubber Research Institute	Thailand
50% Sulfur dispersion	Rubber Research Institute	Thailand
50% Zinc diethyldithiocarbamate dispersion (ZDEC)	Rubber Research Institute	Thailand
50% Zinc-2-mercaptobenzthiazole dispersion (ZMBT)	Rubber Research Institute	Thailand
50% Wingstay®L dispersion	Rubber Research Institute	Thailand
33% Dipropylene Glycol dispersion (DPG)	Rubber Research Institute	Thailand
50% Zinc oxide dispersion (ZnO)	Rubber Research Institute	Thailand
12.5% Sodium silicofluoride dispersion (SSF)	Rubber Research Institute	Thailand

Table 3.2 The equipment in this research

Equipment	Type	Company
Magnetic stirrers	SH7	IKA company, Germany
Oven	ED115	Binder company, Germany
Portable ultrasonic cleaner	NXPC	KODO company, Korea
Vacuum pump	WJ-20	Sibata company, Japan
Elemental analyzer	PE-2400	ParkinElmer, USA
X-ray diffractrometer (XRD)	Bruker D8 advance	Germany
Fourier transform infrared spectrophotometer (FTIR)	Perkin Elmer	Inc., Spectrum one, USA
X-ray photoelectron spectroscopy (XPS)	Perkin Elmer	Inc., USA
Transmission electron microscopy (TEM)	TECNAI 20	Philips
Brunauer-Emmett-Teller	Autosorb-1	Quantachrome, Germany
Scanning electron microscopy (SEM)	JEOL, JSM-6480LV	Japan
Buchner funnel		
Suction flask		
Erlenmeyer flask 500 mL		
Beakers 25, 100, 250 and 500 mL		
Whatman filter paper NO. 40		
Litmus papers : MACHEREY-NAGEL pH-Fix 0-14		
Cake mixer		

3.2 Methodology

3.2.1 Synthesis of GO and rGO

GO was synthesized from graphite waste which was obtained from metal smelting industry, Mahamak Flow Innovation Co., Ltd., Thailand., via a modified Hummer's method (M. T. H. Aunkor et al., 2016). In this typical procedure, graphite powder (3 g) was added into concentrated H_2SO_4 (98% w/v, 60 mL). The resulting suspension was stirred in an ice-water bath with temperature under 10 ℃ for 30 min. Under vigorous stirring, $KMnO_4$ (9 g) was gradually added by maintaining the temperature under 10 ℃ for 1 h. The temperature of mixture solution was then allowed to rise to room temperature for 30 min. After that the reaction was quenched by addition of deionized water (150 mL), leading to brown color. Successively, the suspension was treated by stirring-sonication process in order to compare with the oxidation by thermal process. In the stirring-sonication process, the mixture was stirred at room temperature for 25 min, followed by the sonication in an ultrasonic bath for 5 min. The procedure was repeated for 0, 5 and 10 times (Abdolhosseinzadeh, Asgharzadeh, & Seop Kim, 2015). In case of the thermal-sonication process, the suspension was heated at 95 °C for 15 min, followed by the sonication for 30 min (Wipatkrut & Poompradub, 2017). The resulting suspension was then divided into two equal parts; one washed to obtain GO and the other was processed for rGO preparation. For GO preparation, H_2O_2 (30% w/w, 20 mL) was added into the suspension which was stirred until gas evolution ceased. After that, the suspension was filtered with Whatman paper No. 40 and the obtained solid was washed by of HCl (36% w/w, 5 mL) to remove the sulphate. The solid was washed by deionized water for several times until pH reached to neutral (pH = 6-7) and dried in an oven at 100 ℃ for 24 h, resulting in GO as black solid. The sample codes of these solid products were "GO-5T" and "GO-10T" referred to those obtained from the sonication-sonication 5

and 10 times, respectively, while “GO-H” meant the GO product form thermal-sonication process.

To prepare the rGO, the other part of suspension was adjusted to pH 8-9 by a 1M NaOH solution and followed by sonication for 1 h. L-AA at various concentration (0.25, 0.5 and 1.0 M) used as reducing agent was slowly added into the suspension at room temperature that was then continuously stirred at 95 ℃ for 1 h. After that, the suspension was then cooled down to room temperature and filtered. The resulting black solid was washed by HCl (36% w/w, 5 mL) and deionized water until the pH of suspension became neutral and dried at 100 ℃ for 24 h. The final solid product was referred to rGO. The number codes after “rGO” referred as “rGO-n”, when n is the concentration of L-AA used.

3.2.2 Preparation of NR composite materials

The chemical reagents in set A, B, C and D were mixed in a cake mixer as followed by the formulation and mixing time in Table 3.3. Ungelled NR compounding was quickly poured into an aluminum mould and dried at 100 ^{o}C for 2 h. The resulting NR foam was washed with water to remove unreacted elements and dry in oven at 60 ^{o}C for 24 h. To prepare NR composite foams, the various contents of rGO (0.25, 0.5, 1.0, and 1.5 parts by weight per hundred parts of rubber: phr) were dissolved in 1.5 phr of K-oleate for 15 min and the same procedure was carried out as before. The sample codes used in this part were “NR” for the pure NR foam and “NG-n” for the composite foams, when n is the rGO content used.

Table 3.3 The formulation of rubber compounding.

Set	Chemical agent	Dry weight (phr*)	Wet weight (g)	Time (min)
A	Natural rubber latex	100.00	167	10.0
	10% Potassium oleate solution	1.50	15	
B	50% Sulfur	2.00	4	1.0
	50% Zinc diethyldithiocarbamate (ZDEC)	1.00	2	
	50% Zinc-2-mercaptobenzthiazole (ZMBT)	1.00	2	
	50% Wingstay®L	1.00	2	
C	33% Dipropylene Glycol (DPG)	0.66	2	1.0
	50% Zinc oxide (ZnO)	5.00	10	
D	12.5% Sodium silicofluoride (SSF)	1.00	8	0.5

*Parts by weight per hundred parts of rubber

3.2.3 Characterization

3.2.3.1 Characterization of graphite, GO and rGO

The morphology of graphite, GO and rGO was examined by transmission electron microscopy (TEM) (TECNAI 20, Philips). A sample (0.1 g) in absolute ethanol was sonicated in a sonication bath for 15 min followed by vortex for 5 min and then the colloidal solution was dropped on the TEM grid.

The crystal structure of each sample was characterized by XRD (Bruker D8 advance, Germany) with a CuKα radiation source (λ = 1.5406 Å). X-ray radiation was operated at 40 kV and 40 mA with a scanning rate of 5-50° changing at 0.1° per sec.

The contents of carbon, hydrogen and nitrogen on the sample surface were confirmed by a CHNS analyzer (PE-2400, ParkinElmer, USA). The sample (0.1 g) was added into tin capsules and then burned in a pyrolysis reactor at temperature of 1000 ℃ under constant flow helium steam. The resulting combustion mixture was separated by chromatographic column and detected with a thermo conductivity detector.

Functional groups of samples were determined by fourier transforms infrared spectroscopy (FTIR) (Perkin Elmer, Inc., Spectrum one, USA). The samples were evaluated using KBr pellets and examined in the attenuated total reflectance (ATR) mode. The scans were performed in the range of 500-4000 cm^{-1} with a spectral resolution of 0.5 cm^{-1}.

Elemental binding energy of all samples was measured using X-ray photoelectron spectroscopy (XPS) (Perkin Elmer, Inc., USA). The XPS spectra were taken at a working pressure under 10^{-7} Pa with a monochromatic Al$K\alpha$ radiation source (1486.8 eV).

Surface properties for all samples were performed by a Brunauer-Emmeett-Teller (BET) method (Autosorb-1, Quan tachrome, Germany). Nitrogen (N_2) adsorption isotherm was recorded at 77 K. All samples were degassed at 250 °C for 3 h under vacuum before analysis.

3.2.3.2 Characterization of NR composite materials

The morphology of the NR and composite foam was observed by SEM (JEOL, JSM-6480LV, Japan). The samples were cut and stitched on a SEM stub and then sputter coated with gold before SEM analysis.

3.2.3.3 Adsorption experiment

The oil-seawater sorption capacity of sorbent materials was determined by the Standard Test Method for sorbent performance of adsorbents (ASTM F726-12). Seawater was collected from Seangchan beach, Rayong. The various

types of the petroleum-based oil were used for the oil sorption test including gasohol, kerosene, diesel, crude oil and fuel oil. In the oil-seawater system test, a sample (3 g) of each oil was poured into a 250 mL beaker containing seawater (100 mL). Then, a cubic shape foam sorbent (0.7 × 0.7 × 0.7 cm^3) was weighed before immersing into petroleum-based liquid for 15 min as shown in Figure 3.1.

Table 3.4 Characteristic of seawater.

Properties	Value
Acidity	14 mg/L
Total alkalinity	95 mg/L
Salinity	19 ppt

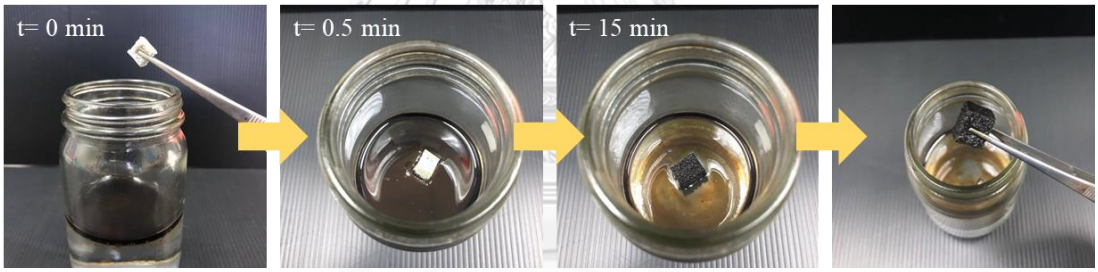

Figure 3.1 Oil adsorption process of sorbent foams.

Following, the fully adsorbed foam was removed from the oil by forceps and allowed to drain for 30 ± 3 s. Finally, the oil sorption capacity (*Q*) of the rubber foam was determined based on Eq. 3.1 (Ratcha et al., 2015). This procedure was carried out 5 times and the mean of the results was reported.

$$Q(g \cdot g^{-1}) = \frac{(W_1 - W_0)}{W_0} \quad (3.1)$$

where *Q* is oil adsorption capacity (g g^{-1}). W_0 and W_1 represent as the initial weight and the fully adsorbed weight of foam, respectively.

3.2.3.4 Environmental parameter setup

Two environmental factors included temperature and turbulence were considered in this study. The effect of the temperature (30, 45 and 60 ^{o}C) on the sorption experiments was investigated. The effect of the turbulence was placed in a shaker (VS-202P, Vision Scientific Co., Ltd., Korea) set at room temperature (30 ^{o}C) and a shaking speed of 100, 150 and 200 rpm. A cubic sorbent was weighted before and after immersing into oil liquid at different conditions. This procedure was carried out 5 times to obtain a mean value for calculating the oil sorption capacity.

3.2.3.5 Adsorption kinetic

Adsorption kinetics was studied by varying the contact time from 0-90 min at room temperature to investigate the reaction rate. The initial concentration of oil was fixed at 3 g in 100 mL of seawater. The cubic sorbent was weighed before and after immersing into oil liquid at different times. The material was drained for 30 ± 3 s and the oil sorption capacity was calculated using Eq. (3.1). The kinetic models applied to this study were pseudo-first-order (Eq. 2.1), pseudo-second-order (Eq. 2.2), Elovich equation (Eq. 2.3), intraparticle diffusion (Eq. 2.4) and liquid film diffusion (Eq. 2.5) models.

3.2.3.6 Adsorption isotherm

The adsorption isotherm experiment was performed to determine and to estimate the maximum amount of adsorbed oil. Langmuir (Eq. 2.8) and Freundlich isotherm (Eq. 2.11) models were analyzed to determine which model give the greatest agreement with the experimental oil sorption data of the NR and composite foam. The initial oil concentration was varied from 0.5-5 g in 100 mL of seawater. The experimental condition in this part was carried out at equilibrium time and room temperature.

3.2.3.7 Oil removal efficiency and reusability

The oil removal efficiency (*Re*) and the foam reusability were determined through adsorption-desorption cycles. After the adsorption, the cubic sorbent was squeezed, re-weighed and placed backed on the oil until it became saturated with the oil. The oil removal efficiency which is a percentage of mass ratio of the saturated weight of foam was calculated for each cycle by Eq. (3.2) (Ratcha et al., 2015). The physical characteristic of the sorbent foams was discussed.

$$Re(\%) = \frac{(W_1 - W_0)}{W_1} \times 100 \quad (3.2)$$

where *Re* is oil removal efficiency. W_0 and W_1 represent as the initial weight and the fully adsorbed weight of foam, respectively.

3.2.3.8 Weathering test

QUV accelerated weathering test was determined damaging effects of long term outdoor exposure of the materials. A typical procedure was followed by the Standard Practice for Operating Fluorescent Light Apparatus for UV Exposure of Nonmetallic Materials (ASTM G 154-00a). All samples were UV exposure (UVA-340) at 70 °C for 8 h, followed by condensation at 50 °C for 4 h. These cycles were repeated for 7 days.

CHAPTER IV

RESULTS AND DISCUSSION

4.1 Structural characterization by XRD and TEM

The interlayer distance is one of significant parameters to access the structural information of the graphite, GO and rGO. The XRD spectra of graphite, GO and rGO are shown in Figure. 4.1. Graphite displayed the characteristic (002), (100), (101) and (004) peaks. The highest reflection peak of (002) at 26.52° indicated the graphite structure consisting of multi-layers carbon planes with *d*-spacing of 0.336 nm. The diffraction peak of (004) at 54.34° was defined as layer spatial arrangement of the graphite structure with the *d*-spacing of 0.169 nm. Two weak peaks were observed at 42.5° (*d*-spacing = 0.212 nm) and 44° (*d*-spacing = 0.206 nm), corresponding to hexagonal order in planes (Howe et al., 2007; Kun, Wéber, & Balázsi, 2011).

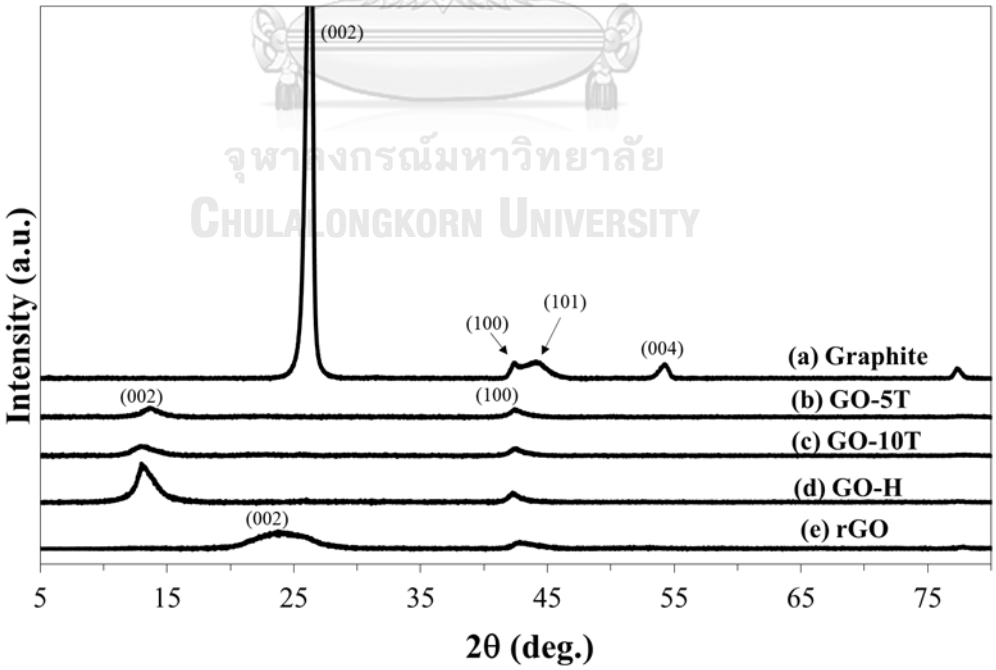

Figure 4.1 The XRD spectra of graphite, GO with different oxidation conditions and rGO.

After the oxidation of the graphite, the XRD patterns of GO-5T, GO-10T and GO-H showed two characteristic peaks of (002) at 12° and (100) at 42.5°. The intensity of the (002) peak was significantly decreased and the peak was shifted to the lower angle. The result indicated that the penetration of oxygen-functional groups after the oxidation process caused the significant increase of the *d*-spacing for the graphene sheets up to 0.63-0.73 nm. Upon the thermal-sonication oxidation method, GO-H showed the high intensity of (002) peak. It could be conducted that the stacking order of the carbon planes in GO-H was higher than those of GO-5T and GO-10T, which were prepared by the stirring-sonication method. The broad (002) peak might refer to the disorder stacking of the carbon planes due to the peeling of graphitic sheets during the oxidation and exfoliation processes. According to the result, the (100) diffraction peak still observed in all oxidation conditions, suggesting that the graphitic structure of the GOs might not be completely distorted through the oxidation processes (Wojtoniszak & Mijowska, 2012; Xiaowei, Jean-Charles, & Suyuan, 2004). After the reduction by L-AA, GO prepared via the stirring-sonication and thermal-sonication methods, showed the identical rGO structure as shown in Figure 4.1(e). The (002) characteristic peak of the rGO was shifted to the higher angle (2θ = 23.93°), confirming the restoration of the graphite structure (Wipatkrut & Poompradub, 2017). However, the interlayer spacing of rGO (0.37 nm) was more than that of the graphite due to the remaining of oxygen-containing groups or other structure defects.

According to the TEM images (Figure. 4.2), the graphite displayed the dark flake due to the stacking of the multi-layers of the graphene sheets by van der Waal force, while the GO-H structure was more transparent and consisted of few-layer sheets after the oxidation process. The oxygen-containing groups destroyed the van der Waal interaction among the graphene sheets of that GO-H structure, thus the graphene sheets was easily separated by the exfoliation step. After the L-AA reduction, the intrinsic features of the rGO such as transparent, and few thin sheets with typical

wrinkled and scrolled structure were observed. Accordingly, the synthesized rGO in this study did not be a single layer structure as in the theory, but as a few layer structure.

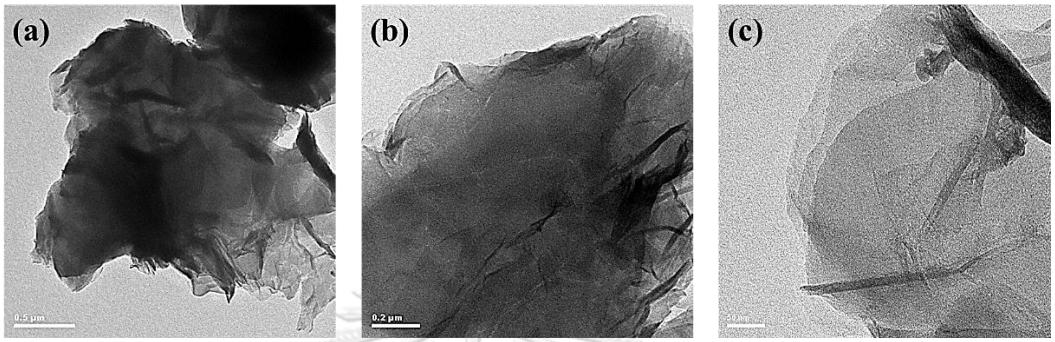

Figure 4.2 TEM images of (a) graphite, (b) GO-H and (c) rGO.

4.2 Surface properties characterization

4.2.1 Elemental analysis

The CHNS elemental analyzer was used to determine the quantitation of carbon, nitrogen and hydrogen of the graphite, GO-H and rGO. As shown in Table 4.1, the carbon content of GO-H was significantly decreased, while its oxygen content became increased after oxidation process, compared with those of the graphite. After the reduction of GO-H, the oxygen-containing groups in rGO structure obviously decreased compared with the oxygen content of GO-H. Moreover, the oxygen content in rGO tended to decline when the concentration of reducing agent used was increased. This indicated that the L-AA led to the removal of the oxygen from GO-H, although some of the oxygen content was still observed.

Table 4.1 Elemental content of the graphite, GO-H and rGO.

Element (%wt)	Graphite	GO-H	rGO-0.25	rGO-0.5	rGO-1.0
Carbon	87.595	51.485	74.035	77.195	89.865
Nitrogen	0.060	0.045	0.060	0.060	0.055
Hydrogen	0.070	2.805	0.845	1.020	0.985
Oxygen	12.275	45.665	25.06	21.725	9.095

4.2.2 Brunauer-Emmett-Teller (BET) analysis

Figure 4.3 shows the N_2 adsorption isotherms of the graphite, GO-H and rGO-0.5 and Table 4.2 summarizes the surface area of the synthesized rGOs prepared by using various L-AA concentration. All adsorption isotherms showed the typical type IV isotherm with type H4 hysteresis loops, corresponding to a mesoporous material with the pore diameter in the range of 20-500 Å (Sing & chemistry, 1985). Additionally, the graphite demonstrated the lowest surface area (33.4 m^2g^{-1}) as seen in Table 4.2, due to the stacking of the carbon planes. The oxidation reaction and exfoliation could separate the graphite structure into few layer sheets, resulting in the increase of surface area in GO-H. After the reduction process, the rGO had the significant increase of surface area, however, still below the theoretical of the value pristine graphene (2,630 m^2 g^{-1}). This result confirmed the existence of few stacked layers in the rGO structure and in agreement with the TEM result (Barroso-Bujans et al., 2012; Nugrahenny et al., 2014).

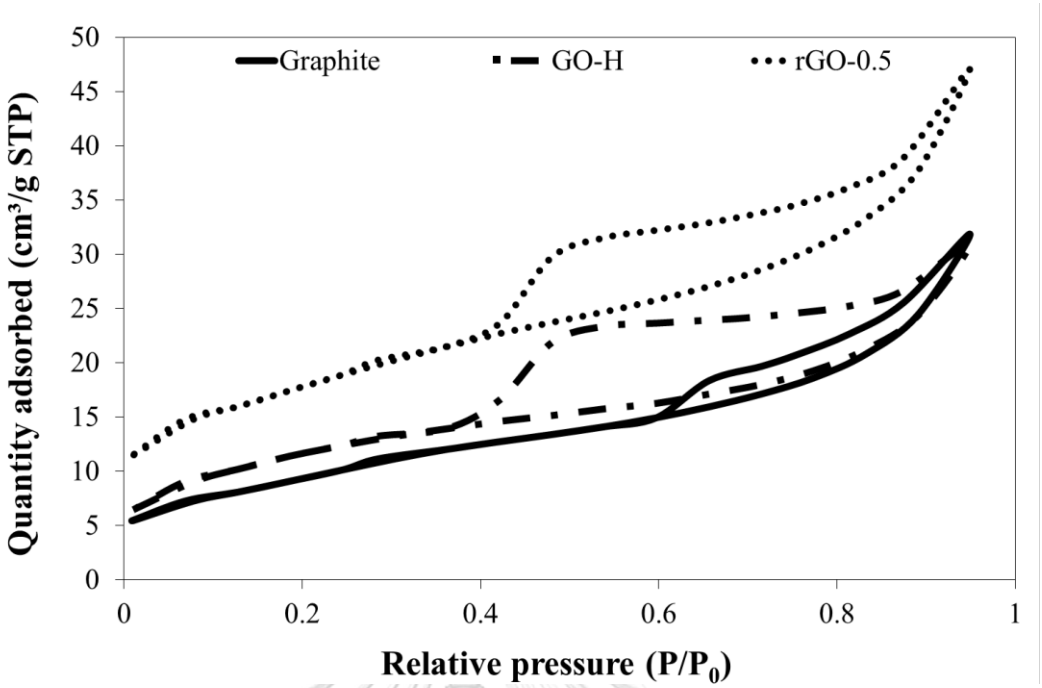

Figure 4.3 N_2 gas adsorption and desorption isotherms of the graphite, GO-H and rGO-0.5.

Table 4.2 Surface area, pore volume and pore size of the graphite, GO-H and rGO prepared by using different reducing agent concentration.

Sample	Surface area (m^2g^{-1})	Pore volume (cm^3g^{-1})	Pore diameter (Å)
Graphite	33.4	0.038	45.315
GO-H	37.9	0.038	39.829
rGO-0.25	48.4	0.048	39.803
rGO-0.5	58.2	0.058	40.102
rGO-1.0	36.8	0.042	45.660

By varying the L-AA concentration, the increase of surface area of the synthesized rGOs was obtained. Nevertheless, when the L-AA concentration was more than 0.5 M, the surface area of the rGO was significantly decreased due to the decreased of the oxygen atoms in GO-H (Table 4.1). Therefore, the graphene sheets

might be reconstructed, resulting in the decrease of surface area (Hu, Chen, & Chen, 2011). According to this result, the reduction of GO-H by 0.5 M L-AA was the best condition, which provided the highest surface area, and the rGO-0.5 was used for further study of the surface properties and oil adsorption capacity.

4.2.3 Fourier transforms infrared spectroscopy (FTIR)

Figure 4.4 shows the FTIR spectrum of the graphite, GO-H and rGO-0.5. The FTIR spectrum of the graphite showed no discernable functional groups, whereas that of GO-H demonstrated various oxygen functional groups that displayed in a series of different absorption peaks such as O-H stretching peak (3418 cm^{-1}), carbonyl peak (C=O) (1727 cm^{-1}), alkoxy peak (C-O-C) (1228 cm^{-1}) and epoxy peak (C-O) (1043cm^{-1}) (M. T. H. Aunkor et al., 2016). All oxygen-functional groups are the hydrophilic groups which made GO-H well dispersed in water (Chen, Yao, Li, & Shi, 2013). The asymmetric stretching of sp^2- hybridized C=C band of GO-H was observed at 1582 cm^{-1}, confirming the sp^2 domains of the graphene structure.

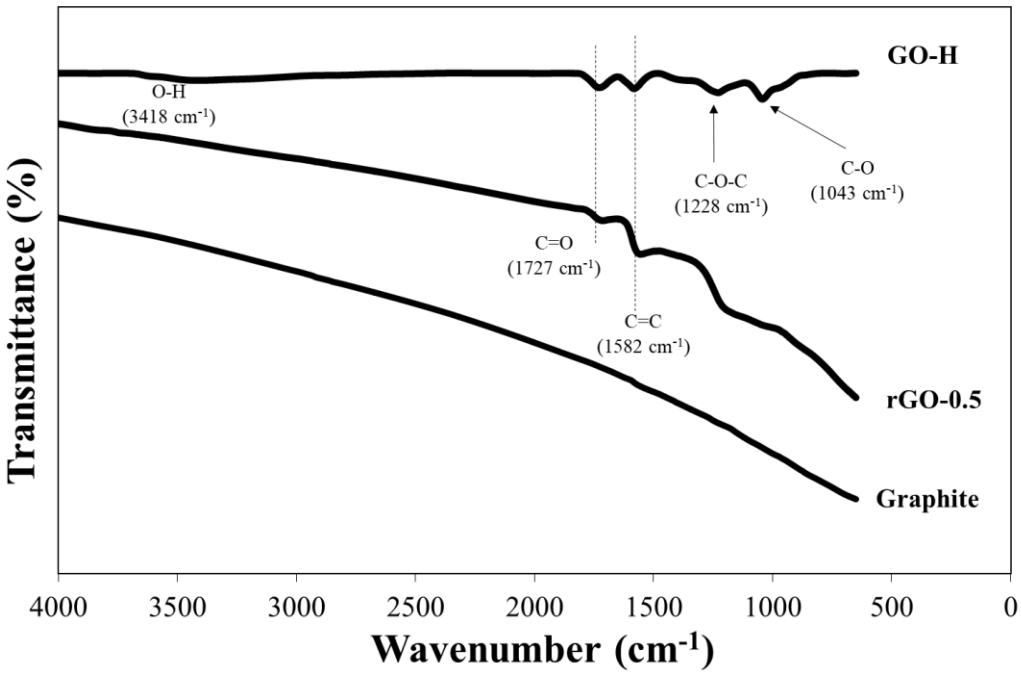

Figure 4.4 FTIR spectra of the graphite, GO-H and rGO-0.5.

After the L-AA reduction, the intensities of oxygen-functional peaks observed in GO-H were obviously decreased. Moreover, the C= C stretching of rGO-0.5 was still observed at 1580 cm^{-1}. This result implied that L-AA successively reduced oxygen containing functional groups from the structure of the GO and the atomic frame of the sp^2 carbons in rGO did not destroyed through the chemical oxidation-reduction process (M. T. H. Aunkor et al., 2016). However, the carbonyl peak (C=O) (1727 cm^{-1}) was found to be weaker in the rGO structure.

4.2.4 X-ray photoelectron spectroscopy (XPS)

The atomic composition and carbon/oxygen (C/O) ratio of the graphite, GO-H and rGO-0.5 characterized by XPS are summarized in Table 4.3. The percentage of the oxygen atoms was observably increased after oxidation process of the graphite, while the oxygen percentage of the rGO was decreased and the C/O ratio was increased. However, the C/O ratio of rGO-0.5 was significant lower than that of the graphite, corresponding to oxygen-containing still remained.

Table 4.3 The elemental composition obtained by XPS spectra of graphite, GO-H and rGO-0.5.

Samples	Composition		C/O ratio
	C 1s	O 1s	
Graphite	98.58	1.42	69.42
GO-H	73.92	26.08	2.83
rGO-0.5	83.75	13.45	6.22

Figure 4.5 shows the XPS spectra of GO-H and rGO-0.5. The spectrum of GO-H had five peaks of carbon and oxygen. The dominating peak of GO-H represented the sp^2 hybridization of the carbon structure at 284.49 eV. The other four peaks in GO-

H were related to oxygen containing functional groups, including the carbon-hydroxyl group (C-OH) at 285.69 eV, epoxy/ether groups (C-O) at 286.29 eV, carbonyl groups (C=O) at 287.19 eV and carboxylate carbon (O-C=O) at 287.99 eV. The rGO-0.5 demonstrated the decrease of the oxygen-containing peaks, indicating a considerable deoxygenation of GO-H by L-AA. Although the reduction process recovered of the sp^2 bonds, some oxygen group peaks were still observed such as the C-OH and C=O peaks at 285.49 and 286.59, respectively (Abdolhosseinzadeh et al., 2015; Johns & Rao, 2011).

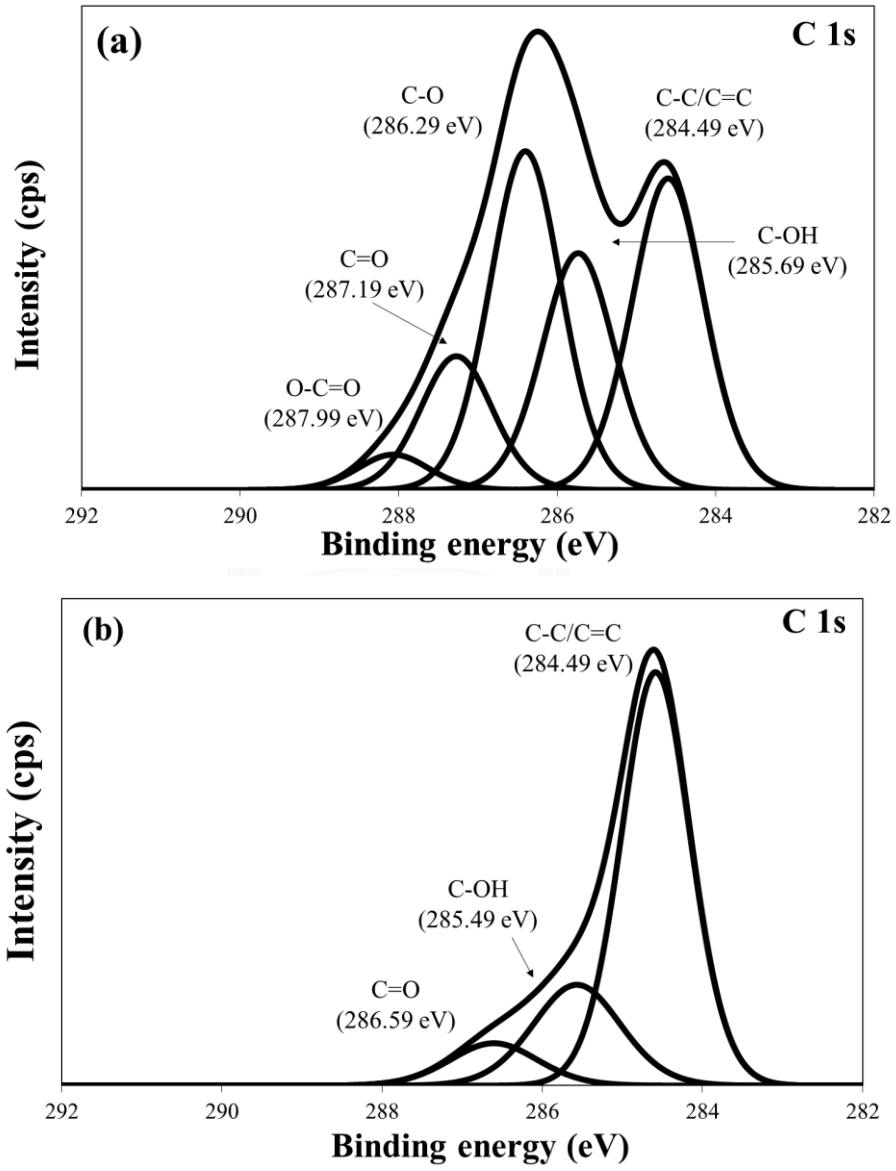

Figure 4. 5 Narrow scans of C 1s XPS spectra of (a) GO-H and (b) rGO- 0.5.

4.3 Morphology of the NR composite foams

The morphology of the NR composite foams having various contents of the rGO was analyzed by SEM as shown in Figure 4.6. The pore size and surface roughness of the NR composite foams tended to be increased with the increase of the rGO content. However, when the addition of the rGO was more than 0.5 phr, the rGO particles were not well dispersed in the NR latex and tended to precipitate at the bottom. Figure 4.6 on the right-hand side confirmed the agglomeration of the rGO in the NR matrix. After the vulcanization, the rubber foam surface of NG-1.0 and NG-1.5 exhibited cracking and big voids inside the foams (Figure 4.6(d) and (e)). This affected the decrease in density and the increase in porosity of the NR composite foams (Table 4.4). Accordingly, the dispersion, compatibility and adhesion between the filler and the rubber significantly influenced on the behavior and properties of the NR composite foams (Idowu et al., 2018).

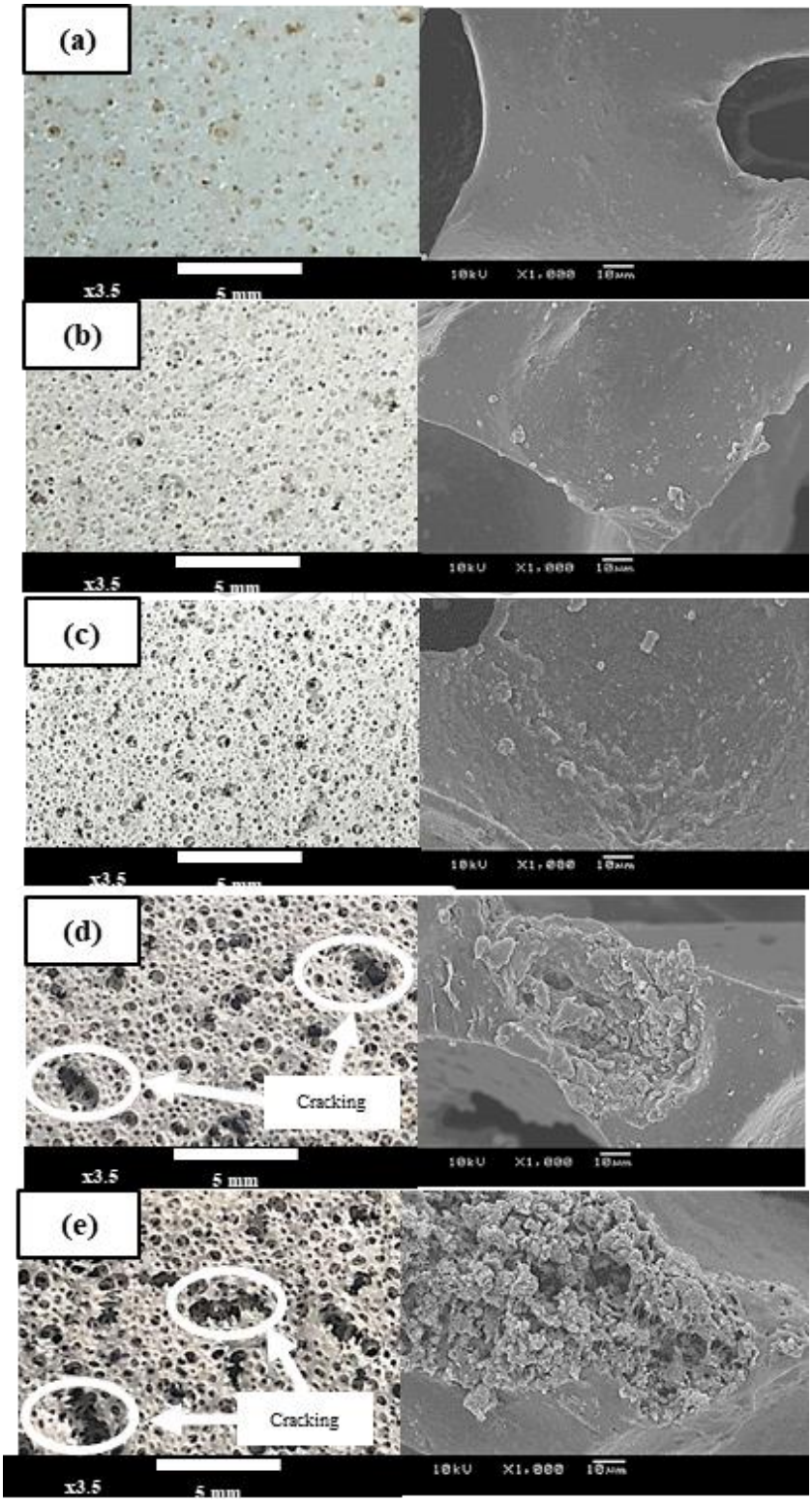

Figure 4.6 Digital and SEM images of (a) NR foam, (b) NG-0.25, (c) NG-0.5, (d) NG-1.0 and (e) NG-1.5.

Table 4.4 Characteristics of the NR composite foams containing different rGO-0.5 contents.

Sample	Density (g/cm^3)	Porosity (%)
NR	0.17	68
NG-0.25	0.17	69
NG-0.5	0.16	71
NG-1.0	0.14	72
NG-1.5	0.15	73

4.4 Oil adsorption

4.4.1 Effect of the oil types

Table 4.5 summaries the properties of the oils used in this study. Five oil types including gasohol, kerosene, crude oil, diesel and fuel oil have the different density and viscosity. Figure 4.7 shows the oil adsorption capacities of the NR composite foams in various oil types. Both NR and NR composite foams could adsorb all five kinds of the oils. However, they showed the best oil sorption performance on gasoline. It is because the low viscous oil can be easily penetrated into the pores of the rubber foams. While the oil adsorption capacity of NR composite foams tended to be decreased when the viscosity of the oils was higher. This result could be explained that the high viscous oil might block the pores at the surface and prevent oil penetration into the foam matrix.

Table 4.5 The characteristic of oils used in this study.

Oil types	Source	Density (g/cm^3)	Viscosity (mPa.s)
Gasoline	Gas station	0.74	1.42
Kerosene	Dinco company	0.80	1.85
Crude oil	Thai oil PCL	0.84	3.80
Diesel	Gas station	0.93	4.56
Fuel oil	Bangchak	1.05	72.40

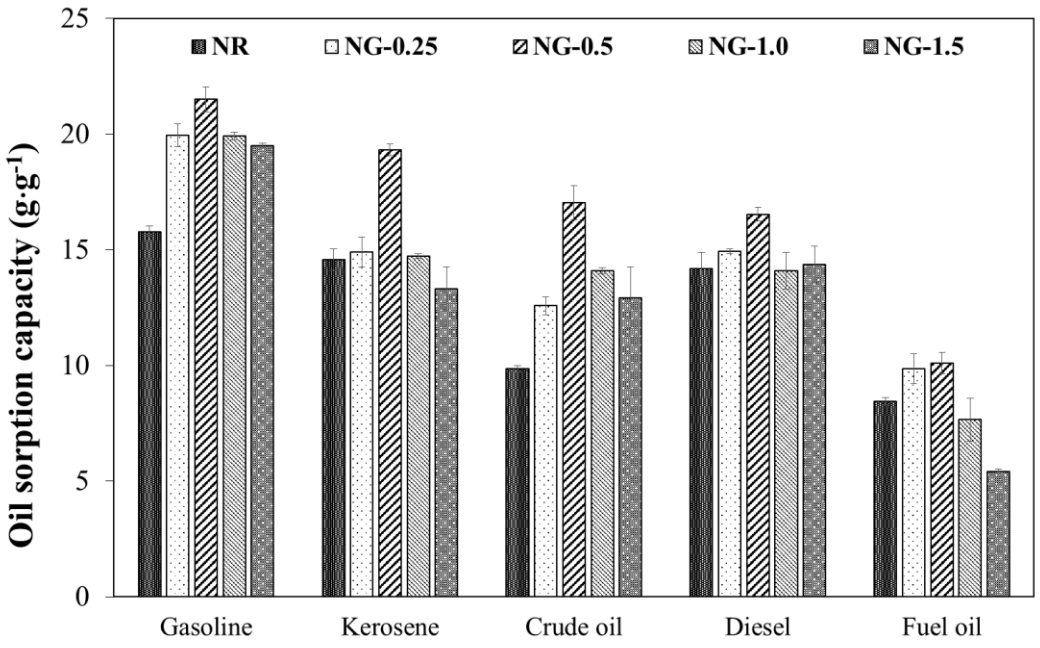

Figure 4.7 Adsorption capacities of the NR composite foams in different oils.

Figure 4.7 also shows the effect of the rGO content on the oil sorption capacities of the NR composite foams. The oil adsorption capacities of the NR foams increased with the increase of the rGO content. However, the oil adsorption capacities of the NR composite foams tended to be decreased after the rGO content was more than 0.5 phr. According to the morphology of NR composite foams, it revealed that the high rGO loading caused the formation of the big pores inside the foam matrix. The

large pores of NR composite foam could not capture and retain oil inside these pores, resulting in the decrease of oil adsorption performance (Ceylan et al., 2009; Pinto, Athanassiou, & Fragouli, 2016). Accordingly, the optimum condition to obtain the highest oil adsorption capacity of the NR composite foam was used of the rGO content at 0.5 phr.

4.4.2 Environmental effect

Generally, the crude oil frequently enters into the marine environment through the natural seepage and human activities. The oil spill accidents caused the harmful effect on human health and also the environmental qualities, thus the spilled oil should be removed immediately. The purpose in this part was to investigate the effect of the environmental conditions (temperature and turbulence) on the oil sorption capacity of the NR composite foams. The crude oil was chosen as a representative for oil sorption studying. As shown in Figure 4.8(a), with an increase in the temperature, the oil uptake in both NR composite foams was also increased due to the reduction of oil viscosity. The NR and NG-0.5 exhibited the highest oil adsorption capacity at 45 ^{o}C but the oil adsorption performance tended to decline when the temperature went beyond 45 ^{o}C. At high temperature, the viscosity of oil was decreased, resulting in the difficult for holding the oil inside the pores of the NR composite foams. Accordingly, the environmental temperature strongly affected on the oil sorption capacity of the NR composite foams.

When the oil was released into the sea surface, wind and wave also affected the oil dispersion. Thus, the effect of horizontal shaking or the turbulence on the oil sorption performance of NR and NG-0.5 was also studied as seen in Figure 4.8 (b). The oil sorption ability of NR and NG-0.5 could be enhanced by turbulence effect owing to the external force improved the diffusion of the oil droplet into the pores. Both NR and NG-0.5 foams had floated on the seawater during the turbulence

experiment, while some sorbents tended to sink into the seawater (Keshavarz et al., 2016). Therefore, it is interesting to note that NR composite foams could be appropriately used as the oil sorbent material under various environmental conditions.

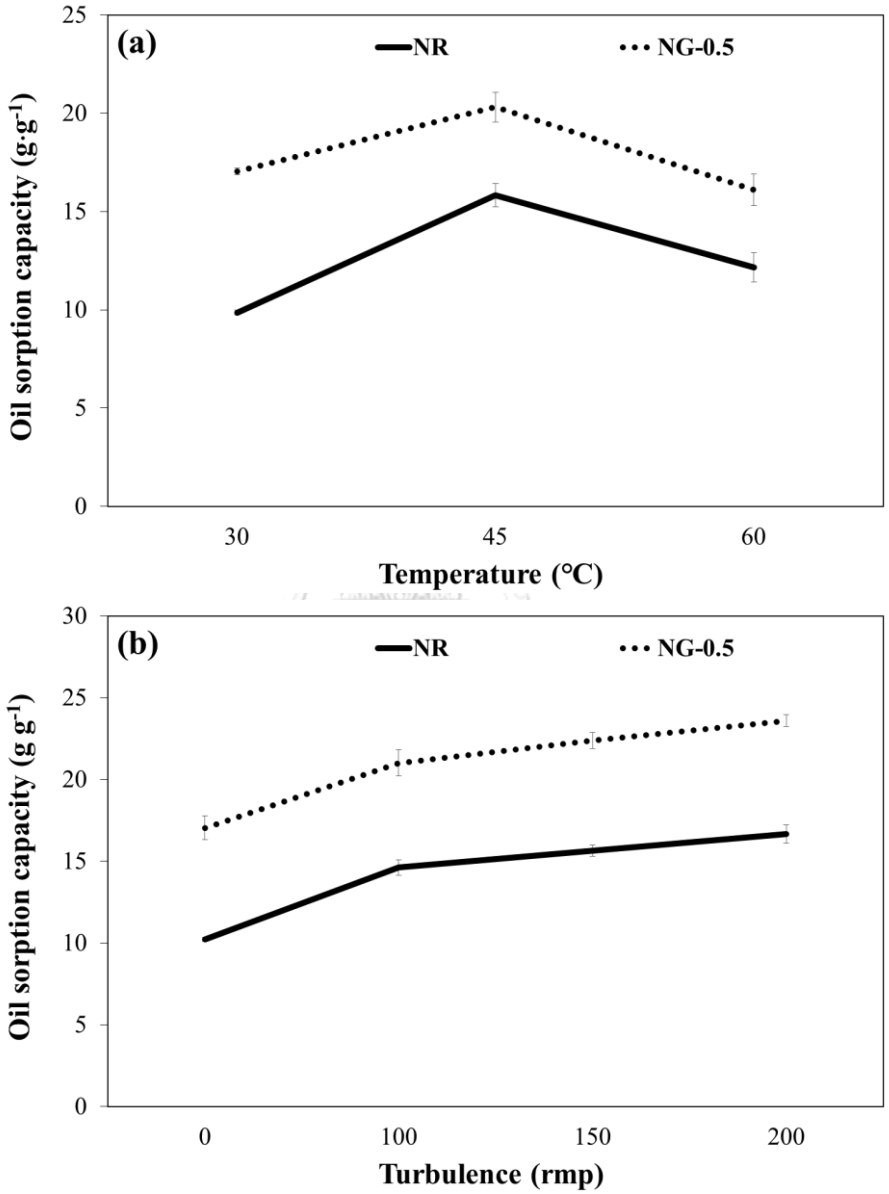

Figure 4.8 Effect of (a) temperature and (b) turbulence of the crude oil adsorption on the NR and NG-0.5 foams at room temperature.

4.4.3 Adsorption kinetic

Figure 4.9 shows the result of the oil adsorption capacity of the NR and NG-0.5 as a function of time. In both cases, the oil adsorption was increased with the increasing contact time and reached the equilibrium before 2 min. The oil adsorption capacities of the NR composite foams was higher than that of the NR foams because the presence of the rGO increased the surface area of the composite material.

Generally, the kinetic models have been proposed to predict the mechanism of the adsorption process. In order to investigate the adsorption kinetic of the crude oil on NR and NG-0.5, the obtained experimental data was used to further calculate the adsorption rate using three kinetic models: pseudo-first-order (Eq. 2.1), pseudo-second-order (Eq. 2.2) and Elovich equation (Eq. 2.3) models. These three models are mostly use to explain the surface reaction between adsorbate and adsorbent. While the intrapartical diffusion (Eq. 2.5) and liquid film diffusion (Eq. 2.6) are described the internal or external diffusion processes.

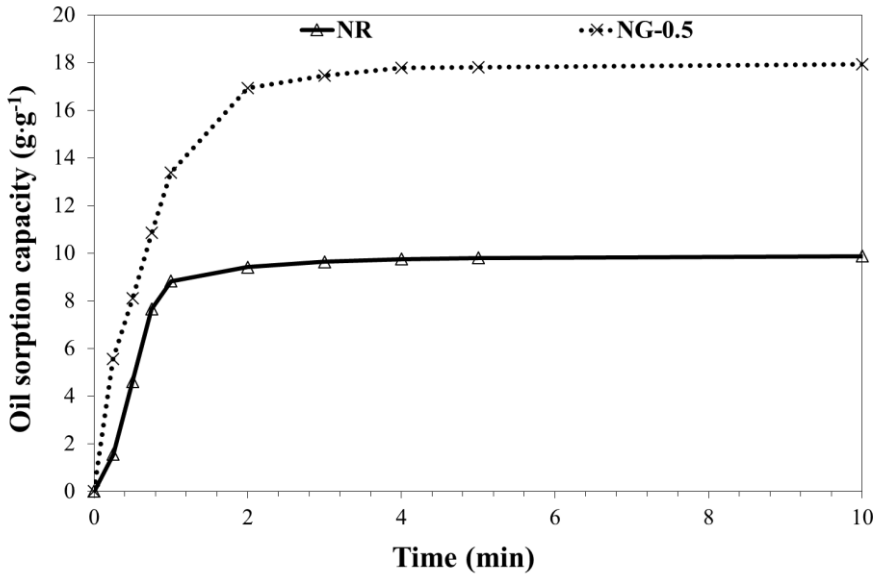

Figure 4.9 Effect of the contact time on the crude oil adsorption process at room temperature.

Figure 4.10 shows a comparison of the kinetic parameter for the crude oil on the NR and NG-0.5 foams. The pseudo-first-order was a plot of $ln(Q_e-Q_t)$ versus t that provided the slope of k_1 and the intercept of lnQ_e. A linear plot of t/Qt versus t of the pseudo-second-order model presented $1/Q_e$ as the slope and $1/k_2Q_e^2$ as the intercept. The Elovich equation which is mostly used to describe the kinetic of the chemisorption demonstrated the linear line of Q_t versus $ln\ t$. The $(1/b)$ and $(1/b)ln(ab)$ which were obtained from the slope and the intercept of the linear plot, respectively, referred to the number of site available for the adsorption and the adsorption quantity, respectively. The comparison of three kinetic models indicated that the correlation coefficient (R^2) for the pseudo-second-order of both NR (0.9997) and NG-0.5 (0.9998) were closely to 1. Moreover, the calculated Q_e values of NR and NG-0.5 were 9.8717 and 17.4520 g/g, respectively, which were in good agreement with the experimental data. The Q_e of NR and NG-0.5 which obtained from the experiment were 9.4728 and 16.8061 g/g, respectively. The calculated k_2 showed that the k_2 value of the NR (0.4772 $g \cdot g^{-1} \cdot min^{-1}$) was lower than that of NG-0.5 (0.5296 $g \cdot g^{-1} \cdot min^{-1}$), indicating that the oil adsorption of the NG-0.5 foam was faster than that of the NR foam. Based on the highest R^2 values of the pseudo-second-order, this model was the most suitable for describing the adsorption process of the crude oil on sorbent foams.

The adsorption process is controlled by one or more stages (e.g. external diffusion, pore diffusion). The above kinetic models only predicted the surface reaction, but did not identify the diffusion mechanism. Therefore, the intraparticle and liquid film diffusion models were also determined. Generally, the sorption of any sorbent from an aqueous phase to a solid phase is a multistep process, involving three consecutive steps. Firstly, the transportation of the adsorbate from a bulk solution to the external surface of the adsorbent was generally known as film diffusion. Next, the particle diffusion is related to the dispersion of the adsorbate into the pores. Finally, the adsorption step occurs on the interior surface of the adsorbent.

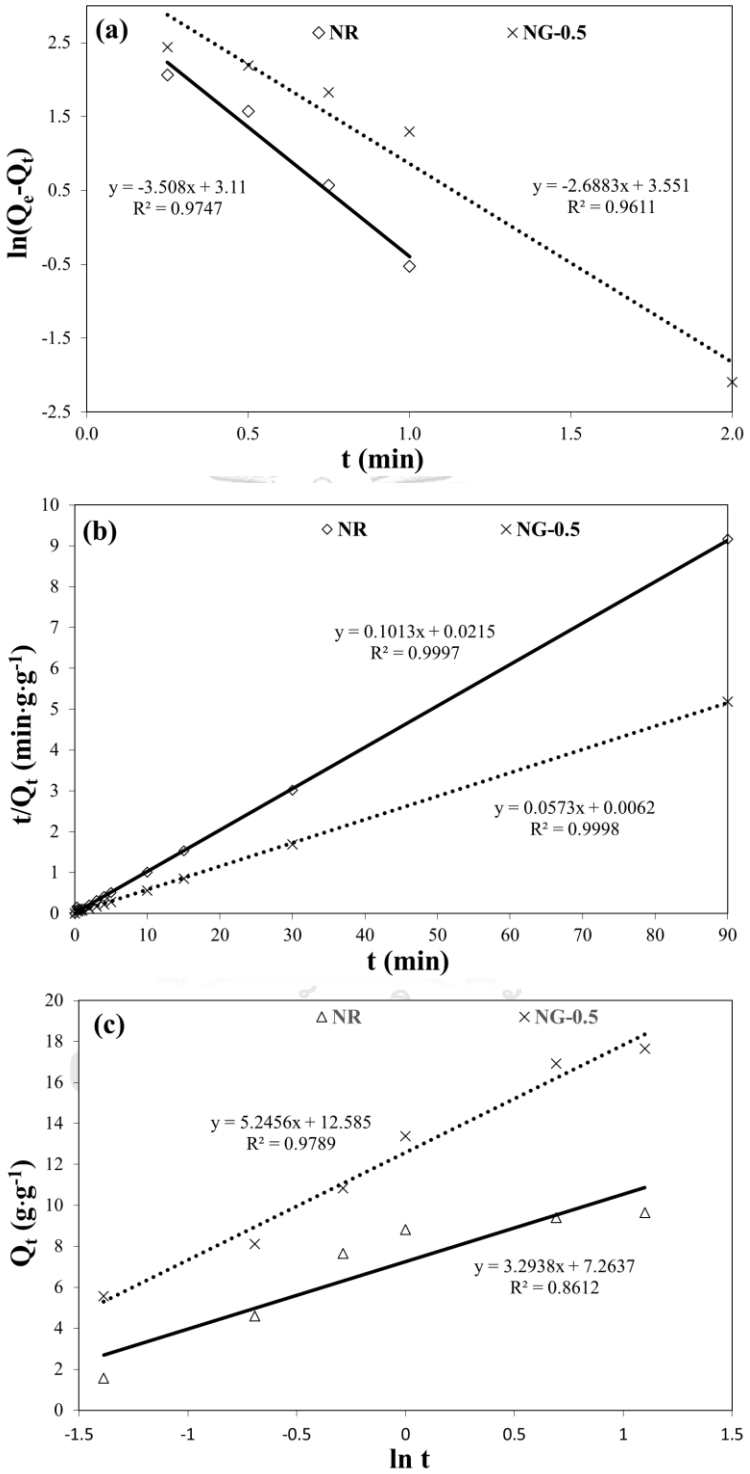

Figure 4.10 Comparison of the (a) pseudo-first-order, (b) pseudo-second-order and (c) Elovich models of crude oil adsorption on the NR and NG-0.5 at room temperature.

Table 4.6 summarizes the intraparicle diffusion constants and correlation coefficient (R^2) for the crude oil adsorption of NR and NG-0.5. The k_d values was divided into three steps which referred the different diffusion steps. The k_{d1} in the first stage of the NR and NG-0.5 foams were 8.1839 and 13.0910 $g \cdot g^{-1} \cdot s^{1/2}$, respectively. While the k_{d2} values in the second stage of NR and NG-0.5 were 1.4233 and 2.2765, respectively. These finding indicated that the first stage was quickly adsorbed due to the instantaneous adsorption or external surface adsorption. Then, the rates were significantly decreased corresponding to the gradual diffusion and adsorption into the pores and reached the final equilibrium. The different rates of adsorption indicated that the adsorption rate was initially faster and then slowed down when the time increased. Moreover, the intercept of stage (*I*), was non-zero that explained about the effect of the boundary layer (Hameed, Tan, & Ahmad, 2008). This result referred to the difference in mass transfer between the initial and final stages of the sorption process (I. Tan, A. Ahmad, & B. Hameed, 2009). The presence of the boundary effect showed that the intraparticle diffusion was not the only rate-limiting step but other processes might control the rate of adsorption.

Table 4.6 Intraparticle diffusion model constant and correlation coefficients for crude oil adsorption.

Sorbent materials	**Intraparticle diffusion model**								
	k_{1d}	k_{2d}	k_{3d}	I_1	I_2	I_3	$(R_1)^2$	$(R_2)^2$	$(R_3)^2$
NR	8.1839	1.4233	0.1489	0.5387	7.3986	9.4298	0.9077	1.0000	0.9989
NG-0.5	13.0910	2.2765	0.1298	0.4603	13.7020	17.519	0.9857	1.0000	0.8488

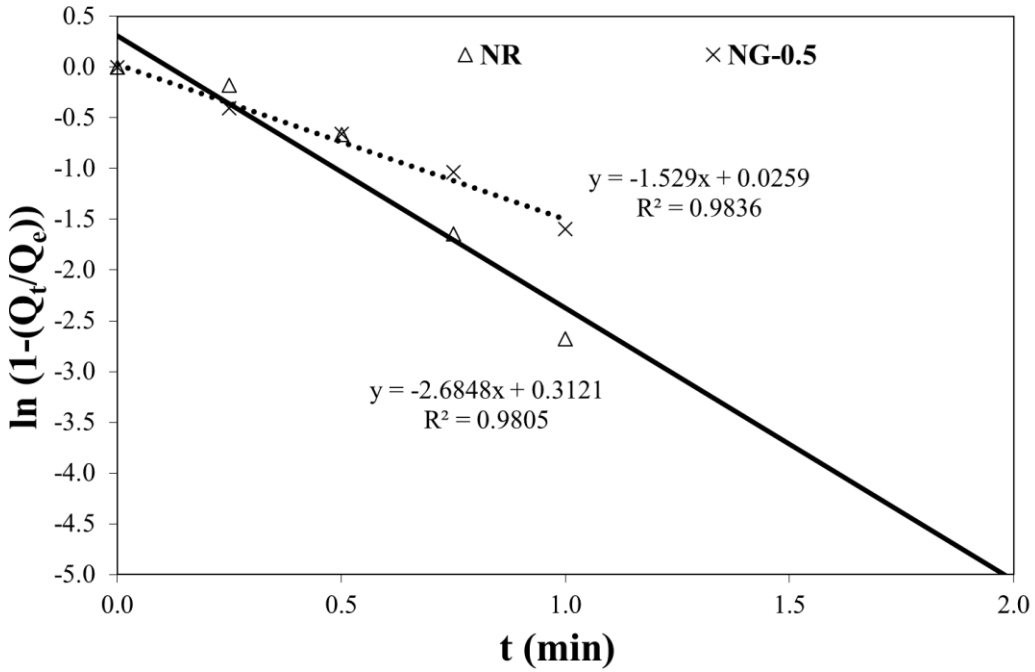

Figure 4.11 A Liquid film diffusion kinetic model of the NR and NG-0.5.

The liquid film diffusion was investigated to confirm that the surface diffusion process of the oil pollutant played a significant mechanism in the adsorption. The rate of the film diffusion (k_{fd}) could be calculated form the plot of $ln(1-Q_t/Q_e))$ as a function of t (min). The linearity of the plot for the liquid film diffusion model indicated the high applicability of this model (Figure 4.11). The liquid film diffusion mechanism produced a better R^2 values than the intraparticle diffusion model for both sorbent foams, indicating that the surface sorption was more predominant than the penetration into the pores of the materials. Additionally, the small intercept values also confirmed that the oil adsorption rate on the NR and NG-0.5 might depend on the thickness of the oil film surrounding the adsorbent. Finally, comparison between the intraparticle and the liquid film diffusion models suggested that the adsorption mechanism was governed by external mass transport where particle diffusion was the rate-determining step.

4.4.4 Adsorption isotherm

Figure 4.12 shows the plot of the oil sorption capacity on NR and NG-0.5 foams and the initial oil concentration because the oil residue was also useful to explain the oil sorption mechanism. This result exhibited that the oil sorption capacity of the composite foam was higher that of the NR foam. It was observed that the oil uptake of both sorbent foams increased with the initial oil concentration range from 5-50 g L^{-1}. The oil adsorption capacities of the NR and NG-0.5 foams reached equilibrium at 0.75 and 1.25 g/100mL, respectively. The addition of the small amount of oil enhanced the mass transfer into the sorbent foams, resulting in the higher oil adsorption capacity. However, at an excessing oil concentration of more than 1.25 g/100mL, the oil adsorption capacity was a constant. This result demonstrated that at the low initial concentration the adsorption sites were available for the adsorption of the oil on the sorbent matrix. On the contrary, the sorbent foams could not adsorb any more oil at the high initial oil concentration due to the saturation of the sorbent foams. Furthermore, the oil adsorption capacities of the NR and NG-0.5 were used to determine the adsorption isotherm. In this study, two common isotherm models, including Langmuir and Freundlich models, were investigated.

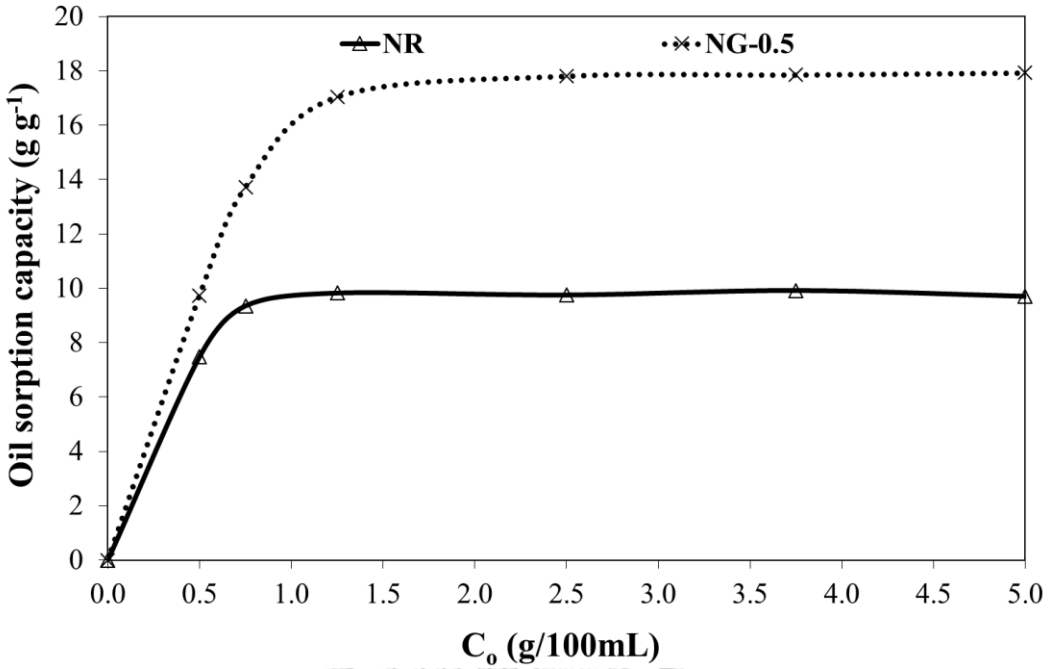

Figure 4.12 Effect of the initial oil concentration on the adsorption process.

Figure 4.13 shows a comparison between Langmuir and Freundlich models for the oil adsorption capacities of the NR and NG-0.5. The Langmuir isotherm assumes that the oil adsorption mechanism on the sorbent surface is monolayer and homogenous, whereas the Freundlich model defines the multilayer of the oil adsorption on the heterogeneous sorbent surface. When C_e/Q_e was plotted against C_e of the Langmuir isotherm, a straight line with the slope of $1/Q_m$ and the intercept of $1/Q_m k_L$ were obtained. The obtained Q_m values of the NR and NG-0.5 were 9.8039 and 17.9211 respectively, which were close to the experimental data. The k_L values corresponding to the Langmuir constant of the NR and NG-0.5 were found to be 102 and 186 (100L/g), respectively. This k_L values indicated the strong interface energy between the adsorbate and the adsorbent. Moreover, the separation factor (R_L) which is an essential characteristic of the Langmuir isotherm of both the NR (0.0192) and NG-0.5 (0.0132) demonstrated the favorable sorption of the crude oil on the sorbent foams. Accordingly, the correlation coefficient (R^2) of both sorbent foams were almost

equal to unity. This result indicated a monolayer of the adsorbed oil covered the entire surface of the NR composite foams

In case of Freundlich isotherm model, a plot of *Log* Q_e versus *Log* C_e gave a straight line with the slop of *1/n* and the intercept of *log* k_f. This isotherm provided the lower R^2 values than the Langmuir model. Furthermore, the *1/n* Freundlich constants of the NR and NG-0.5 was 0.0733 and 0.0675, respectively, indicating a normal Langmuir isotherm (Hameed et al., 2008). Therefore, these finding implied the possible monolayer of the crude oil covered on the NR composite foam surface through homogenous sites with uniform energy-level distribution.

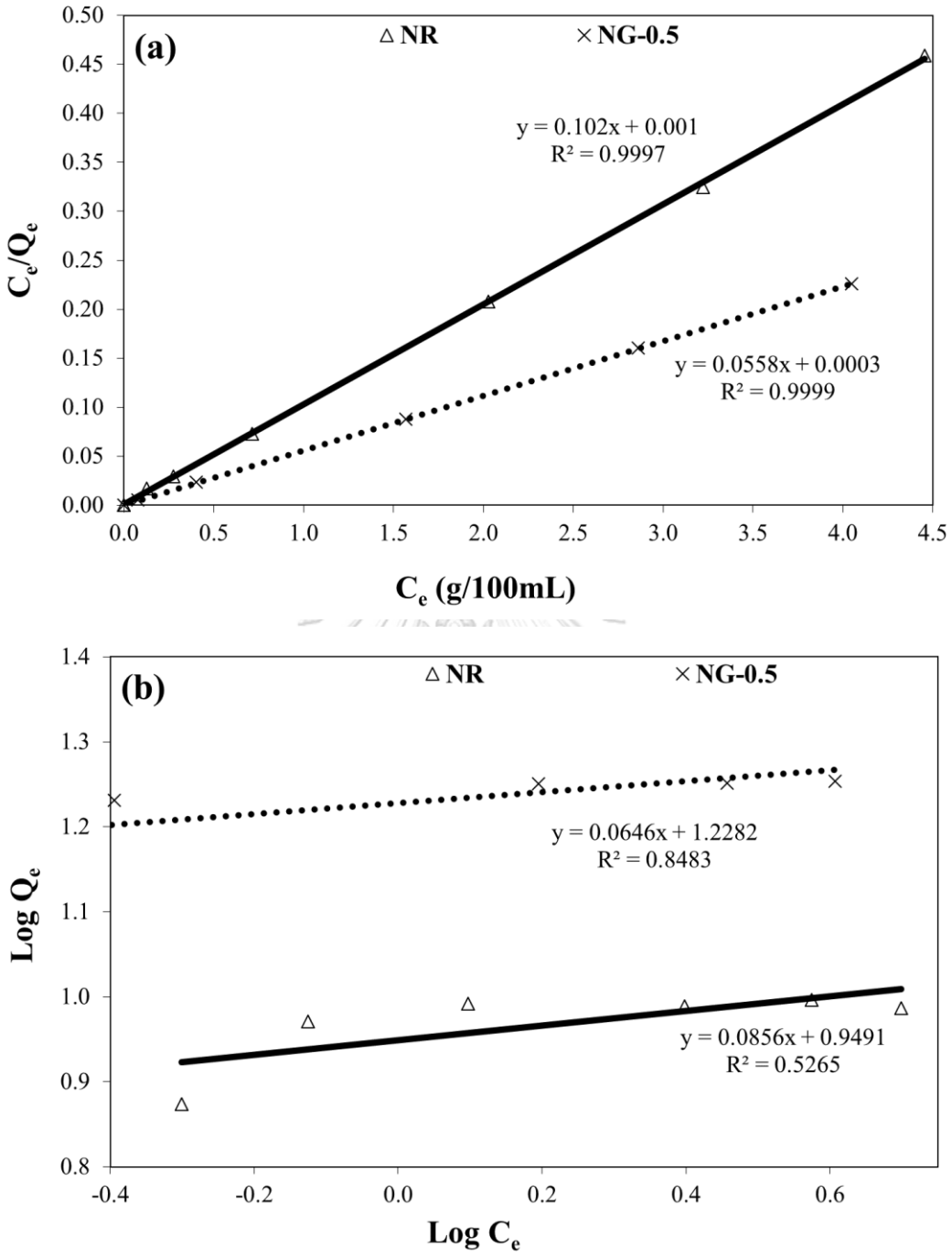

Figure 4. 13 Comparison between the (a) Langmuir and (b) Freundlich model with oil adsorption by the NR and NG-0.5 foams.

4.4.5 Reusability of the NR composite foams

The reusability of the oil sorbent materials is a critical criteria because it affects the cost of the material production and the waste management. Thus, the efficiencies of the sorbent foams during fifteen continuous cycles were investigated as shown in Figure 4.14. The result presented that both the NR and NG-0.5 was the high oil removal efficiency more than 90% in the first cycle. Then, their performances tended to decrease, corresponding to the incomplete oil desorption and then the removal efficiencies of the NR and NG-0.5 became stable up to fifteen cycles. The small residual oil was trapped inside the pore structure and the NR network after the oil adsorption process, resulting in the decrease of available sites of the NR composite foams. Another reason might be the loss of the rGO from the sorbent foams as the crude oil contained different types of inorganic and organic substances that adversely affected the bond between the rGO particles and the foams surface (Keshavarz et al., 2016). Additionally, the NR composite foam could be reused in several times due to the flexibility and elasticity of the NR properties. This result confirmed the reusability performance of the sorbent foams for oil removal from seawater.

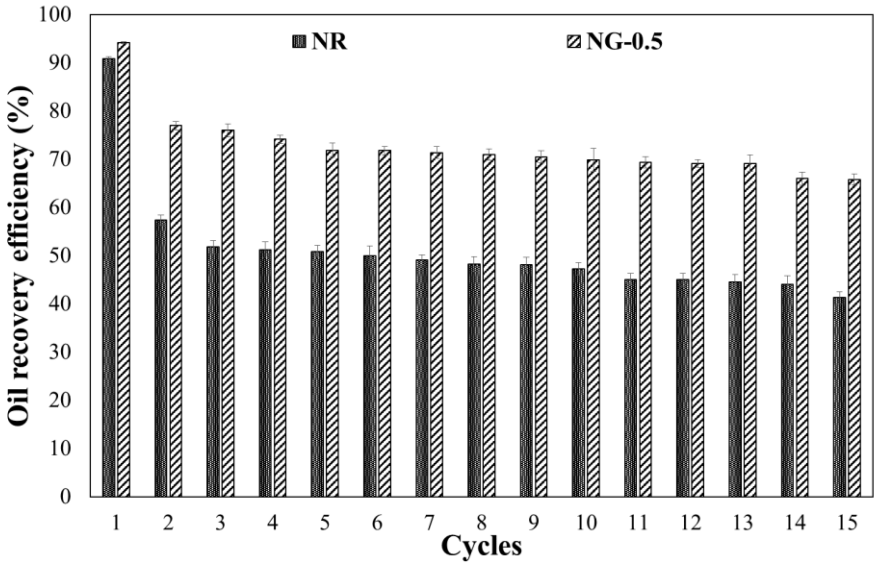

Figure 4.14 The oil recovery efficiency of NR and NG-0.5 foams.

Table 4.7 Comparative the oil adsorption capacity with other oil sorbent foam.

Sorbent foam	Oil type	Maximum oil adsorption (g g^{-1})	Reference
PUF-nanoclay (3 wt%)	Crude oil	21.5	(Nikkhah, Zilouei, Asadinezhad, & Keshavarz, 2015)
PUF-lignin (10 wt%)	Crude oil	28.9	(Santos, da Silva, Silva, Mussel, & Yoshida, 2017)
GN@PU	Lubricate oil	31.0	(Zhang, Liu, Ma, Nie, & Sui, 2017)
NR	Crude oil	9.8	This study
NG-0.5	Crude oil	17.9	This study

Table 4.7 shows a comparative of oil adsorption capacity of several oil sorbent materials. Several works suggested that the addition of filler could enhance the oil adsorption capacity of sorbent foam. This results demonstrated that the oil adsorption capacities of NR and NG-0.5 were lower than that of literatures. It is because the oil adsorption capacity is depending on several factors such as the hydrophobic property of sorbent materials or the characteristic of oil.

4.4.6 Production cost

Table 4.8 presents the estimation cost of NG-0.5 production. In this study, the size of prepared composite foam per batch was 30x30x0.7 cm^3, while the commercial sorbent was in a dimension of 40x50x0.2 cm^3. The estimated cost of composite foam in the lab scale (219.79 Baht/sheet) was found to be higher than that of commercial sorbent (35 Baht/sheet). However, based on this study the advantages of this foam are more flexibility and reusability than the commercial one.

Table 4.8 Estimation of NG-0.5 production cost

Chemical	Weight (unit/batch)	Chemical cost (Baht/batch)	Electricity cost (Baht/batch)			Cost (Baht/batch)
			Stirrer	Sonication	Oven	
rGO synthesis						
$KMnO_4$	9 g	19.44				
H_2SO_4	60 mL	9.25				
HCl	5 mL	0.67				
H_2O_2	20 mL	10.00				
L-AA	8 g	17.12				
NaOH	80 g	41.60				
Total cost		**98.08**	**8.81**[a]	**0.17**[b]	**71.54**[c]	**178.60**[e]
NR composite foam prepartion						
NR latex	250.50	26.50				
10% K-oleate	22.50	0.56				
50 % Sulfur	6.00	0.69				
50% ZDEC	3.00	0.50				
50% ZMBT	3.00	0.73				
50% Wingstay®L	3.00	1.12				
33% DPG	3.00	0.53				
50% ZnO	15.00	4.05				
12.5% SSF	12.00	0.54				
Total cost		**35.22**			**5.97**[d]	**41.19**[e]
NR composite foam preparation cost (178.60 + 41.19)						**219.79**

[a] **Electricity cost**: 1.05 kW*4.5 h = 4.73 kWh (1 kWh = 1.863 Baht)
= 4.73 kWH*1.863 = 8.81 Baht

[b] **Electricity cost**: 0.18 kW*0.5 h = 0.09 kWh (1 kWh = 1.863 Baht)
= 0.09 kWH*1.863 = 0.17 Baht

[c] **Electricity cost**:: 1.60 kW*24 h = 38.40 kWh (1 kWh = 1.863 Baht)
= 38.40 kWH*1.863 = 71.54 Baht

[d] **Electricity cost**: 1.60 kW*2 h = 3.20 kWh (1 kWh = 1.863 Baht)
= 3.20 kWH*1.863 = 5.97 Baht

[e] Cost = Chemical cost + Electricity cost

4.5 Weathering test

The weathering test was used to determine the degradation of polymer. The influence of weather on the visual appearances of the NR and NR composite foams was investigated by exposing NR and composite foam to QUV-A for 7 days. The original NR and NG-0.5 foams demonstrated light yellow color and light grey color, respectively. The result from the QUV-A exposure was reported in terms of greyscale level 1 with surface cracking. It was clearly to seen that the surface of NG-0.5 foam was more destroyed than that of the NR foam. This result implied that the presence of rGO filler affect the cracking of the NG-0.5 foam. Moreover, the surface cracking of the foams referred to the degradation of the elastomers by photo-oxidation. Therefore, prolonged outdoor exposure to UV was the limitation of the use of the NR composite foams.

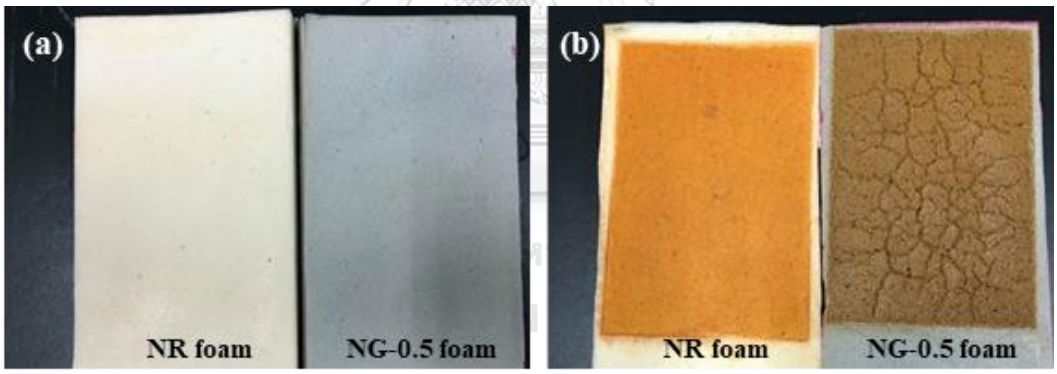

Figure 4.15 Physical appearance of the NR and NG-0.5 foams (a) before and (b) after expose use to UV-A for 7 days.

CHAPTER V

CONCLUSIONS AND RECOMMENDATIONS

5.1 Conclusion

In this study, the NR composite foams was successfully prepared by mixing the NR latex and the rGO filler. The rGO could be synthesized from the graphite waste through the oxidation and reduction processes. In the oxidation step, the thermal-sonication was an appropriate method provided the highest interlayer spacing of 0.73 nm for GO-H. The reduction of GO-H by 0.5 M L-AA could mostly remove the oxygen-containing groups. Moreover, the surface area of rGO-0.5 was increased up to 58.2 m^2 g^{-1} due to the exfoliation step. Finally, the obtained rGO-0.5 showed as the few layer structure with transparency and wrinkle. Therefore, rGO-0.5 was used as a representative in order to prepare NR composite foams.

The presence of rGO content in the NR foam directly affected the foam morphology and the oil sorption capacity. The addition of rGO-0.5 could enhance the pore size of NR foam led to the highest oil sorption capacities of various oil types including gasohol, kerosene, crude oil, diesel and the fuel oil. However, the NR composite foams was more selective with the low-viscous oils than the high viscous oil. The increase of the environmental temperature, which reduction of the oil viscosity, enhanced the oil adsorption capacity of the NR composite foams. Besides, the oil was easily dispersed into the foam by the stimulation of turbulence. The rate of oil adsorption process was also studied using five kinetic models. The pseudo-second-order model was found to be the best fit for the oil adsorption of the NR and NG-0.5 and the oil sorption mechanism was mainly controlled by the intraparticle diffusion as the rate-determining step. The equilibrium isotherm was described by the Langmuir isotherm model, indicating the maximum adsorption capacity were 9.8039 and 17.9211 g g^{-1} for NR and NG-0.5, respectively. Additionally, the sorbent foams could

be reused up to fifteen cycles. This study has significant environmental relevance such as (i) utilization of graphite waste for rGO synthesis (ii) increasing value of natural product (iii) positive results in oil adsorption of NR composite foam (iv) applicable large-scale production and (v) decreasing of waste management cost due to the reusability of sorbent foam. Therefore, the NR composite foams are proven to be a promising alternative sorbent for the oil spill removal.

5.2 Recommendations

5.2.1 The synthesized RGO in this study provided the low surface area, thus the synthesized method should be improved by using thermal reduction.

5.2.2 The high rGO loading in the NR latex, the rGO tended to precipitate in the bottom and caused the non-homogenous dispersion in the NR matrix. Hence, the further improvement, such as use of surfactant for the dispersion, modification of the filler surface and development of the NR composite formulation, should be studied.

5.2.3 As a result of the oil adsorption capacity, the NR composite foams had the oil adsorption efficiency of the high-viscous oils. Therefore, the adsorption of the high-viscous oil on the NR composite foam should be developed through increase of the pore size of the NR composite foams by adjusting the K-oleate ratio in the NR formulation.

5.2.4 The prepared sorbent foams were sensitive to the environmental condition, especially UV. Then the weathering resistance of the NR composite foams should be improved, such as addition of antioxidant agents.

REFERENCES

VITA

NAME	Siripak Songsaeng
DATE OF BIRTH	29 Apr 1994
PLACE OF BIRTH	Bangkok
INSTITUTIONS ATTENDED	She graduated her Bachelor's degree of Science, Faculty of Environment and Resources Studies, Mahidol University in 2016. She pursued her Master's degree in Internation Program in Hazardous Substance and Environmental Management, Graduate School, Chulalongkorn University in 2016.
PUBLICATION	Siripak Songsaeng, Patchanita Thamyongkit and Sirilux Poompradub. EFFECT OF FOAMING AGENT ON NATURAL RUBBER FOAM FOR OIL SPILL CLEANUP. The proceeding of The International Polymer Conference of Thailand (PCT-8) June 14-15, 2018 at Amari Watergate Bangkok Hotel, Bangkok Thailand.

REFERENCES

Abdolhosseinzadeh, S., Asgharzadeh, H., & Seop Kim, H. (2015). Fast and fully-scalable synthesis of reduced graphene oxide. *Sci Rep, 5*, 10160. doi:10.1038/srep10160

Abdullah, M., Rahmah, A. U., & Man, Z. (2010). Physicochemical and sorption characteristics of Malaysian Ceiba pentandra (L.) Gaertn. as a natural oil sorbent. *Journal of Hazardous Materials, 177*(1-3), 683-691.

Adebajo, M. O., Frost, R. L., Kloprogge, J. T., Carmody, O., & Kokot, S. (2003). Porous materials for oil spill cleanup: a review of synthesis and absorbing properties. *Journal of Porous materials, 10*(3), 159-170.

Akbari, A., Talebanfard, S., Hassan, A. J. P.-P. T., & Engineering. (2010). The effect of the structure of clay and clay modifier on polystyrene-clay nanocomposite morphology: A review. *49*(14), 1433-1444.

Al-Jammal, N., & Juzsakova, T. (2017). Review on the Effectiveness of Adsorbent Materials in Oil Spills Clean Up. *Sea, 25*, 36.

Al-Majed, A. A., Adebayo, A. R., & Hossain, M. E. (2012). A sustainable approach to controlling oil spills. *Journal of environmental management, 113*, 213-227.

Ali, N., El-Harbawi, M., Jabal, A. A., & Yin, C.-Y. J. E. t. (2012). Characteristics and oil sorption effectiveness of kapok fibre, sugarcane bagasse and rice husks: oil removal suitability matrix. *33*(4), 481-486.

Allen, A. J. S., Woodinville, WA. (1988). In-situ burning: a new technique for oil spill response.

Arayapranee, W. (2012). Rubber abrasion resistance. In *Abrasion Resistance of Materials*: InTech.

Asadpour, R., Sapari, N. B., Tuan, Z. Z., Jusoh, H., Riahi, A., & Uka, O. K. (2013). Application of Sorbent materials in Oil Spill management: A review. . *Caspian Journal of Applied Sciences Research, 2*(2).

Aunkor, M., Mahbubul, I., Saidur, R., & Metselaar, H. J. R. A. (2016). The green reduction of graphene oxide. *6*(33), 27807-27828.

Aunkor, M. T. H., Mahbubul, I. M., Saidur, R., & Metselaar, H. S. C. (2016). The green reduction of graphene oxide. *RSC Advances, 6*(33), 27807-27828. doi:10.1039/c6ra03189g

Ayalew, A., Gonte, R. R., & Balasubramanian, K. J. I. J. o. G. N. (2012). Development of polymer composite beads for dye adsorption. *4*(4), 440-454.

Azizian, S. J. J. o. c., & Science, I. (2004). Kinetic models of sorption: a theoretical analysis. *276*(1), 47-52.

Bacon, R., Farmer, E. J. R. C., & Technology. (1939). The interaction of maleic anhydride with rubber. *12*(2), 200-209.

Bansal, S., von Arnim, V., Stegmaier, T., & Planck, H. (2011). Effect of fibrous filter properties on the oil-in-water-emulsion separation and filtration performance. *Journal of Hazardous Materials, 190*(1-3), 45-50.

Barlow, F. W. (1988). *Rubber compounding: principles, materials, and techniques*: M. Dekker.

Barroso-Bujans, F., Fernandez-Alonso, F., Pomposo, J. A., Enciso, E., Fierro, J. L. G., & Colmenero, J. (2012). Tunable uptake of poly(ethylene oxide) by graphite-oxide-based materials. *Carbon, 50*(14), 5232-5241. doi:10.1016/j.carbon.2012.07.008

Behabtu, N., Lomeda, J. R., Green, M. J., Higginbotham, A. L., Sinitskii, A., Kosynkin, D. V., . . . Kesselman, E. J. N. n. (2010). Spontaneous high-concentration dispersions and liquid crystals of graphene. *5*(6), 406.

Behnood, R., Anvaripour, B., Jaafarzade Haghighi Fard, N., & Farasati, M. (2013). Application of natural sorbents in crude oil adsorption. *Iranian Journal of Oil & Gas Science and Technology, 2*(4), 1-11.

Bernard, H., & Jakobson, K. (1972). *Effectiveness of Devices for the Control And Clean up of Oil Spills.* Paper presented at the Offshore Technology Conference.

Bhuyan, M. S. A., Uddin, M. N., Islam, M. M., Bipasha, F. A., & Hossain, S. S. J. I. N. L. (2016). Synthesis of graphene. *6*(2), 65-83.

Board, M., Board, O. S., & Council, N. R. (2003). *Oil in the sea III: inputs, fates, and effects*: national academies Press.

Boysen, E., & Nancy, C. M. J. N. f. D., 2nd Edn., ISBN. (2009). Graphene: Sheets of carbon-based Nanoparticles. 978-970.

Brydson, J. A. (1978). *Rubber chemistry*: Applied Science Publishers.

Ceylan, D., Dogu, S., Karacik, B., Yakan, S. D., Okay, O. S., Okay, O. J. E. s., & technology. (2009). Evaluation of butyl rubber as sorbent material for the removal of oil and polycyclic aromatic hydrocarbons from seawater. *43*(10), 3846-3852.

Chabot, V., Higgins, D., Yu, A., Xiao, X., Chen, Z., & Zhang, J. (2014). A review of graphene and graphene oxide sponge: material synthesis and applications to energy and the environment. *Energy & Environmental Science, 7*(5), 1564. doi:10.1039/c3ee43385d

Chaitoglou, S. (2016). Growth Study and Characterization of Single Layer Graphene Structures Deposited on Copper Substrate by Chemical Vapor Deposition.

Chapman, A. J. T. (2007). Natural rubber and NR-based polymers: renewable materials with unique properties. *5*(8).

Chen, J., Yao, B., Li, C., & Shi, G. (2013). An improved Hummers method for eco-friendly synthesis of graphene oxide. *Carbon, 64*, 225-229. doi:10.1016/j.carbon.2013.07.055

Chiou, C. T. (2003). *Partition and adsorption of organic contaminants in environmental systems*: John Wiley & Sons.

Choi, H. M., Cloud, R. M. J. E. s., & technology. (1992). Natural sorbents in oil spill cleanup. *26*(4), 772-776.

Choi, W., Lahiri, I., Seelaboyina, R., Kang, Y. S. J. C. R. i. S. S., & Sciences, M. (2010). Synthesis of graphene and its applications: a review. *35*(1), 52-71.

Ciesielski, A. (1999). *An introduction to rubber technology*: iSmithers Rapra Publishing.

Clark, R. B., Frid, C., & Attrill, M. (1989). *Marine pollution* (Vol. 4): Clarendon Press Oxford.

Cornish, K. (2014). Biosynthesis of natural rubber (NR) in different rubber-producing species. In *Chemistry, Manufacture and Applications of Natural Rubber* (pp. 3-29): Elsevier.

Dąbrowski, A. J. A. i. c., & science, i. (2001). Adsorption—from theory to practice. *93*(1-3), 135-224.

Darmanin, T., & Guittard, F. (2015). Superhydrophobic and superoleophobic properties in nature. *Materials Today, 18*(5), 273-285.

Dave, D. A. E. G., & Ghaly, A. E. (2011). Remediation technologies for marine oil spills: A critical review and comparative analysis. . *American Journal of Environmental Sciences, 7*(5).

Davies, M. B., Partridge, D. A., & Austin, J. (2007). *Vitamin C: its chemistry and biochemistry*: royal society of chemistry.

De Silva, K., Huang, H.-H., Joshi, R., & Yoshimura, M. J. C. (2017). Chemical reduction of graphene oxide using green reductants. *119*, 190-199.

Doerffer, J. W. (2013). *Oil spill response in the marine environment*: Elsevier.

Dong, T., Xu, G., & Wang, F. (2015). Oil spill cleanup by structured natural sorbents made from cattail fibers. *Industrial Crops and Products, 76*, 25-33.

Donnet, J.-B., & Custodero, E. (2005). Reinforcement of elastomers by particulate fillers. In *Science and Technology of Rubber (Third Edition)* (pp. 367-400): Elsevier.

Doshi, B., Sillanpää, M., & Kalliola, S. (2018). A review of bio-based materials for oil spill treatment. *Water research, 135*, 262-277.

Emergency, U. S. E. P. A. O. o., Response, R., & Division, U. S. E. P. A. E. R. (1993). *Understanding oil spills and oil spill response* (Vol. 9200): The Office.

EO, O., FA, K., & DA, O. (2014). Techniques of Oil Spill Response in the sea. *IOSR Journal of Applied Physics, 6*, 36-41.

Fan, X., Peng, W., Li, Y., Li, X., Wang, S., Zhang, G., & Zhang, F. J. A. M. (2008). Deoxygenation of exfoliated graphite oxide under alkaline conditions: a green route to graphene preparation. *20*(23), 4490-4493.

Fernández-Merino, M. J., Guardia, L., Paredes, J., Villar-Rodil, S., Solís-Fernández, P., Martínez-Alonso, A., & Tascon, J. J. T. J. o. P. C. C. (2010). Vitamin C is an ideal substitute for hydrazine in the reduction of graphene oxide suspensions. *114*(14), 6426-6432.

Fingas, M. (2012). *The basics of oil spill cleanup*: CRC press.

Fingas, M. (2014). *Handbook of oil spill science and technology*: John Wiley & Sons.

Fingas, M. (2016). *Oil spill science and technology*: Gulf professional publishing.

Funck, A., Kaminsky, W. J. C. S., & Technology. (2007). Polypropylene carbon nanotube composites by in situ polymerization. *67*(5), 906-915.

Gandhi, M. R., Vasudevan, S., Shibayama, A., & Yamada, M. J. C. (2016). Graphene and Graphene-Based Composites: A Rising Star in Water Purification-A Comprehensive Overview. *1*(15), 4358-4385.

Gao, J., Liu, F., Liu, Y., Ma, N., Wang, Z., & Zhang, X. J. C. o. M. (2010). Environment-friendly method to produce graphene that employs vitamin C and amino acid. *22*(7), 2213-2218.

Ge, J., Zhao, H. Y., Zhu, H. W., Huang, J., Shi, L. A., & Yu, S. H. (2016). Advanced sorbents for Oil-Spill cleanup: Recent advances and future perspectives. *Advanced materials, 28*(47), 10459-10490.

Gong, J. R. (2011). Graphene-Synthesis, Characterization, Properties and Applications.

Gupta, S., & Tai, N.-H. (2016). Carbon materials as oil sorbents: a review on the synthesis and performance. *Journal of Materials Chemistry A, 4*(5), 1550-1565.

Hameed, B., Tan, I., & Ahmad, A. J. C. E. J. (2008). Adsorption isotherm, kinetic modeling and mechanism of 2, 4, 6-trichlorophenol on coconut husk-based activated carbon. *144*(2), 235-244.

Hariwongsanupab, N. (2017). *Development of green natural rubber composites: Effect of nitrile rubber, fiber surface treatment and carbon black on properties of pineapple leaf fiber reinforced natural rubber composites.* Université de Haute Alsace-Mulhouse,

Ho, Y.-S., & McKay, G. J. P. b. (1999). Pseudo-second order model for sorption processes. *34*(5), 451-465.

Hou, D., Liu, Q., Wang, X., Quan, Y., Qiao, Z., Yu, L., & Ding, S. J. J. o. M. (2018). Facile synthesis of graphene via reduction of graphene oxide by artemisinin in ethanol.

Howe, J. Y., Cavin, B. O., Drakeford, A. E., Peascoe, R. A., Zontek, T. L., Miller, D. J. J. I. I. R., & Discussion. (2007). Influence of Bulk Graphite Thickness on the Accuracy of X-Ray Diffraction Measurement. 1-5.

Hu, Z., Chen, Y., & Chen, H. (2011). Comparative study on the formation mechanism of graphene oxide-derived carbon/Pd composites. *Micro & Nano Letters, 6*(8), 709. doi:10.1049/mnl.2011.0354

Hummers Jr, W. S., & Offeman, R. E. J. J. o. t. a. c. s. (1958). Preparation of graphitic oxide. *80*(6), 1339-1339.

Iakovleva, E. J. A. U. L. (2018). Novel sorbents from low-cost materials for water treatment.

Idowu, A., Boesl, B., & Agarwal, A. J. C. (2018). 3D graphene foam-reinforced polymer composites–A review.

Idris, J., Eyu, G., Mansor, A., Ahmad, Z., & Chukwuekezie, C. J. T. S. W. J. (2014). A preliminary study of biodegradable waste as sorbent material for oil-spill cleanup. *2014*.

Ivshina, I. B., Kuyukina, M. S., Krivoruchko, A. V., Elkin, A. A., Makarov, S. O., Cunningham, C. J., . . . Philp, J. C. (2015). Oil spill problems and sustainable response strategies through new technologies. *Environmental Science: Processes & Impacts, 17*(7), 1201-1219.

Johns, J., & Rao, V. J. I. J. o. P. M. (2011). Adsorption of methylene blue onto natural rubber/chitosan blends. *60*(10), 766-775.

Jokuty, P., Whiticar, S., Wang, Z., Fingas, M., Fieldhouse, B., Lambert, P., & Mullin, J. (1999). Properties of crude oils and oil products. *EE-165. Ottawa, Ontario: Environment Canada*.

Kalaitzidou, K., Fukushima, H., Drzal, L. T. J. C. P. A. A. S., & Manufacturing. (2007). Mechanical properties and morphological characterization of exfoliated graphite–polypropylene nanocomposites. *38*(7), 1675-1682.

Kampa, A. L., Casarotto, T., Maria, A., Woodard-Wallace, C. G., & Whyte, J. S. (2014). Documentation and analysis of the Rayong oil spill: characterizing the health, economic, and social impacts of the incident and response.

Kemp, K. C., Seema, H., Saleh, M., Le, N. H., Mahesh, K., Chandra, V., & Kim, K. S. J. N. (2013). Environmental applications using graphene composites: water remediation and gas adsorption. *5*(8), 3149-3171.

Keshavarz, A., Zilouei, H., Abdolmaleki, A., Asadinezhad, A., Nikkhah, A. J. I. j. o. e. s., & technology. (2016). Impregnation of polyurethane foam with activated carbon for enhancing oil removal from water. *13*(2), 699-710.

Kuilla, T., Bhadra, S., Yao, D., Kim, N. H., Bose, S., & Lee, J. H. J. P. i. p. s. (2010). Recent advances in graphene based polymer composites. *35*(11), 1350-1375.

Kun, P., Wéber, F., & Balázsi, C. J. C. E. J. o. C. (2011). Preparation and examination of multilayer graphene nanosheets by exfoliation of graphite in high efficient attritor mill. *9*(1), 47-51.

Langmuir, I. J. J. o. t. A. C. s. (1918). The adsorption of gases on plane surfaces of glass, mica and platinum. *40*(9), 1361-1403.

Largitte, L., Pasquier, R. J. C. E. R., & Design. (2016). A review of the kinetics adsorption models and their application to the adsorption of lead by an activated carbon. *109*, 495-504.

Li, J., Sham, M. L., Kim, J.-K., Marom, G. J. C. S., & Technology. (2007). Morphology and properties of UV/ozone treated graphite nanoplatelet/epoxy nanocomposites. *67*(2), 296-305.

Li, J., Zeng, X., Ren, T., & Van Der Heide, E. J. L. (2014). The preparation of graphene oxide and its derivatives and their application in bio-tribological systems. *2*(3), 137-161.

Limousin, G., Gaudet, J.-P., Charlet, L., Szenknect, S., Barthes, V., & Krimissa, M. J. A. g. (2007). Sorption isotherms: a review on physical bases, modeling and measurement. *22*(2), 249-275.

Ltd., I. T. O. P. F. (2012). *Response to Marine Oil Spills* (2nd Edition ed.).

Michel, J., & Fingas, M. (2016). Oil Spills: Causes, Consequences, Prevention, and Countermeasures. In *Fossil Fuels: Current Status and Future Directions* (pp. 159-201): World Scientific.

Mohajeri, L., Aziz, H. A., Zahed, M. A., & Isa, M. H. (2008). *Oil spill cleanup and response in Malaysian shorelines*. Paper presented at the Technology and Innovation for Sustainable Development Conference (TISD2008)

Mohan, V. B., Lau, K.-t., Hui, D., & Bhattacharyya, D. J. C. P. B. E. (2018). Graphene-based materials and their composites: a review on production, applications and product limitations.

Monks, P., Farmer, J. G., Graham, M., De Mora, S. J., Pulford, I., & Hulsall, C. (2007). *Principles of Environmental Chemistry*: Royal Society of Chemistry.

Moriwaki, H., Kitajima, S., Kurashima, M., Hagiwara, A., Haraguchi, K., Shirai, K., . . . Kiguchi, K. J. J. o. H. M. (2009). Utilization of silkworm cocoon waste as a sorbent for the removal of oil from water. *165*(1-3), 266-270.

Musin, E. (2013). Adsorption Modelling.

Nair, A., & Joseph, R. (2014). Eco-friendly bio-composites using natural rubber (NR) matrices and natural fiber reinforcements. In *Chemistry, Manufacture and Applications of Natural Rubber* (pp. 249-283): Elsevier.

Nair, K. P. (2010). *The agronomy and economy of important tree crops of the developing world*: Elsevier.

Najib, N., Ariff, Z. M., Bakar, A., Sipaut, C. S. J. M., & Design. (2011). Correlation between the acoustic and dynamic mechanical properties of natural rubber foam: Effect of foaming temperature. *32*(2), 505-511.

National Academies of Sciences, E., & Medicine. (2016). *Spills of Diluted Bitumen from Pipelines: A Comparative Study of Environmental Fate, Effects, and Response*: National Academies Press.

Nikkhah, A. A., Zilouei, H., Asadinezhad, A., & Keshavarz, A. J. C. E. J. (2015). Removal of oil from water using polyurethane foam modified with nanoclay. *262*, 278-285.

Nishi, Y., Iwashita, N., Sawada, Y., & Inagaki, M. (2002). Sorption kinetics of heavy oil into porous carbons. *Water research, 36*(20), 5029-5036.

Novoselov, K. S., Geim, A. K., Morozov, S. V., Jiang, D., Zhang, Y., Dubonos, S. V., . . . Firsov, A. A. J. s. (2004). Electric field effect in atomically thin carbon films. *306*(5696), 666-669.

Nugrahenny, A. T. U., Kim, J., Kim, S.-K., Peck, D.-H., Yoon, S.-H., & Jung, D.-H. (2014). Preparation and application of reduced graphene oxide as the conductive material for capacitive deionization. *Carbon letters, 15*(1), 38-44. doi:10.5714/cl.2014.15.1.038

Nwadiogbu, J. O., Ajiwe, V. I. E., & Okoye, P. A. C. (2018). Removal of crude oil from aqueous medium by sorption on hydrophobic corncobs: Equilibrium and kinetic studies. *Journal of Taibah University for Science, 10*(1), 56-63. doi:10.1016/j.jtusci.2015.03.014

Nwadiogbu, J. O., Okoye, P. A., Ajiwe, V. I., & Nnaji, N. J. (2014). Hydrophobic treatment of corn cob by acetylation: kinetics and thermodynamics studies. *Journal of Environmental Chemical Engineering, 2*(3), 1699-1704.

Parker, J. G. (1997). Oil Spill Response. *The Global Environment: Science, Technology and Management*, 955-972.

Paulauskiene, T. J. E. S., & Research, P. (2018). Ecologically friendly ways to clean up oil spills in harbor water areas: crude oil and diesel sorption behavior of natural sorbents. *25*(10), 9981-9991.

Pei, S., & Cheng, H.-M. J. C. (2012). The reduction of graphene oxide. *50*(9), 3210-3228.

Perera, D., Kumanayaka, T., & Walpalage, S. J. I. J. S. R. (2015). Effect of zeolite on the properties of natural rubber foams. *5*, 1-4.

Phinyocheep, P. (2014). Chemical modification of natural rubber (NR) for improved performance. In *Chemistry, manufacture and applications of natural rubber* (pp. 68-118): Elsevier.

Phiri, J., Gane, P., Maloney, T. C. J. M. S., & B, E. (2017). General overview of graphene: Production, properties and application in polymer composites. *215*, 9-28.

Pinto, J., Athanassiou, A., & Fragouli, D. J. J. o. P. D. A. P. (2016). Effect of the porous structure of polymer foams on the remediation of oil spills. *49*(14), 145601.

Poompradub, S. (2014). Soft bio-composites from natural rubber (NR) and marine products. In *Chemistry, Manufacture and Applications of Natural Rubber* (pp. 303-324): Elsevier.

Puskas, J., Chiang, K., & Barkakaty, B. (2014). Natural rubber (NR) biosynthesis: perspectives from polymer chemistry. In *Chemistry, Manufacture and Applications of Natural Rubber* (pp. 30-67): Elsevier.

Qiu, H., Lv, L., Pan, B.-c., Zhang, Q.-j., Zhang, W.-m., & Zhang, Q.-x. J. J. o. Z. U.-S. A. (2009). Critical review in adsorption kinetic models. *10*(5), 716-724.

Radhika, M., & Palanivelu, K. J. J. o. h. m. (2006). Adsorptive removal of chlorophenols from aqueous solution by low cost adsorbent—Kinetics and isotherm analysis. *138*(1), 116-124.

Rao, C., Maitra, U., Matte, H. J. G., GmbH, W.-V. V., & Co. KGaA: Weinheim, G. (2012). Synthesis, characterization, and selected properties of graphene. 1-47.

Ratcha, A., Samart, C., Yoosuk, B., Sawada, H., Reubroycharoen, P., & Kongparakul, S. (2015). Polyisoprene modified poly(alkyl acrylate) foam as oil sorbent material. *Journal of Applied Polymer Science, 132*(42), n/a-n/a. doi:10.1002/app.42688

Repo, E. (2011). *EDTA-and DTPA-functionalized silica gel and chitosan adsorbents for the removal of heavy metals from aqueous solutions*: Lappeenranta University of TechnologyLaboratory of Green Chemistry.

Riyajan, S., & Sakdapipanich, J. J. K. K., Gummi, Kunststoffe. (2006). Cationic cyclization of deproteinized natural rubber latex using sulfuric acid. *59*(3), 104-109.

Roberts, A. D. (1988). *Natural rubber science and technology*: Oxford University Press.

Sakdapipanich, J. T., & Rojruthai, P. (2012). Molecular structure of natural rubber and its characteristics based on recent evidence. In *Biotechnology-Molecular Studies and Novel Applications for Improved Quality of Human Life*: InTech.

Sakthivel, T., Reid, D. L., Goldstein, I., Hench, L., & Seal, S. (2013). Hydrophobic high surface area zeolites derived from fly ash for oil spill remediation. *Environmental science & technology, 47*(11), 5843-5850.

Saleem, J., Riaz, M. A., & Gordon, M. (2018). Oil sorbents from plastic wastes and polymers: a review. *Journal of Hazardous Materials, 341*, 424-437.

Santos, O., da Silva, M. C., Silva, V., Mussel, W., & Yoshida, M. J. J. o. h. m. (2017). Polyurethane foam impregnated with lignin as a filler for the removal of crude oil from contaminated water. *324*, 406-413.

Schratzberger, M., Daniel, F., Wall, C. M., Kilbride, R., Macnaughton, S. J., Boyd, S. E., . . . Swannell, R. P. J. (2003). Response of estuarine meio- and macrofauna to in situ bioremediation of oil-contaminated sediment. *Marine Pollution Bulletin, 46*(6), 430-443.

Sentheshanmuganathan, S., Yapa, P., Nadarajah, M., & Kasinathan, S. (1975). *Some aspects of lipid chemistry of natural rubber [Hevea].* Paper presented at the International Rubber Conference, Kuala Lumpur (Malaysia), 20 Oct 1975.

Shams, S. S., Zhang, R., & Zhu, J. J. M. S.-P. (2015). Graphene synthesis: a Review. *33*(3), 566-578.

Silva, M., Alves, N. M., & Paiva, M. C. J. P. f. A. T. (2018). Graphene-polymer nanocomposites for biomedical applications. *29*(2), 687-700.

Sing, K. S. J. P., & chemistry, a. (1985). Reporting physisorption data for gas/solid systems with special reference to the determination of surface area and porosity (Recommendations 1984). *57*(4), 603-619.

Singh, V., Kendall, R. J., Hake, K., Ramkumar, S. J. I., & Research, E. C. (2013). Crude oil sorption by raw cotton. *52*(18), 6277-6281.

Speight, J. G. (2014). *The chemistry and technology of petroleum*: CRC press.

Speight, J. G. (2016). *Environmental Organic Chemistry for Engineers*: Butterworth-Heinemann.

Sweetman, M., May, S., Mebberson, N., Pendleton, P., Vasilev, K., Plush, S., & Hayball, J. J. C. (2017). Activated carbon, carbon nanotubes and graphene: Materials and composites for advanced water purification. *3*(2), 18.

Tan, I., Ahmad, A., & Hameed, B. (2009). Adsorption isotherms, kinetics, thermodynamics and desorption studies of 2, 4, 6-trichlorophenol on oil palm empty fruit bunch-based activated carbon. *Journal of Hazardous Materials, 164*(2-3), 473-482.

Tan, I., Ahmad, A., & Hameed, B. J. J. o. H. M. (2009). Adsorption isotherms, kinetics, thermodynamics and desorption studies of 2, 4, 6-trichlorophenol on oil palm empty fruit bunch-based activated carbon. *164*(2-3), 473-482.

Tewari, S., & Sirvaiya, A. (2015). Oil spill remediation and its regulation. *International Journal of Engineering Research and General Science, 1*(6), 1-7.

Thakur, S., & Karak, N. J. C. (2015). Alternative methods and nature-based reagents for the reduction of graphene oxide: A review. *94*, 224-242.

Tour, J. M. J. C. o. M. (2013). Top-down versus bottom-up fabrication of graphene-based electronics. *26*(1), 163-171.

Van Veersen, G. J. R. C., & Technology. (1951). The structure of cyclized rubber. *24*(4), 957-969.

Venkatanarasimhan, S., & Raghavachari, D. J. J. o. M. C. A. (2013). Epoxidized natural rubber–magnetite nanocomposites for oil spill recovery. *1*(3), 868-876.

Ventikos, N. P., Vergetis, E., Psaraftis, H. N., & Triantafyllou, G. (2004). A high-level synthesis of oil spill response equipment and countermeasures. *Journal of Hazardous Materials, 107*(1-2), 51-58.

Wahi, R., Chuah, L. A., Choong, T. S. Y., Ngaini, Z., & Nourouzi, M. M. (2013). Oil removal from aqueous state by natural fibrous sorbent: an overview. *Separation and Purification Technology, 113*, 51-63.

Wang, X., Liu, B., Lu, Q., & Qu, Q. J. J. o. C. A. (2014). Graphene-based materials: Fabrication and application for adsorption in analytical chemistry. *1362*, 1-15.

Warren-Thomas, E., Dolman, P. M., & Edwards, D. P. (2015). Increasing demand for natural rubber necessitates a robust sustainability initiative to mitigate impacts on tropical biodiversity. *Conservation Letters, 8*(4), 230-241.

White, I. C. (2000). Oil spill response: experience, trends and challenges. *Ports & Harbors*.

Wipatkrut, P., & Poompradub, S. (2017). Exfoliation approach for preparing high conductive reduced graphite oxide and its application in natural rubber composites. *Materials Science and Engineering: B, 218*, 74-83. doi:10.1016/j.mseb.2017.02.007

Wojtoniszak, M., & Mijowska, E. (2012). Controlled oxidation of graphite to graphene oxide with novel oxidants in a bulk scale. *J Nanopart Res, 14*(11), 1248. doi:10.1007/s11051-012-1248-z

Wu, B., & Zhou, M. J. W. M. (2009). Recycling of waste tyre rubber into oil absorbent. *29*(1), 355-359.

Wu, D., Fang, L., Qin, Y., Wu, W., Mao, C., & Zhu, H. J. M. p. b. (2014). Oil sorbents with high sorption capacity, oil/water selectivity and reusability for oil spill cleanup. *84*(1-2), 263-267.

Xiao, M., Sun, L., Liu, J., Li, Y., & Gong, K. J. P. (2002). Synthesis and properties of polystyrene/graphite nanocomposites. *43*(8), 2245-2248.

Xiaowei, L., Jean-Charles, R., & Suyuan, Y. (2004). Effect of temperature on graphite oxidation behavior. *Nuclear Engineering and Design, 227*(3), 273-280. doi:10.1016/j.nucengdes.2003.11.004

Xue, Z., Cao, Y., Liu, N., Feng, L., & Jiang, L. (2014). Special wettable materials for oil/water separation. *Journal of Materials Chemistry A, 2*(8), 2445-2460.

Yi, M., & Shen, Z. J. J. o. M. C. A. (2015). A review on mechanical exfoliation for the scalable production of graphene. *3*(22), 11700-11715.

Zhang, X., Liu, D., Ma, Y., Nie, J., & Sui, G. J. A. S. S. (2017). Super-hydrophobic graphene coated polyurethane (GN@ PU) sponge with great oil-water separation performance. *422*, 116-124.

Zheng, Q., & Kim, J.-K. (2015). Synthesis, structure, and properties of graphene and graphene oxide. In *Graphene for Transparent Conductors* (pp. 29-94): Springer.

Zhu, H., Qiu, S., Jiang, W., Wu, D., & Zhang, C. (2011). Evaluation of electrospun polyvinyl chloride/polystyrene fibers as sorbent materials for oil spill cleanup. *Environmental science & technology, 45*(10), 4527-4531.

Zhu, H., Qiu, S., Jiang, W., Wu, D., Zhang, C. J. E. s., & technology. (2011). Evaluation of electrospun polyvinyl chloride/polystyrene fibers as sorbent materials for oil spill cleanup. *45*(10), 4527-4531.

Zhu, X., Venosa, A. D., Suidan, M. T., & Lee, K. (2001). Guidelines for the bioremediation of marine shorelines and freshwater wetlands. *US Environmental Protection Agency*.

Zweben, C. J. M. E. H. (2014). Composite materials. 1-37.

Appendix

Table A.1 Composition of graphite waste

Samples	Composition (ppm)								
	C	S	Cl	Si	Fe	Zn	Ca	K	Cu
Graphite waste	~100%	42.9	98.9	59.7	115.0	63.1	183.0	154.0	6.0

Table A.2 Oil adsorption capacity of NR composite foams.

Samples	Gasoline				Kerosene				Crude oil			
	W_0	W_1	Q	SD	W_0	W_1	Q	SD	W_0	W_1	Q	SD
NR	0.0700	1.2730	17.1857	0.5716	0.0540	0.8610	15.0340	0.3325	0.0580	0.6320	9.8850	0.9124
	0.0560	1.0250	17.3036		0.0610	0.9370	14.4830		0.0600	0.5770	8.6760	
	0.0580	1.0260	16.6897		0.0560	0.8410	14.1020		0.0560	0.6040	9.7150	
	0.0620	1.0550	16.0161		0.0560	0.8690	14.6030		0.0570	0.5050	7.8820	
	0.0670	1.2320	17.3881		0.0510	0.7970	14.5400		0.0500	0.5530	9.9660	
	Average		16.9166		Average		14.5524		Average		9.2248	
NG-0.25	0.0640	1.3120	19.5000	0.7167	0.0570	0.9190	15.2050	1.0324	0.0520	0.8770	15.8654	1.2491
	0.0530	1.1250	20.2264		0.0520	0.8410	15.3380		0.0580	0.8760	14.1034	
	0.0650	1.3100	19.1538		0.0530	0.9600	17.0190		0.0500	0.8717	16.4340	
	0.0530	1.0250	18.3396		0.0560	0.9280	15.6220		0.0550	0.8770	14.9455	
	0.0570	1.1280	18.7895		0.0540	0.8210	14.1460		0.0570	0.8193	13.3737	
	Average		19.2019		Average		15.4660		Average		14.9444	
NG-0.5	0.0530	1.1950	21.5472	0.6883	0.0530	1.0570	18.9434	1.3534	0.0600	1.0090	15.9360	0.7302
	0.0510	1.1380	21.3137		0.0580	1.0410	16.9483		0.0590	1.0950	17.6520	
	0.0510	1.0850	20.2745		0.0510	1.1050	20.6667		0.0550	0.9690	16.7510	
	0.0570	1.2550	21.0175		0.0530	1.0850	19.4717		0.0540	1.0160	17.7020	
	0.0560	1.2960	22.1429		0.0520	1.0600	19.3846		0.0530	0.9540	17.1730	
	Average		21.2592		Average		19.0829		Average		17.0428	
NG-1.0	0.0640	1.3490	19.9470	0.3440	0.0610	0.9650	14.7200	0.6680	0.0590	0.9000	14.1960	0.5400
	0.0590	1.2670	20.5140		0.0550	0.9400	16.0040		0.0570	0.8140	13.2610	
	0.0660	1.4170	20.5270		0.0570	0.8710	14.2330		0.0540	0.8540	14.7560	
	0.0620	1.3110	20.0750		0.0630	0.9960	14.8280		0.0590	0.8820	13.9440	
	0.0650	1.3410	19.7590		0.0630	0.9780	14.6040		0.0600	0.9120	14.1660	
	Average		20.1644		Average		14.8778		Average		14.0646	
NG-1.5	0.0650	1.2810	18.6220	0.9260	0.0620	0.9240	13.9720	1.2550	0.0610	0.9290	14.1760	1.2320
	0.0590	1.1690	18.9850		0.0630	1.0060	15.0900		0.0590	0.9220	14.6730	
	0.0620	1.3450	20.6240		0.0780	1.0170	12.0860		0.0600	0.8360	12.9330	
	0.0600	1.1650	18.4200		0.0610	0.8970	13.7320		0.0680	0.8450	11.5030	
	0.0590	1.1430	18.4390		0.0650	0.8610	12.2670		0.0600	0.8430	13.0700	
	Average		19.0180		Average		13.4294		Average		13.2710	

Table A.3 Oil adsorption capacity of NR composite foams (continuous).

Samples	Diesel				Fuel oil			
	W_0	W_1	Q	SD	W_0	W_1	Q	SD
NR	0.059	0.86	13.509	1.009	0.058	0.552	8.558	0.727
	0.059	0.812	12.738		0.053	0.586	10.06	
	0.055	0.823	14.103		0.056	0.534	8.502	
	0.055	0.883	15.193		0.052	0.535	9.2	
	0.052	0.822	14.921		0.053	0.495	8.264	
	Average		14.0928		Average		8.9168	
NG-0.25	0.059	0.939	14.836	0.431	0.063	0.73	10.572	0.951
	0.06	0.96	15.055		0.059	0.624	9.627	
	0.057	0.97	15.89		0.062	0.56	8.045	
	0.06	0.985	15.393		0.055	0.532	8.734	
	0.057	0.904	14.921		0.061	0.63	9.337	
	Average		15.219		Average		9.263	
NG-0.5	0.0590	1.1070	17.9150	0.8540	0.0650	0.6880	9.5670	1.0980
	0.0640	1.0940	16.0450		0.0600	0.5990	8.9570	
	0.0650	1.2050	17.4530		0.0680	0.8800	11.8830	
	0.0630	1.2000	18.2030		0.0660	0.7440	10.3410	
	0.0620	1.1060	16.9460		0.0600	0.6840	10.3760	
	Average		17.3124		Average		10.2248	
NG-1.0	0.0580	0.8290	13.1970	0.6030	0.0630	0.5000	6.9670	0.7720
	0.0550	0.8290	14.0470		0.0640	0.5000	6.7660	
	0.0560	0.8610	14.4630		0.0620	0.5410	7.7710	
	0.0550	0.8630	14.7480		0.0640	0.6190	8.7020	
	0.0570	0.8730	14.4420		0.0620	0.5150	7.2910	
	Average		14.1794		Average		7.4994	
NG-1.5	0.0530	0.8530	15.2090	0.6200	0.0610	0.3930	5.4180	0.2860
	0.0540	0.8310	14.3830		0.0620	0.3990	5.4700	
	0.0550	0.8130	13.7750		0.0670	0.4700	6.0420	
	0.0560	0.8200	13.6380		0.0630	0.3980	5.3380	
	0.0600	0.9130	14.2610		0.0610	0.3940	5.4170	
	Average		14.2532		Average		5.5370	

Table A.4 Effect of temperature on crude oil adsorption capacity of NR and NG-0.5.

Temperature (°C)	NR				NG-0.5			
	W_0	W_1	Q	SD	W_0	W_1	Q	SD
30	0.0581	0.6324	9.8847	0.5904	0.0525	1.1247	20.4229	0.2314
	0.0596	0.5767	8.6762		0.0561	1.1995	20.3815	
	0.0564	0.6043	9.7145		0.0507	1.0711	20.1262	
	0.0509	0.5054	8.9293		0.0516	1.0908	20.1395	
	0.0504	0.5527	9.9663		0.0511	1.1082	20.6869	
	Average		9.4342		Average		20.3514	
45	0.0464	0.7327	14.7909	0.1498	0.0528	1.2337	22.3655	0.5627
	0.0452	0.7163	14.8473		0.0508	1.1574	21.7835	
	0.0524	0.8328	14.8931		0.0517	1.255	23.2747	
	0.0519	0.8172	14.7457		0.0522	1.2309	22.5805	
	0.053	0.8549	15.1302		0.0561	1.3409	22.902	
	Average		14.88144		Average		22.58124	
60	0.0499	0.6416	11.8577	0.7856	0.0519	0.9216	16.7572	0.4151
	0.0526	0.7174	12.6388		0.0503	0.8696	16.2883	
	0.056	0.7078	11.6393		0.0529	0.9416	16.7996	
	0.0549	0.673	11.2587		0.0512	0.9431	17.4199	
	0.0551	0.7822	13.196		0.0568	0.9989	16.5863	
	Average		12.1181		Average		16.77026	

Table A. 5 Effect of turbulence on crude oil adsorption capacity of NR and NG-0.5.

Turbulence (rmp)	NR				NG-0.5			
	W_0	W_1	Q	SD	W_0	W_1	Q	SD
0	0.0581	0.6324	9.8847	0.2625	0.0600	1.0090	15.9360	0.7302
	0.0596	0.6767	10.3540		0.0590	1.0950	17.6520	
	0.0564	0.6043	9.7145		0.0550	0.9690	16.7510	
	0.0509	0.5454	9.7151		0.0540	1.0160	17.7020	
	0.0504	0.5527	9.9663		0.0530	0.9540	17.1730	
	Average		9.9269		**Average**		17.0428	
100	0.0598	0.9458	14.8161	0.3729	0.0550	1.1833	20.5146	0.5909
	0.0584	0.9323	14.9640		0.0527	1.1388	20.6091	
	0.0688	1.0380	14.0872		0.0515	1.1805	21.9223	
	0.0521	0.8212	14.7620		0.0512	1.1309	21.0879	
	0.0526	0.8049	14.3023		0.0508	1.0970	20.5945	
	Average		14.5863		**Average**		20.9457	
150	0.0659	1.1000	15.6920	0.4902	0.0535	1.2412	22.2000	0.3471
	0.0689	1.1042	15.0261		0.0532	1.2730	22.9286	
	0.0554	0.9147	15.5108		0.0529	1.2182	22.0284	
	0.0519	0.8730	15.8208		0.0527	1.2231	22.2087	
	0.0571	0.9922	16.3765		0.0546	1.2769	22.3864	
	Average		15.6852		**Average**		22.3504	
200	0.0659	1.1341	16.2094	0.4390	0.0544	1.3551	23.9099	0.6804
	0.0689	1.2042	16.4775		0.0543	1.3148	23.2136	
	0.0554	1.0148	17.3177		0.0581	1.4341	23.6833	
	0.0504	0.8730	16.3214		0.0525	1.2331	22.4876	
	0.0511	0.8922	16.4599		0.0568	1.3297	22.4102	
	Average		16.5572		**Average**		23.1409	

Table A.6 Effect of the contact time on the crude oil adsorption of NR and NG-0.5

NR				NG-0.5		
Time (min)	W_0	W_1	Q	W_0	W_1	Q
0.25	0.0569	0.1567	1.754	0.0516	0.353	5.8411
	0.0492	0.1055	1.1443	0.0568	0.3456	5.0845
	0.0567	0.1496	1.6384	0.0529	0.3406	5.4386
	0.0571	0.1435	1.5131	0.0536	0.3843	6.1698
	0.0565	0.1545	1.7345	0.0553	0.3492	5.3146
	Average		1.5569	Average		5.5697
0.5	0.0558	0.2845	4.0986	0.0557	0.4699	7.4363
	0.0598	0.3835	5.413	0.0517	0.4672	8.0368
	0.0544	0.3462	5.364	0.0539	0.4932	8.1503
	0.0422	0.2141	4.0735	0.0535	0.4858	8.0804
	0.0422	0.2148	4.09	0.0556	0.5497	8.8867
	Average		4.6078	Average		8.1181
0.75	0.0565	0.4461	6.8956	0.0562	0.6651	10.8345
	0.0538	0.4632	7.6097	0.0521	0.5901	10.3263
	0.0577	0.4995	7.6568	0.0549	0.6206	10.3042
	0.0586	0.5092	7.6894	0.0524	0.6062	10.5687
	0.0524	0.4917	8.3836	0.0565	0.5645	8.9912
	Average		7.647	Average		10.205
1	0.0492	0.5498	10.1748	0.0563	0.7035	11.4956
	0.0568	0.5705	9.044	0.0543	0.6083	10.2026
	0.0456	0.457	9.0219	0.0553	0.7129	11.8915
	0.0464	0.4966	9.7026	0.0559	0.7148	11.7871
	0.0494	0.5148	9.4211	0.0547	0.6887	11.5905
	Average		9.47288	Average		11.39346

Table A.7 Effect of the contact time on the crude oil adsorption of NR and NG-0.5 (continuous)

Time (min)	NR			NG-0.5		
	W_0	W_1	Q	W_0	W_1	Q
2	0.0493	0.5011	9.1643	0.0544	0.8353	14.3548
	0.0446	0.4474	9.0314	0.0539	0.7657	13.2059
	0.0498	0.5891	10.8293	0.0514	0.7904	14.3774
	0.0468	0.4913	9.4979	0.0583	0.8777	14.0549
	0.0518	0.5823	10.2413	0.0564	0.8243	13.6152
	Average		9.75284	Average		13.92164
3	0.0515	0.4955	8.6214	0.0509	0.8375	15.4538
	0.0471	0.5474	10.6221	0.05	0.8191	15.382
	0.0526	0.5641	9.7243	0.0529	0.8693	15.4329
	0.0465	0.5426	10.6688	0.0559	0.8879	14.8837
	0.0435	0.4529	9.4115	0.0516	0.8318	15.1202
	Average		9.80962	Average		15.25452
4	0.0516	0.6045	10.7151	0.0618	1.0874	16.5955
	0.0515	0.5629	9.9301	0.0534	0.9447	16.691
	0.0486	0.5634	10.5926	0.055	0.8968	15.3055
	0.0561	0.5989	9.6756	0.0526	0.9878	17.7795
	0.0503	0.5726	10.3837	0.0544	0.9835	17.079
	Average		10.25942	Average		16.6901
5	0.0539	0.6611	11.2653	0.0574	1.0094	16.5854
	0.0595	0.6475	9.8824	0.0563	0.9949	16.6714
	0.0529	0.6115	10.5595	0.0539	0.9692	16.9814
	0.0522	0.5638	9.8008	0.0573	1.0155	16.7225
	0.0536	0.5704	9.6418	0.0528	0.9541	17.0701
	Average		10.2299	Average		16.8066

Table A. 8 Effect of the contact time on the crude oil adsorption of NR and NG-0.5 (continuous)

Time (min)	NR			NG-0.5		
	W_0	W_1	Q	W_0	W_1	Q
10	0.0585	0.6291	9.7538	0.0595	1.069	16.9664
	0.0529	0.6177	10.6767	0.0533	0.9667	17.137
	0.0574	0.6726	10.7178	0.0591	1.0704	17.1117
	0.0588	0.5725	8.7364	0.0568	1.0018	16.6373
	0.0564	0.5741	9.1791	0.0546	0.9717	16.7967
	Average		9.8127	Average		16.9298
15	0.0581	0.5831	9.0361	0.0596	1.0094	15.9362
	0.0596	0.6717	10.2701	0.0587	1.0949	17.6525
	0.0564	0.5977	9.5975	0.0546	0.9692	16.7509
	0.0569	0.667	10.7223	0.0543	1.0155	17.7017
	0.0534	0.6547	11.2603	0.0525	0.9541	17.1733
	Average		10.1772	Average		17.0429
30	0.0577	0.5731	8.9324	0.0569	0.996	16.5044
	0.0587	0.6324	9.7734	0.0585	1.0198	16.4325
	0.0483	0.5421	10.2236	0.0558	0.9952	16.8351
	0.0563	0.6292	10.1758	0.0549	0.9916	17.0619
	0.0537	0.6275	10.6853	0.0504	0.8901	16.6607
	Average		9.9581	Average		16.6989
90	0.0566	0.5645	8.9735	0.0593	1.0302	16.3727
	0.0575	0.6445	10.2087	0.0543	1.0703	18.7109
	0.058	0.7268	11.5314	0.0583	1.074	17.422
	0.0547	0.5622	9.2779	0.0503	0.9348	17.5845
	0.0559	0.5666	9.136	0.0523	0.9293	16.7686
	Average		9.8254	Average		17.3717

Table A.9 Effect of the initial oil concentration on the adsorption capacity of NR and NG-0.5.

Initial concentration (g/100ml)	NR			NG-0.5		
	W_0	W_1	Q	W_0	W_1	Q
0.5	0.0489	0.4307	7.8077	0.0526	0.5922	10.2585
	0.0449	0.4385	8.7661	0.0538	0.536	8.9628
	0.0439	0.4072	8.2756	0.0535	0.605	10.3084
	0.0478	0.4012	7.3933	0.059	0.5634	8.5491
	0.0486	0.4215	7.6728	0.0556	0.6431	10.5665
	Average		7.9831	Average		9.7290
0.75	0.0506	0.5136	9.1501	0.0474	0.6552	12.8227
	0.0496	0.4871	8.8205	0.0551	0.6344	10.5136
	0.0549	0.5857	9.6684	0.0566	0.7456	12.1731
	0.0519	0.4814	8.2755	0.0548	0.7842	13.3102
	0.0544	0.5629	9.3474	0.0555	0.8201	13.7765
	Average		9.0524	Average		12.5192
1.25	0.0598	0.5607	8.3762	0.049	0.8648	16.6489
	0.0534	0.6101	10.425	0.0489	0.9352	18.1247
	0.0536	0.5876	9.9626	0.0454	0.8166	16.9867
	0.0524	0.6111	10.6622	0.0548	0.9228	15.8394
	0.0549	0.5871	9.6939	0.0582	0.949	15.3058
	Average		9.8240	Average		16.5811

Table A.10 Effect of the initial oil concentration on the adsorption capacity of NR and NG-0.5 (continuous).

Initial concentration (g/100ml)	NR			NG-0.5		
	W_0	W_1	Q	W_0	W_1	Q
2.5	0.0493	0.5011	9.1643	0.0574	1.0094	16.5853
	0.0446	0.4474	9.0313	0.0563	0.9949	16.6714
	0.0498	0.5891	10.8293	0.0539	0.9692	16.9814
	0.0468	0.4913	9.4978	0.0573	1.0155	16.7225
	0.0518	0.5823	10.2413	0.0528	0.9541	17.0700
	Average		9.7528	Average		16.8061
3.75	0.0509	0.5279	9.3713	0.052	0.9399	17.0750
	0.0521	0.6134	10.7735	0.0578	0.9651	15.6972
	0.0528	0.5704	9.8030	0.0533	0.9526	16.8724
	0.0538	0.5642	9.4869	0.0519	0.8761	15.8805
	0.0572	0.638	10.1538	0.0579	0.9772	15.8773
	Average		9.9177	Average		16.2805
5	0.0581	0.6324	9.8846	0.0596	1.0094	15.9362
	0.0596	0.5767	8.6761	0.0587	1.0949	17.6524
	0.0564	0.6403	10.3528	0.0546	0.9692	16.7509
	0.0569	0.6054	9.6397	0.0543	1.0155	17.7016
	0.0504	0.5527	9.9662	0.0525	0.9541	17.1733
	Average		9.7039	Average		17.0429

Table A.11 The oil recovery efficiency of NR and NG-0.5 foams.

Time	NR		NG-0.5	
	W_0	W_1	W_0	W_1
1	0.0509	0.5279	0.052	0.9399
	0.0521	0.6134	0.0578	0.9651
	0.0528	0.5704	0.0533	0.9526
	0.0538	0.5642	0.0519	0.8761
	0.0572	0.638	0.0579	0.9772
2	0.1782	0.6348	0.1928	0.8517
	0.1767	0.6693	0.2058	0.9476
	0.1719	0.6181	0.2054	0.8526
	0.1688	0.6293	0.179	0.8517
	0.1525	0.5947	0.221	0.9662
3	0.175	0.6226	0.1985	0.8654
	0.193	0.6857	0.2173	0.9205
	0.1771	0.6098	0.1915	0.8434
	0.1933	0.6351	0.195	0.871
	0.1588	0.5931	0.197	0.9161
4	0.201	0.6643	0.1805	0.8869
	0.184	0.626	0.2103	0.959
	0.1815	0.6153	0.1879	0.8394
	0.1889	0.6025	0.1802	0.7903
	0.1621	0.6106	0.2009	0.8504
5	0.1858	0.6581	0.2034	0.8706
	0.1855	0.6729	0.2082	0.9515
	0.196	0.7417	0.1997	0.85
	0.1989	0.6859	0.2119	0.8516
	0.1513	0.6031	0.2126	0.935
6	0.1824	0.6318	0.2082	0.84
	0.1803	0.6708	0.223	0.9832
	0.1851	0.6975	0.201	0.8476
	0.1829	0.6945	0.1592	0.8618
	0.1749	0.5849	0.2103	0.9615

Table A.12 The oil recovery efficiency of NR and NG-0.5 foams (continuous).

Time	NR		NG-0.5	
	W_0	W_1	W_0	W_1
7	0.1919	0.7195	0.1904	0.8801
	0.1889	0.667	0.2089	0.9691
	0.1807	0.7288	0.1908	0.8526
	0.2004	0.7725	0.1783	0.8763
	0.1555	0.609	0.2012	0.9833
8	0.1827	0.6326	0.1852	0.79
	0.1953	0.6993	0.2298	0.9086
	0.1752	0.6605	0.1883	0.8268
	0.1899	0.6385	0.1883	0.8224
	0.1647	0.5644	0.2004	0.9216
9	0.1711	0.6533	0.1888	0.8255
	0.2016	0.682	0.2142	0.9975
	0.2012	0.7025	0.1896	0.878
	0.1952	0.6508	0.1776	0.8475
	0.1726	0.5888	0.2009	0.9722
10	0.1709	0.6166	0.1906	0.8998
	0.1721	0.6751	0.2115	0.933
	0.1785	0.6244	0.1904	0.824
	0.1905	0.6597	0.1851	0.8678
	0.1618	0.5798	0.194	0.9658
11	0.113	0.5834	0.1329	0.8665
	0.1176	0.648	0.1343	0.919
	0.1294	0.6614	0.1457	1.0407
	0.1266	0.7321	0.1464	0.9215
	0.1268	0.7202	0.131	0.82
12	0.1569	0.626	0.199	0.9214
	0.1697	0.6535	0.1993	0.9148
	0.1742	0.6595	0.2025	1.0129
	0.1731	0.7573	0.1795	0.9107
	0.17	0.7393	0.1977	1.0654

Table A.13 The oil recovery efficiency of NR and NG-0.5 foams (continuous).

Time	NR		NG-0.5	
	W_0	W_1	W_0	W_1
13	0.1584	0.6197	0.1958	0.8631
	0.1637	0.669	0.177	0.922
	0.1994	0.693	0.2127	0.9547
	0.1782	0.6214	0.187	0.8403
	0.1745	0.676	0.2037	0.9949
14	0.1648	0.7543	0.1935	0.8279
	0.1679	0.7782	0.1882	0.8635
	0.1844	0.7503	0.1984	0.9777
	0.1886	0.7914	0.1876	0.8482
	0.1629	0.7317	0.2142	0.9433
15	0.1648	0.5684	0.1887	0.7665
	0.176	0.5735	0.1768	0.8819
	0.1996	0.6211	0.211	0.9007
	0.2041	0.6745	0.1863	0.7891
	0.1911	0.6029	0.2055	0.9116